Solving the Matter

Crystal Engineering and Particle Design of Poorly Soluble Drugs via Rapid Expansion of Supercritical Solutions

Dissertation

der Mathematisch-Naturwissenschaftlichen Fakultät

der Eberhard Karls Universität Tübingen

zur Erlangung des Grades eines

Doktors der Naturwissenschaften

(Dr. rer. nat.)

vorgelegt von

Katrin Christine Müllers

aus Koblenz

Tübingen 2015

Tag der mündlichen Qualifikation:	12.06.2015
Dekan:	Prof. Dr. Wolfgang Rosenstiel
1. Berichterstatter:	Prof. Dr. Martin A. Wahl
2. Berichterstatter:	Prof. Dr. Rolf Daniels

ACKNOWLEDGEMENTS

The second part of this work "Formation of Nanosuspensions with RESS" was conducted in cooperation with the department of pharmaceutical technology of the university of Lisbon, Portugal and funded by "*Fundação para a Ciência e a Tecnologia*", Lisbon, Portugal (PTDC/CTM/098688/2008 and SFRH/BD/90118/2012). I would like to thank Prof. João Pinto for his professional input and for his donation of olanzapine samples. I also wish to thank Ms. Maria Paisana for her valuable advice in all questions concerning the solid state characterization of olanzapine and for conducting the FTIR measurements and data evaluation of olanzapine. Ms. Paisana also performed all PXRD measurements described in this thesis.

TABLE OF CONTENTS

ABBREVIATIONS

API	Active Pharmaceutical Ingredient
BCS	Biopharmaceutics Classification System
BET	Brunauer-Emmet-Teller Method
BSA	Bovine Serum Albumin
CNT	Classical Nucleation Theory
CPD	Controlled Particle Deposition
CRM	Confocal Raman Microscopy
DSC	Differential Scanning Calorimetry
DLS	Dynamic Light Scattering
FTIR	Fourier Transform Infrared Spectroscopy
GAS	Gas Antisolvent Process
HCl	Hydrochloric Acid
HPMC	Hydroxypropylmethylcellulose
IBU	Ibuprofen
MDT	Mean Dissolution Time
NA	Nicotinamide
NCE	New Chemical Entity
OLZ	Olanzapine
PCA	Precipitation from Compressed Antisolvent

PEG	Polyethylenglycole
PGSS	Particles from Gas-Saturated Solutions
Ph. Eur.	European Pharmacopeia
PLA	Polylactic Acid
PSD	Particle Size Distribution
PVP	Polyvinylpyrrolidone
PVA	Polyvinyl Alcohol
PXRD	Powder X-Ray Diffractometry
PY	Product Yield
RESOLV	Rapid Expansion of Supercritical Solutions into Liquid Solvent
RESS	Rapid Expansion of Supercritical Solutions
RESSAS	Rapid Expansion from Supercritical Solution to Aqueous Solution
SAS-EM	Supercritical Antisolvent Process with Enhanced Mass Transfer
scCO2	Supercritical Carbon Dioxide
SCF	Supercritical Fluid
SEDS	Solution-Enhanced Dispersion by Supercritical Fluids
SEM	Scanning Electron Microscopy
TP	Theophylline
WHO	World Health Organization

NOMENCLATURE

A	Surface Area	m^2
c	Concentration	mg/ml
c*	Concentration of critical nuclei	Eq. 9
D	Diffusion coefficient	$m^2\ s^{-1}$
F_b	Buoyancy force measured in contact angle measurements	N
F_n	Free energy of nucleus formation	J; Eq. 2
F_n*	Nucleation barrier	J; Eq. 6
F_{tot}	Vertical force in contact angle measurements	N
ΔG_m	Activation free energy of interface crossing	J; Eq. 10
h	Thickness of diffusion layer	m
ΔH_f	Specific heat of fusion	$J\ g^{-1}$
J	Nucleation rate	$m^{-3}\ s^{-1}$; Eq. 12
k_B	Boltzmann constant	1.38×10^{-23} Nm K^{-1}
l	Wetted length in contact angle measurements	m
m	Mass	kg
m_D	Mass of the API dissolved in $scCO_2$	g
m_E	Mass of the RESS product recovered from the expansion chamber	g
M	Molecular mass	$g\ mol^{-1}$
n*	Critical nucleus size	Eq. 5
p	Pressure	MPa

PY	Process yield	%; Eq. 14
R	Gas constant	8.314 J $mol^{-1}K^{-1}$
rpm	Rounds per minute	min^{-1}
s	Solubility in water	mg/ml
s_{CO2} (p;T;t)	Solubility in $scCO_2$ as mass fraction	g/kg CO_2; Eq. 15
S	Supersaturation (dimensionless)	Eq. 1
spm	Shakes per minute	min^{-1}
t	Time	min
T	Temperature	°C
T_{on}	Onset temperature of melting	°C
Δu	Propagated error	Eq. 20
V	Volume	l
V_{Ext}	Volume of extraction chamber	l
w	Mass fraction	m/m
wt. %	Weight percent	%
x_{c^*}	Fraction of nuclei with critical size	Eq. 7
y (p;T;t)	Solubility in $scCO_2$ as molar fraction	mol/mol CO_2; Eq. 16
y*	Equilibrium mol fraction at expansion	Eq. 1
y_E (p;T)	Mol fraction at extraction (p;T)	Eq. 1

Greek Letters

α	Cocrystal yield	(Eq. 23)
α_f	Shape factor (dimensionless)	(Eq. 2)
γ	Interfacial tension	(N m^{-1})
δ	Deformation vibration (Raman, FTIR)	(m^{-1})
η	Kinematic viscosity	(cSt)
θ	Diffraction angle in PXRD measurements	(°)
θ_C	Contact angle of water on powders	(°)
$\Delta\mu$	Difference in chemical potential between bulk phase and newly created phase	(Eq. 3)
ν	Stretching vibration (Raman, FTIR)	(m^{-1})
ν_{inc}	Frequency of molecule incorporation into nuclei	(s^{-1})
ν_{mol}	Molecular vibration frequency	(s^{-1})
ρ	CO_2 density	(kg m^{-3})
σ	Surface tension of test liquid in contact angle measurements	(Jm^{-2})

ZUSAMMENFASSUNG

Eine wachsende Anzahl neu entwickelter Arzneistoffe ist durch hohe Lipophilie charakterisiert und dadurch bedingt nur schwer und langsam in wässrige Lösung zu überführen. Das schlechte Auflösungsverhalten dieser Arzneistoffe führt oft zu geringer Bioverfügbarkeit, was die therapeutische Wirksamkeit dieser Stoffe so stark beeinträchtigen kann, dass die Entwicklung von pharmazeutischen Darreichungsformen nicht praktikabel ist. Aus pharmazeutisch-technologischer Sicht können Löslichkeit und Lösungsgeschwindigkeit durch gezieltes Partikel-Design und "crystal engineering" erheblich verbessert werden.

Viele der etablierten pharmazeutisch-technologischen Techniken wie Mahlen, Umkristallisieren aus Lösemitteln oder Sprühtrocknen greifen dafür jedoch auf hohe Temperaturen, mechanische Belastung und organische Lösemittel zurück, was Kristalldefekte, chemische Zersetzung und/oder organische Lösungsmittel-Verunreinigungen verursachen kann. Im Gegensatz dazu bietet Rapid Expansion of Supercritical Solutions (RESS) ein alternatives Verfahren, bei dem weder organische Lösemittel noch aggressive Prozessbedingungen zur Anwendung kommen. Trotz dieser Vorteile befindet sich das Verfahren noch im Frühstadium der wissenschaftlichen und prozesstechnischen Entwicklung. Das Ziel dieser Arbeit ist es daher, RESS als alternatives Verfahren für crystal engineering und Partikel-Design schwer löslicher Arzneistoffe zu untersuchen.

In **Kapitel 2** wurde ein Prozess zur RESS Mikronisierung unter Verwendung von organischem Cosolvens entwickelt, da viele Stoffe mit höherem Molekulargewicht und polaren Funktionen eine zu geringe Löslichkeit in überkritischem Kohlenstoffdioxid aufweisen und daher nicht für das RESS Verfahren geeignet sind. Durch die Zugabe von 4 wt. % Methanol zur überkritischen Phase konnte die Löslichkeit des Modell-Arzneistoffs Theophyllin um einen Faktor von beinahe 25 gesteigert werden bei gleichzeitiger Ausbeutesteigerung von rund 0 auf 25 %.

Durch die RESS Mikronisierung wurde dabei eine 14fache Steigerung der spezifischen Oberfläche erzielt. Mit steigender Expansionstemperatur konnte die Abscheidung von flüssigem Methanol unterdrückt werden, so dass Umkristallisierung und Partikelwachstum des Produkts minimiert wurden. Durch diese Weiterentwicklung des klassischen RESS Prozesses kann nun eine weitaus größere Anzahl an Stoffen mit dem RESS Verfahren mikronisiert werden.

In **Kapitel 3** wurde die Produktion von Nanopartikeln und Nanosuspensionen mit Olanzapin, einem schwer löslichen BCS Klasse II Stoff, beschrieben. Mittels RESS konnten Nanopartikel und Nanosuspensionen mit einer mittleren Partikelgröße von 160-340 nm und einer engen Partikelgrößenverteilung produziert werden. Besonders die Expansionstemperatur und der CO_2 Fluss durch die Düse während der Expansion stellten kritische Prozessparameter dar, da bei mangelnder Kontrolle das Stabilisatormedium zum Einfrieren neigte oder mit dem expandierenden Gas aus dem Auffangbehälter ausgetragen wurde.

Je nach verwendetem Stabilisatormedium konnte eine Prozess-Ausbeute von fast 100 % erzielt werden. Aus prozesstechnischer Sicht eigneten sich sterische Stabilisatoren besser als elektrostatische, da sie weniger zur Schaumbildung neigten und die Viskosität des Stabilisatormediums erhöhten. Olanzapin zeigte allerdings bereits wenige Stunden nach der Herstellung der Nanosuspensionen ein mit Hydratbildung einhergehendes Partikelwachstum in diesen Medien. Dies konnte durch Zugabe von Natriumlaurylsulfat im Anschluss an den Produktionsprozess verhindert werden. Letztlich zeigten die Nanosuspensionen eine deutliche Steigerung der Auflösegeschwindigkeit von Olanzapin im Vergleich zur Referenz. Im Hinblick auf den Verzicht von Lösemitteln, die milden Prozessbedingungen und das erreichte Partikelgrößenspektrum kann das RESS Verfahren insgesamt eine bessere Alternative zu konventionellen Verfahren zur Herstellung von Nanopartikeln und Nanosuspensionen bieten.

In **Kapitel 4** wurde RESS zur Produktion und gleichzeitigen Mikronisierung von Cokristallen aus Ibuprofen und Nicotinamid eingesetzt. Die beiden Stoffe wurden in unterschiedlichen molaren Verhältnissen aus der überkritischen Lösung ausgefällt. Bei einem Überschuss an Nicotinamid wurde der komplette Arzneistoff zum Cokristall umgesetzt, während bei einem molaren Verhältnis von 1:1 ein reines cokristallines Produkt erhalten wurde. RESS Cokristalle verfügten über eine deutlich erhöhte spezifische Oberfläche und eine erhöhte Auflösegeschwindigkeit im Vergleich zu Cokristallen, die durch konventionelle Evaporation von organischem Lösemittel hergestellt wurden. Im Hinblick auf die hohe Produkt-Reinheit und die Zusammenfassung von Produktion und Mikronisierung in einem einzelnen Schritt ist das RESS Verfahren eine vielversprechende Alternative zu herkömmlichen Techniken des crystal engineerings.

Abschließend kann aus pharmazeutischem Blickwinkel gesagt werden, dass das RESS Verfahren eine vielseitige technologische Plattform mit bisher unausgeschöpftem Potenzial für crystal engineering und Partikel-Design niedermolekularer Arzneistoffe bietet. Als umweltfreundliches Verfahren kann RESS den Sektor der bereits verfügbaren Technologien sinnvoll ergänzen, da einerseits Produkte mit vergleichbarer oder sogar überlegener pharmazeutischer Qualität erhalten werden können, während andererseits keine organischen Lösemittelabfälle anfallen oder Lösungsmittelrückstände die Toxizität der finalen Arzneiform erhöhen.

CHAPTER 1 | INTRODUCTION AND AIM OF THIS THESIS

Introduction

Aqueous solubility and fast dissolution are key parameters to achieve adequate bioavailability of active pharmaceutical ingredients (API's). But many new drug candidates present poor pharmacokinetic properties due to their low solubility and poor dissolution performance. Statistically, 40 % of new molecules are thus excluded from further development at the early stages of pharmaceutical research (1). This is a problem not only from an economical standpoint, as increasing costs of pharmaceutical development and limited output of successful drug candidates from the pipeline are the consequences. Today, a majority of the recently developed drugs on the market is classified as poorly soluble according to BCS (2) (Figure 1). In contrast, most entities listed on the World Health Organization's list of essential medicines from 10 years ago were still classified as well soluble, which clearly shows that there is an evolving trend towards more hydrophobic compounds (Figure 1).

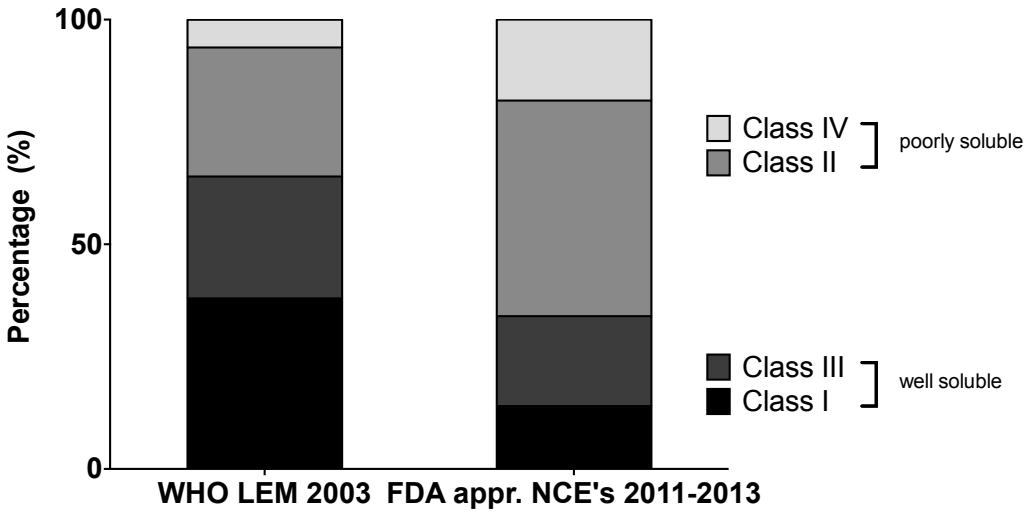

Figure 1 Distribution over the BCS classes of API's on the World Health Organization's essential list of medicines (WHO LEM) from 2003 and of new chemical entities approved by the Food and Drug Administration (FDA appr. NCE's) from 2011-2013 (3, 4)

This means that there is a growing demand for strategies and processing technologies to increase the bioavailability of intrinsically poorly soluble compounds. From a pharmaceutical technological standpoint, crystal engineering and particle design are valuable tools to improve dissolution-limited bioavailability. There are a number of established processing technologies such as milling, spray drying or recrystallization from organic solvents, but most of them suffer from drawbacks arising from the use of harsh process conditions such as high temperature, mechanical stress or organic solvents.

Given the evident trend in recent drug development towards poorly soluble drugs and the stability issues related with conventional procedures, it is particularly important to develop alternative technologies. As such, the Rapid Expansion of Supercritical Solutions (RESS) shows great potential, because it can circumvent many of the problems associated with traditional techniques. RESS involves the use of little or no organic solvents and thus provides contaminant-free products. In addition, low-molecular weight drugs with poor aqueous solubility often show good solubility in $scCO_2$, which makes BCS Class II and IV compounds an interesting target group for processing with RESS. The versatility of the process has attracted growing scientific attention in the last years, which is mirrored by a high number of reviews, research papers and patents available in the literature, but much of the research is still on an experimental level (5, 21-25).

Up to date, there is no pharmaceutical product on the market that exploits RESS as a tool for particle design. Clearly, further scientific attention is required before RESS can become common practice in pharmaceutical production and development. For a more profound insight into the RESS process, the following sections describe its history, the theory of particle formation and its current status viewed from a pharmaceutical perspective.

Supercritical fluids as solvents

In 1879, Hannay and Hogarth first observed that solids with low vapor pressure could be dissolved in supercritical fluids (5). They further observed that by rapidly reducing the pressure in a system containing a fluid and a solute, a crystalline deposit and "a cloud of fine crystals floating in the menstruum" were formed (5). The supercritical state is reached, when a gas is compressed and heated beyond its critical point, where the phase boundary between the liquid and the gaseous state ceases to exist. The critical point is located on the vapor pressure curve and is a unique property of the respective gas (Figure 2). The fluid state is characterized by properties similar to gases and liquids, but it also has unique physical characteristics. The viscosity is as low as in gases, facilitating both pumping and natural convection (6). The density, especially in the near critical region, is a function of the applied pressure and reaches liquid-like values at higher pressures. Because the solvent capacity of the SCF varies exponentially with its density, small changes in the operating conditions can specifically tailor the solubility of the solute or trigger precipitation. Finally, surface tension is literally non-existent in supercritical fluids, while the diffusivity is, with 1 or 2 orders of magnitude, substantially higher than in a liquid (7).

These properties account for the solvent power of SCF's and for their application in mass-transfer and phase-transition processes. Figure 2 shows that by choosing a pathway through the supercritical region, the gaseous state can be reached from the liquid state without phase separation. The fluid of choice in SCF processing is $scCO_2$, since its critical point is at 7.38 MPa and 31.1 °C, which provides relatively mild process conditions. It is also inert, non-flammable, non-toxic and environmentally friendly (8). CO_2 is a nonpolar, hydrophobic molecule (O=C=O) with a polarity comparable to that of n-hexane (9). Its solvent power is thus negligible for polar substances and macromolecules. But for low molecular weight drugs with low aqueous solubility and polarizability, the solubility profile of $scCO_2$ is often convenient.

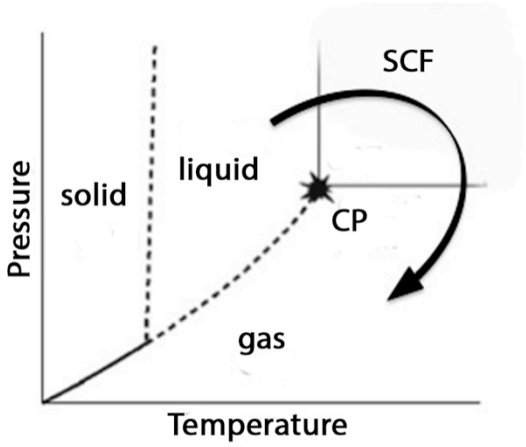

Figure 2 p-T phase diagram showing the critical point (CP) and the transition from the liquid to the gaseous state through the supercritical region. Modified after (7)

Supercritical fluids in particle and solid state design

Despite the fact that SCF's have been discovered over a century ago, commercial applications were only established in the 1970's for the decaffeination of coffee beans and tea leafs (10). Most of the other industrial applications of SCF technology are in the field of extraction, such as hops and essential oils, and analytical chromatography (10). Apart from extraction and chromatography, SCF technology comprises several applications for particle formation and design. These techniques are particularly interesting from a pharmaceutical perspective, but are so far only used on laboratory scale. One reason for this is that the cost of instrumentation and operation in high-pressure systems is comparably high (10).

SCF technology for particle design can be broadly classified into 2 groups, namely solvent and antisolvent techniques (Table 1). In solvent techniques, the processed compound is dissolved in a SCF; sufficient solubility is thus a prerequisite. In antisolvent techniques, an API is dissolved in an organic solvent and emulsified with an aqueous phase containing optional excipients. The organic solvent is then extracted with $scCO_2$, so that micelles of the API in the watery phase remain.

On the one hand, antisolvent techniques allow processing of a wider range of materials because solubility in the fluid is not a prerequisite. But on the other hand, un-extracted residual solvents can lead to re-agglomeration of the products and increase their toxic potential, thus contradicting one of the most important initial advantages of SCF technology (10). Controlled Particle Deposition (CPD) and the Rapid Expansion of Supercritical Solutions (RESS) are solvent-based techniques that use SCF's (Table 1). In CPD, the pressure is released from the dissolution chamber, so that the dissolved material is precipitated directly into porous carriers that are placed in the chamber together with the API. It has been used for the formation of drug-loaded carriers and an inclusion complex of ibuprofen in cyclodextrins (11, 12). Disadvantages of this technique are solute loss via the vent, when the reaction chamber is depressurized, and unspecific particle deposition inside the reaction chamber. In addition, it is difficult to ensure homogeneous conditions throughout the dissolution chamber and throughout the duration of the expansion, so that broad particle size distributions may result.

In contrast to this, the expansion of the supercritical solution in the RESS process is controlled through a capillary nozzle. The spray expansion lasts for less than 10^{-5}s, so that the pressure and density of the fluid drop very rapidly. At the same time, the solvent power of the SCF, which is a direct function of the fluid density, is reduced drastically. As a result, the solute is precipitated on a submicron or micron scale (13, 14).

Table 1 Supercritical Fluid based techniques for particle formation

Solvent based techniques	Antisolvent based techniques
• Rapid Expansion of Supercritical Solutions (RESS) (13, 14) • Controlled Particle Deposition (CPD) (11, 12)	• Particles from Gas-Saturated Solutions (PGSS) (15) • Gas Antisolvent Process (GAS) (16) • Supercritical Antisolvent Process (SAS) (17, 18) • Precipitation from Compressed Antisolvent (PCA) (19), • Solution Enhanced Dispersion by Supercritical Fluids (SEDS) (20) • Supercritical Antisolvent Process with Enhanced Mass Transfer (SAS-EM) (21)

Particle formation with RESS

The supersaturation S is the driving force for all solution crystallization processes. The supersaturation is the difference between the actual concentration and the equilibrium concentration of a solute at given conditions and is a determining factor for the resulting particle size distribution. S is defined as:

$$S = \frac{y_E \ (p_E;T_E)}{y^* \ (p;T)} \qquad \textit{Eq. 1}$$

Where y_E is the solute mole fraction at the extraction temperature and pressure (T_E; p_E) and y^* is the equilibrium mole fraction of the solute at the actual temperature and pressure of expansion (p;T) (22). Nucleation means the birth of new crystal nuclei via random aggregation of molecules.

It is followed and partially superposed by particle growth that is driven by condensation, when single molecules are added at the particle surface, and coagulation, when collisions of separate particles form bigger ones (23). The supersaturation controls these competing mechanisms and influences the resulting crystal size. At low supersaturation, crystals can grow faster than they actually nucleate, so that fewer and larger crystals are formed (Figure 3). With increasing supersaturation, the nucleation rate increases exponentially, which is why in these cases; a high number of small crystals are formed. This is the underlying principle of RESS micronization.

The theory of nucleation in RESS can be explained analogous to classical nucleation theory (CNT) and the kinetic models assumed for nucleation and particle growth developed by Volmer and Weber (24) and Becker and Döring (25). In CNT, the free energy of nucleus formation F_n for a nucleus comprising n molecules is described as:

$$F_n = \gamma \alpha n^{\frac{2}{3}} - n\Delta\mu \qquad \textit{Eq. 2}$$

Where γ is the interfacial tension between the medium and the newly created bulk phase, α is a shape factor to account for nuclei that are not spherical in shape, and $\Delta\mu$ is the difference in chemical potential between the phases.

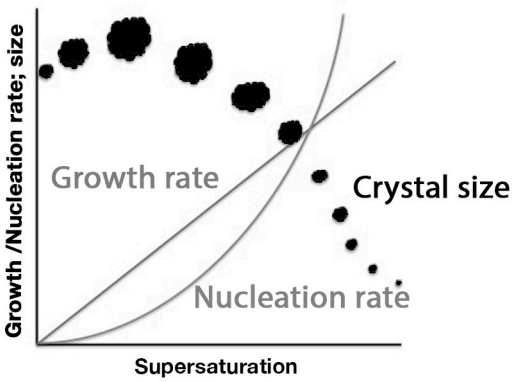

Figure 3 Influence of supersaturation on crystal size through growth and nucleation rate

$\Delta\mu$ is the driving force for the phase change and can be expressed as:

$$\Delta\mu = k_B T \, lnS \qquad \textit{Eq. 3}$$

Where k_B is the Boltzmann constant, T is the temperature and S is the supersaturation[1]. Basically speaking, the term $\gamma\alpha n^{\frac{2}{3}}$ describes the energy cost of the system due to the creation of a new interface, while the term $n\Delta\mu$ describes the energy gain due to the formation of a new stable phase from a metastable state. To account for the fact that not all nuclei are spherical, a shape factor α can be introduced in Eq. 2 while replacing r with n as the number of molecules inside the nuclei. By plugging Eq. 3 into Eq. 2, F_n becomes:

$$F_n = \gamma\alpha n^{\frac{2}{3}} - nk_B T \, lnS \qquad \textit{Eq. 4}$$

In Figure 4, the free energy of nucleus formation F_n is plotted against the nucleus size. As the creation of a new interface costs energy, nucleation will not proceed if the formed nucleus is too small, because the energy released by forming its volume is not enough to create its surface. This is only the case when the critical nucleus size n^* is reached. At n^*, the sum of these energies reaches a maximum $F_n{}^*$, which is also called the nucleation barrier. At this point, the free energy F_n of the system will be reduced, whether the nucleus grows or dissolves. Nuclei with critical size are thus in a thermodynamically metastable state.

[1] In many publications, Eq. 3 is expressed as $\Delta\mu = k_B T \ln\left(\frac{a_0}{a_{Sat}}\right)$. The activity ratio $\frac{a_0}{a_{Sat}}$ can however be approximated by the ratio of concentrations, or S.

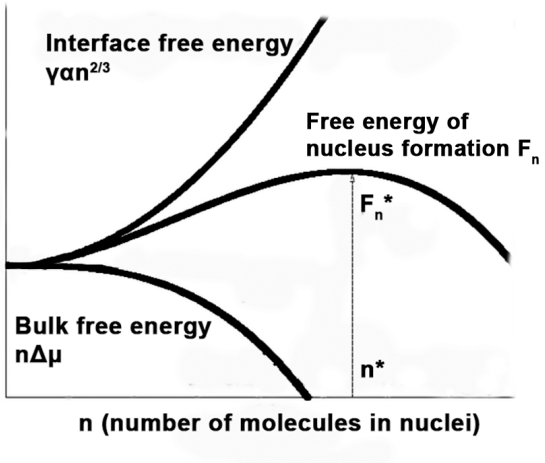

Figure 4 Free energy of nucleus formation F_n as sum of interface free energy and bulk free energy in dependence of the nucleus size. Modified after (26)

The critical nucleus can be calculated by setting the first derivative of Eq. 4 to zero and solving it for n:

$$n^* = \left(\frac{2\gamma\alpha}{3k_B\mathrm{T}\,\ln\mathrm{S}}\right)^3 \qquad \textit{Eq. 5}$$

The critical energy or nucleation barrier can then be calculated as:

$$F_n^* = \frac{4(\gamma\alpha)^3}{27(k_BT\ lnS)^2} \qquad \textit{Eq. 6}$$

Nucleation is basically the result of random fluctuations that bring together sufficient numbers of molecules to form a nucleus that exceeds the critical size. The smaller the critical nucleus size becomes, the higher is the probability for this energy fluctuation to occur. This is exactly the case, when the supersaturation S is increased.

The probability of energy fluctuation of the size $F_n{}^*$ is given by:

$$x_{c*} \cong exp\left(\frac{-F_n^*}{k_BT}\right) \qquad \textit{Eq. 7}$$

Where x_{c^*} is the fraction of nuclei with critical size, which is defined as:

$$x_{c*} \cong \frac{c^*}{c_1} \qquad \textit{Eq. 8}$$

With c_1 being the concentration of monomers in the system, assuming that it is much greater than the concentration of critical nuclei c^*, T is the temperature and k_B is the Boltzmann constant. Combining Eq. 7 and Eq. 8, the concentration of critical nuclei c^* is given by

$$c^* \cong c1\ exp\left(\frac{-F_n^*}{k_B T}\right) \qquad \textit{Eq. 9}$$

For the nucleus to grow, an atom or molecule must overcome the energy barrier ΔG_m to cross the interface separating the nucleus and the matrix.

The frequency of atom or molecule incorporation into the nucleus ν_{inc} is described by another Boltzmann distribution:

$$\nu_{inc} = \nu_{mol} exp\left(\frac{-\Delta G_m}{k_B T}\right) \qquad \textit{Eq. 10}$$

Where ν_{mol} is the vibration frequency of the molecule at a temperature T, ΔG_m is the activation free energy for the molecule to cross the interface, k_B is the Boltzmann constant and T is the temperature. Combining the 2 conditions given by Eq. 9 and Eq. 10, one arrives at a simplified description for the nucleation rate J, which is defined as number of nuclei formed per unit volume in unit time:

$$J = c\ Z\ exp\left(-\frac{F_n{}^*}{k_B T}\right) exp\left(-\frac{\Delta G_m}{k_B T}\right) \qquad \textit{Eq. 11}$$

Where c is the number of atoms or molecules per unit volume and Z is the Zeldovich factor, which essentially expresses the probability of a nucleus with the energy $F_n{}^*$ going on to form the new solid phase instead of dissolving back (27). Using Eq. 6, Eq. 11 can be written as:

$$J = Z\ exp\left(\frac{B\gamma^3}{S^2}\right) \qquad \textit{Eq. 12}$$

Here, all other factors except the supersaturation and the interfacial tension are grouped into a factor B. Eq. 12 shows how strongly J depends on the supersaturation S and the interfacial tension γ, as they come in the 2nd and 3rd powers in the argument of an exponential.

Modeling of the particle size in RESS

For RESS to become a common processing technique for particle formation, control over both particle size and morphology is crucial for its further development up to commercial feasibility. For that reason, mathematic modeling has been important from the early stages of RESS research (22, 28, 29). Models to predict particle size include the nucleation process analogous to CNT and, as a significant determinant of the final particle size, the particle growth due to condensation and coagulation (22, 23, 30). CNT was derived on the assumption of equilibrium conditions, which is not the case in RESS (13). Corrections of CNT are thus necessary due to the non-ideality of SCF's. For example, their liquid-like density coupled with high compressibility causes a decrease of the solute concentration upon expansion and a sharp drop of the temperature, thus increasing the critical nucleus size and decreasing the attainable nucleation rates (28, 29).

The so far developed RESS models focus on the influence of the process conditions and equipment on the expansion process, such as pre- and post expansion temperature and pressure, nozzle geometry and length. The variables included are the fluid density, the flow area, the velocity of the fluid, the distance along the expansion device, friction in the capillary, and the enthalpy, heat and pressure of the system (31). Given the necessary simplifications for reasonable calculations, the diversity of particle growth mechanisms taking place simultaneously[2] and the difficulty of accounting for all flow phenomena inside the exact geometry of the expansion chamber, the predictability of particle size and morphology with the current models is to a certain degree inaccurate. In addition, many of the proposed calculations yield reasonable results when applied to the particular study in which they were derived, but often contradict those of other publications in the field (23).

[2] These include particle growth due to condensation, coagulation and/or Ostwald ripening.

According to most models, the particle size at the end of the supersonic freejet expansion is in the range of 10- 50 nm (23, 31). Although the calculation models somewhat lack precision, this raises the question why experiments yield particle sizes that exceed these models by 1 or 2 orders of magnitude. The reason for this is probably that particle growth in the supersonic expansion freejet is unfinished, but continues during the subsonic freejet and/or the residence time of the particles inside the expansion chamber (31). The major part of the growth time is spent outside the nozzle, which means that the influence of the pre-expansion conditions on the final particle size might be over-estimated, while the conditions inside the expansion chamber are key factors that are often not yet included in the models (23, 31). Restriction of particle growth inside the expansion chamber could, for example, be achieved by lowering the collision frequency and efficiency by choosing low pre-expansion solute mol fractions and lower temperatures (23, 32). All in all, there are promising approaches to be found for modeling of the RESS process, but it is still in development and especially the issue of particle growth during the residence time needs to be investigated more thoroughly.

Is there a place for RESS in pharmaceutical technology?

As explained initially, most applications of RESS are still on an experimental level. To date, no commercial applications for particle formation and design exist in the pharmaceutical field. The reasons for this can be mainly seen in the following issues:

- **Predictability and control of the particle size and size distribution are often poor.**

RESS modeling often does not yet succeed to reliably predict the final particle sizes, because the determining factors that influence particle growth are not yet fully understood (page 12). As a result, micron-sized particles with broad size distributions are often obtained.

- **The solubility of many compounds in $scCO_2$ is too low.**

As discussed initially, the solubility profile of $scCO_2$ is restricted to low molecular weight drugs and such that are rather non-polar (page 4). Even if these properties are met, it is still difficult to achieve solute concentrations that are comparable to organic solvents. The process is thus often regarded as economically unfeasible because of the low throughput rates.

- **The process yield of RESS is often low due to inefficient separation of the small particles from the gaseous stream.**

Similar to spray drying, where a solution of a drug is atomized via a nozzle and collected in a tower or cyclone, optimization of the particle yield in RESS is of utmost importance. The separation efficiency depends on the speed of the travelling particles, their size and of course the geometry of the expansion device. With the currently used equipment, presumably a large fraction of the fine material is not separated from the gaseous stream. This becomes evident by the low process yields often reported in the literature, which are mostly below 5 % (33). It is also possible that the discrepancy between calculated and experimental particle size is partially caused because of this phenomenon (see page 12).

- **Joule-Thompson cooling during the expansion process can cause process disruptions because of (dry) ice formation or nozzle blockage.**

As described before, the spray expansion of the supercritical solution occurs in less than 10^{-5} s (page 5). Due to the rapid expansion of a large amount of gas, the temperature inside the expansion chamber can drop to -50 °C within seconds. Heating mantles can often not compensate that, so that it is vital to control the mass flow of CO_2 through the nozzle. The drastic temperature drop can cause formation of dry ice, freezing of water if present, and blockage of the nozzle so that the expansion process is disrupted.

So clearly, there is a need to dedicate further scientific attention to these issues before RESS can become common practice as a pharmaceutical processing technique. And although the research published on RESS for the improvement of solubility and dissolution is promising, there are fundamental questions that remain to be addressed. At the same time, RESS offers a number of advantages over established processing techniques that justify further scientific effort and make its development worthwhile. Figure 5 summarizes the advantages of RESS from a pharmaceutical perspective. The most important aspect certainly is that in contrast to traditional procedures, it involves the use of little or no organic solvents. This avoids large organic waste streams and renders the process environmentally friendly, which is particularly important in today's environment that is increasingly focused on sustainability (34). At the same time, RESS avoids organic solvent contamination in the products, which would increase their toxic potential, call for complex purification steps and analytical control of the residual levels.

In contrast to organic solvents, $scCO_2$ is non-toxic, environmentally friendly, non-flammable, relatively cheap and inert. With its critical point located at 7.38 MPa and 31.1 °C, $scCO_2$ offers very mild processing conditions. In contrast, conventional size reduction techniques often impart high mechanical stresses on the material, which can cause degradation of thermo-labile compounds due to heat generated by attrition, polymorphic conversions and damage of the crystallinity.

Compressed gases can be easily recycled after expansion without the need of further purification, because once returned to the gaseous state, they have negligible solvent power (13). From a process-engineering standpoint, this allows easy in-process recycling of the SCF, which helps to reduce the production cost in a pharmaceutical batch operation or could even help to design a continuous process (10). In addition, the solubility profile of $scCO_2$ is convenient for processing of hydrophobic, low-molecular weight drugs, which is also the target group usually processed by conventional micronization techniques.

Finally, one of the most attractive features of the RESS process is clearly its versatility, as a number of applications can be realized with basically the same technology. In the pharmaceutical literature, the largest part of the research is focused on micronization of poorly soluble drugs (14, 35-39). There are also a number of publications that describe RESS as a tool for the production of nanoparticles and nanosuspensions (40-44). In addition, a few reports assess RESS in the field of crystal engineering, i.e. for the formation of different polymorphs or crystal doping (45-47). Polymer processing with RESS has high potential but lies beyond the scope of this work and will therefore not be addressed further. For these aspects, reference is made to previous publications (40-42, 44, 48-51).

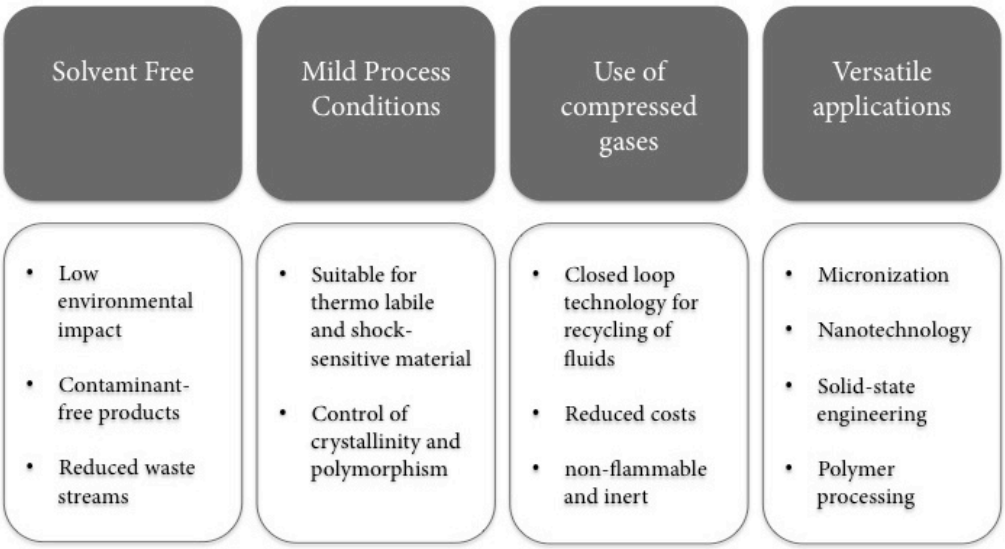

Figure 5 Summary of process advantages of the Rapid Expansion of Supercritical Solutions (RESS)

Aim of this thesis

A growing number of newly developed drug candidates often need to be excluded from pharmaceutical development due to insufficient solubility and, as a result, poor pharmacokinetics. At the same time, traditional pharmaceutical techniques to process such compounds can cause instabilities that arise from using harsh process conditions such as elevated temperature, mechanical stress or organic solvents. In this light, there is a definite need to develop alternative technologies such as the Rapid Expansion of Supercritical Solutions (RESS). Although the technique offers immanent advantages such as little or no use of organic solvents and very mild process conditions, its use in the field of pharmaceutical particle design and crystal engineering is still on an experimental level. Clearly, some fundamental issues need to be addressed before the technique can become common practice in pharmaceutical development and production. These issues concern:

- Control of the critical product parameters such as the particle size distribution
- Solubility in supercritical carbon dioxide
- Process yield
- Control of the critical process parameters such as the expansion cooling

The aim of this thesis is to investigate the potential of RESS as an alternative pharmaceutical processing technique for crystal engineering and particle design to improve aqueous solubility and the dissolution performance of poorly soluble drugs. To this end, each of the central chapters focuses on the development of a specific RESS application. **Chapter 2** investigates whether liquid-cosolvent assisted RESS micronization is a feasible approach to increase drug solubility in supercritical carbon dioxide and thus RESS process yields. **Chapter 3** assesses RESS as an alternative technology for the production of nanosuspensions as a potential pharmaceutical

dosage form. **Chapter 4** investigates RESS as a tool for the simultaneous formation and micronization of pharmaceutical cocrystals. Each chapter includes a pharmaceutical characterization of the products to evaluate the quality of the processed material in terms of purity, particle characteristics and, in **Chapter 3** and **4**, dissolution rate. At the same time, the above-mentioned issues associated with RESS are addressed and discussed in the respective context. Ultimately, this thesis should help to disclose the potential of processing low molecular weight API's with poor aqueous solubility via RESS and thus support the technique's further development in a pharmaceutical environment.

CHAPTER 2 | COSOLVENT-ASSISTED RESS MICRONIZATION

Introduction

A large fraction of research conducted in the field of RESS is focused on micronization of poorly soluble drugs to enhance solubility and dissolution (14, 31, 36, 39, 52, 53). But the restricted solvent capacity of SCF's does not allow a wide range of material to be processed with RESS (54). The described advantages of using CO_2 as a fluid in the pharmaceutical sector are opposed by its low polarizability. CO_2 is a Lewis base, because it can donate an electron pair to Lewis acceptors. Acid/base, induced dipole and quadrupole interactions provide $scCO_2$ with a limited solvation power, which is however not great enough for high molecular weight and/or polar compounds (55). The solubility in $scCO_2$ of these compounds is not sufficient to be economically acceptable.

From the field of SCF chromatography and extraction, it is known that the polarity of the SCF can be modified by addition of a cosolvent to increase the solubility of many compounds (56). A commonly used polar modifier in SCF chromatography and extraction is methanol (57). The p-T-x behavior of the binary system CO_2 + methanol has been thoroughly examined (58-63). Methanol is highly soluble in CO_2 and completely miscible with $scCO_2$ above 15.6 MPa in a temperature range from 0 - 120 °C and at 0 - 20 mol % (55). Depending on the fraction of methanol added to CO_2 and the applied pressure, the dielectric constant of the mixture can be increased distinctly.

In the case of xanthines, this was found to significantly enhance their solubility in $scCO_2$ (56). Theophylline (TP) is a methylxanthine drug used in the treatment of respiratory diseases, since it acts as a competitive nonselective phosphodiesterase inhibitor and raises intracellular cAMP (Figure 6). At 40 °C and 22 MPa, the solubility of TP in $scCO_2$ is very low with 9.77×10^{-6} mol fraction (64). It has thus been mainly processed with supercritical antisolvent techniques (65-69). With the addition of methanol to the supercritical phase, it is however possible to increase the solubility of TP by an order of magnitude (56).

The solubility enhancement in $scCO_2$ is a prerequisite for TP to be successfully micronized with RESS. It is however vital to consider what happens to the cosolvent when the ternary mixture of $scCO_2$, cosolvent and API is sprayed into the expansion chamber. Upon depressurization, it is possible that the supercritical mixture is separated into a liquid methanol phase and a gaseous CO_2 + methanol phase. In that case, the cosolvent that is precipitated in liquid state can cause dissolution and recrystallization of the micronized product during the residence time in the expansion chamber (70). The product might also be contaminated with remnant solvent and need further purification steps. Due to these issues, liquid cosolvents have been rarely applied in the RESS process and the literature on that matter is sparse (43, 51, 54, 71, 72). Up to date, there is no systematic investigation about the effect that a phase separation of the organic solvent has on the product and how that could be avoided.

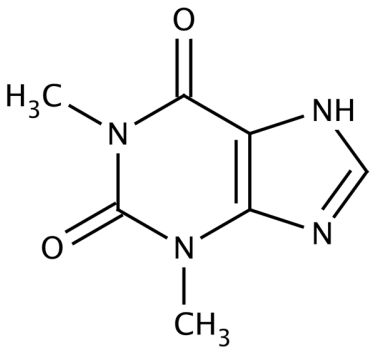

Figure 6 Chemical structure of theophylline

The p-T region, where such a phase separation can be expected to occur, can be derived from the isothermal phase equilibria of binary mixtures of methanol and CO_2 (Figure 7a). In that representation, the area inside the envelopes is two-phase, gas and liquid, while the outside of the envelopes consists of a single phase. The implications of this shall be explained with the following example: The process conditions **P** in Figure 7 mark a cosolvent mass percentage of 4 wt. % and a post expansion pressure of 1.0 MPa. If the temperature during RESS expansion is at 25 °C, the liquid-vapor line will be crossed resulting in a phase separation. If the temperature during the expansion was

to be kept at 50 °C, then these process conditions would fall outside the envelope, meaning that a homogeneous gaseous phase would be maintained. It is hypothesized that by careful control of the expansion temperature and pressure, a liquid phase separation of methanol during liquid cosolvent-assisted RESS can be suppressed, so that a micronized product with a homogeneous particle size distribution can be obtained. To test this hypothesis, the solubility of TP with different amounts of cosolvent was measured. With a suitable cosolvent addition, RESS products of theophylline were produced at 3 different temperature intervals and the particle morphology, specific surface area and size distribution for each product was analyzed. In addition, a solid state analysis via FTIR and PXRD was included to assess the influence of RESS precipitation and the presence of methanol on the polymorphism of the drug.

a)

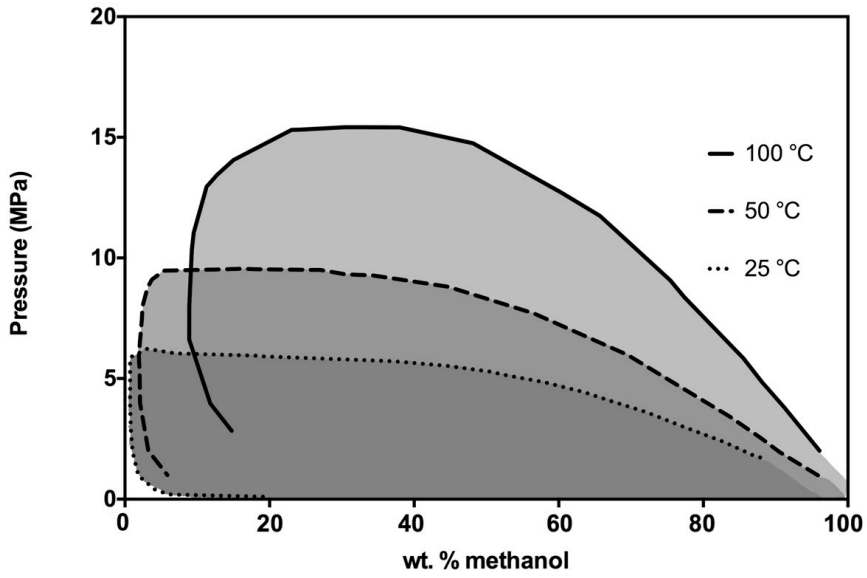

b)

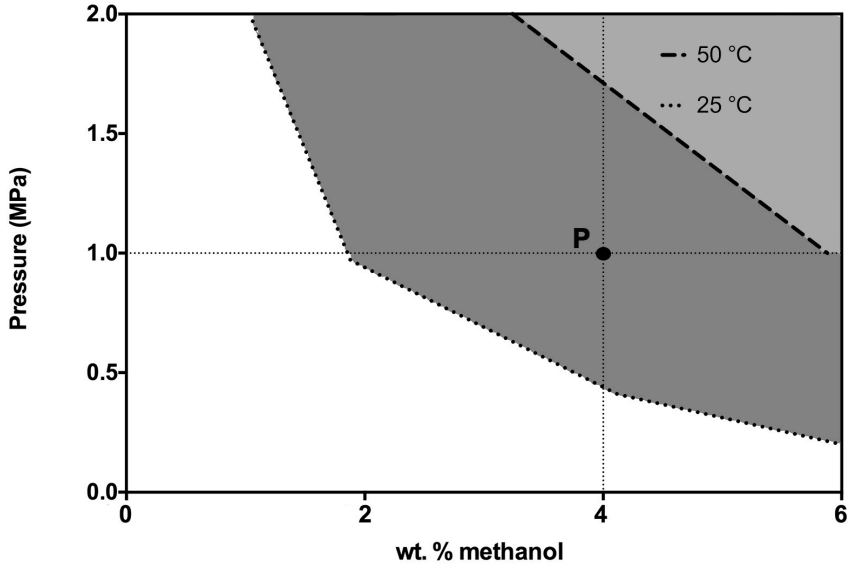

Figure 7 a) Binary isothermal phase equilibria of CO_2 + methanol at 25, 50 and 100 °C. The area inside the envelopes is two-phase. Data from (58); b) exemplary process conditions P (1 MPa, 4 wt. % methanol)

Materials and Methods

Materials

Theophylline was obtained from Böhringer Ingelheim, Biberach, Germany. Methanol was purchased from Avantor, Deventor, The Netherlands, and carbon dioxide was purchased from Air liquide, Düsseldorf, Germany.

Methods

Pilot unit for high-pressure micronization

The pilot unit that was used for high-pressure micronization is shown in Figure 8 (Sietec-Sieber, Maur, Switzerland). Carbon dioxide (CO_2) was used as solvent in all experiments. The machine comprises a tank, where CO_2 is cooled down to liquid state (Figure 9). Liquid CO_2 is then conveyed via a high-pressure pump into the extraction chamber, heated and pressurized to supercritical conditions.

Figure 8 Pilot unit used for high pressure micronization

The CO_2 flow can be adjusted in a range of 0 to 30 kg/h and the mantle temperature of the extraction chamber can be heated up to 70 °C. After the equilibrium time, the supercritical solution is expanded into the expansion chamber through a capillary nozzle with a diameter of 150 µm. The flux through the nozzle needs to be controlled manually with a micro-metering valve. The process parameters (temperature and

pressure of the extraction and expansion chamber, mass flow, CO_2 density in the extraction chamber) are monitored with the software VisiDAQ Runtime version 3.11. To increase the particle yield and the process efficiency, several modifications of the original expansion path that was designed by Sietec-Sieber were tested. Further details can be found in the Appendix.

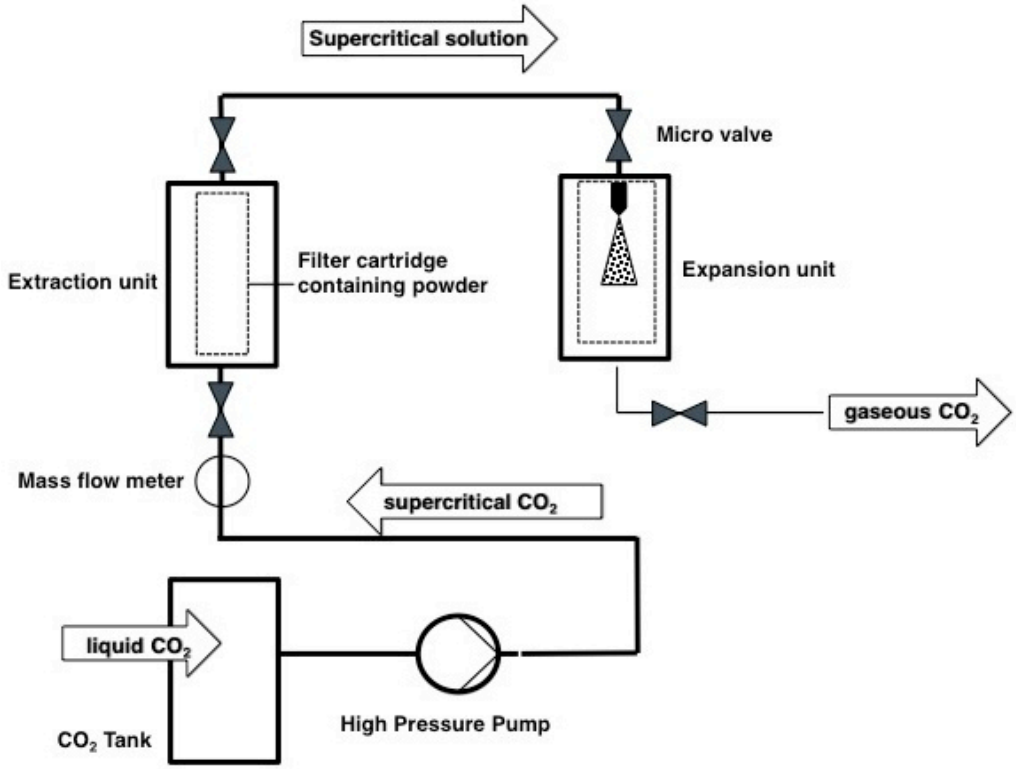

Figure 9 Schematic of the pilot unit for high-pressure micronization

Micronization of theophylline with the RESS process

1.0 g of anhydrous theophylline was placed into the extraction chamber, which was then flooded with CO_2, heated to 50.0 °C and pressurized to 30 MPa. If cosolvent was used (2 or 4 wt. % in $scCO_2$), it was placed into the extraction chamber together with the solid material. The cosolvent mass was calculated as

$$m_{MetOH} = w_{MetOH} \cdot \rho\, CO_2(p_E; T_E) \cdot V_{Ext} \qquad \textit{Eq. 13}$$

Where w_{MetOH} is the mass fraction of methanol, $\rho\, CO_2(p_E; T_E)$ is the CO_2 density at the respective extraction conditions (9) and V_{Ext} is the volume of the extraction chamber. The solution was left to equilibrate for 3 h or 18.5 h. After the equilibration time, the solution was expanded into the expansion chamber at a post expansion pressure of 1.0 MPa and 3 different temperature intervals (Table 2). The expansion chamber was equipped with a filter cartridge for particle collection as shown in Figure 10.

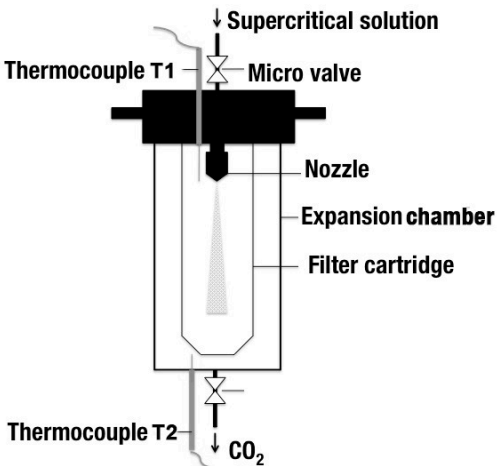

Figure 10 Device for particle collection used in the expansion chamber

The heating mantle of the expansion chamber was set to 70.0 °C. This alone was however not sufficient to compensate the expansion cooling so that the actual temperature control was achieved via adjusting the mass flow of CO_2 through the

micro-metering valve (Table 2). This naturally reduced the throughput of the process, which is why longer expansion times were chosen for RESS experiments conducted at the higher temperature intervals (Table 2). To monitor the temperature, 2 thermocouples T1 and T2 were used (Figure 10). T1 was placed in close proximity to the fluid exit at the nozzle and T2 at the bottom of the expansion chamber. It was assumed that the maximum temperature drop occurred in close proximity to the nozzle exit, so that the positioning of T1 allowed the detection of the lowest temperature inside the expansion chamber. The temperature fluctuations measured with T1 were quite drastic, because partial or total blockage of the nozzle could cause a difference of more than 10 °C in a couple of seconds. Without a nozzle heating or an automated control, this could not be prevented effectively. But, more importantly, the temperature at the bottom of the expansion chamber was more stable and generally at least 15 °C higher than at T1. The temperature at T2 was considered crucial, because liquid methanol collected in the lower part of the chamber would certainly cause recrystallization of the product during the residence time.

Table 2 Process conditions for the production of RESS theophylline at temperature intervals 1-3. Mean values represent average values ± standard deviation of 3 individual RESS experiments

Sample	Temperature in the expansion chamber (°C)		Mass flow CO_2 (kg/h)	Time of expansion (min)
	T1	T2		
RESS TP 1	> 0	< 15	11.2 ± 0.39	120
RESS TP 2	> 15	< 30	1.49 ± 0.12	300
RESS TP 3	> 30	> 50	0.51 ± 0.22	300

Calculation of the RESS process yield

The process yield *PY* of RESS experiments was calculated as wt. % in relation to the dissolved material m_D :

$$PY = \frac{m_E}{m_D} \cdot 100 \qquad \textit{Eq. 14}$$

Where m_E is the mass of the RESS product recovered from the expansion chamber.

Solubility measurements in supercritical carbon dioxide and calculation of solubility

The solubility *s* of the employed materials in $scCO_2$ was measured with a static gravimetric approach (9). An accurately weighed amount of the respective material was placed inside the extraction chamber, which was subsequently flooded with CO_2, heated and pressurized to the desired experimental conditions. After the equilibration time, the extraction chamber was depressurized and the remaining solid was removed and weighed again. The solubility s_{CO2} was calculated as g/kg of dissolved API in $scCO_2$ (m_D) at the respective extraction conditions or as molar fraction *y* of the API in $scCO_2$:

$$s_{CO2} = \frac{m_D\,(API)}{m\,(CO_2\,p_E;T_E)} \qquad \textit{Eq. 15}$$

$$y = \frac{mol\,(API)}{mol\,(CO_2 p_E;T_E)} \qquad \textit{Eq. 16}$$

The mass of CO_2 was calculated as

$$m\,CO_2 = \rho\,CO_{2\,p;T} \cdot V_{Ext} \qquad \textit{Eq. 17}$$

Where $\rho\,CO_{2\,p;T}$ is the density of $scCO_2$ at the respective extraction conditions. The pressure (p) and temperature (T) were recorded over the extraction time (VisiDAQ Runtime software version 3.11) and the respective density data was taken from the literature (9). The volume of the extraction chamber V_{Ext} was 5.033 l.

Particle size measurement via Laser Diffractometry in dry dispersion

A Mastersizer 2000 (Malvern, Herrenberg, Germany) equipped with a dry dispersion unit (Scirocco 2000) was used. For The disperser pressure was set to 0.35 MPa. The particle size distribution (PSD) was characterized by the median particle size (D_v50) and the particle size distribution width (span) was calculated based on the 10 %, 50 % and 90 % quantile:

$$Span = \frac{D_v90 - D_v10}{D_v50} \qquad Eq.\ 18$$

Particle size measurement via Dynamic Light Scattering (DLS)

The particle size and particle size distribution (PSD) of RESS theophylline produced at the third temperature interval was measured using a Zetasizer Nano ZS (Malvern, Herrenberg, Germany). An amount of 10 mg of RESS TP particles was suspended in 1 ml of demineralized water that was previously saturated with theophylline. All samples were diluted 1:4 and equilibrated during 120 s at a cell temperature of 20 °C. Each sample was measured 3 times and the average values of 3 individual RESS batches are reported.

Measurement of the specific surface area with the Brunauer-Emmet-Teller (BET) method

The specific surface area was measured with nitrogen gas adsorption at -196 °C. The material was accurately weighed and analyzed with a SA 3100 Beckman Coulter system (Beckman Coulter, Krefeld, Germany). The outgas temperature was set to 100 °C at an outgas time of 120 min. The average results reported are those of 2 individual RESS batches.

Scanning Electron Microscopy (SEM)

The surface morphology and particle shape were examined using a scanning electron microscope (DSM 940 A, Zeiss, Oberkochen, Germany). Pictures were taken using the Orion 5 frame grabber system (E.L.I. Microscopy, Charleroi, Belgium). The RESS

material was directly precipitated onto microscopic slides, which were then coated with gold with a sputter coater (E5100, BioRad, München, Germany). All samples were sputtered 4 times over 60 s at 2.1 kV and 20 mA.

Differential Scanning Calorimetry (DSC)

Measurements were performed using a DSC system (TA 8000, DSC 820, Mettler Toledo, Germany). The samples (4.5 – 5.5 mg per run) were placed in perforated 40 µl aluminium standard pans and crimped with punched lids. An empty aluminum sample pan was used as reference. A temperature range from 25 °C to 300 °C was scanned at a heating rate of 10 K to determine the melting points (onset temperature, T_{on}) and the specific heat of fusion (ΔH_f). The heat of fusion was obtained by integration of the melting peak areas (software STAR^e SW 8.10). The average results reported are those of 3 individual RESS batches.

Powder X-Ray Diffraction (PXRD)

The X-ray powder diffractograms were recorded at room temperature (Philips PW 1730 diffractometer, NL) using a Cu Kα radiation source with an automatic data acquisition (APD Philips v.35B). The equipment was set to a range of 2θ from 7 to 35 $^\circ$ in the continuous mode, with a step size of 0.015° (2θ) and an acquisition time of 1 s/step. Samples were mounted on an aluminum sample holder and the current and voltage of the tube set to 30 mA and 40 kV, respectively.

Fourier Transform Infrared Spectroscopy (FTIR)

Measurements were performed using a Nicolet 380 FT-IR spectrometer in absorbance mode (Thermo scientific, Karlsruhe, Germany). A total of 30 scans was performed over a range of 4000-400 cm^{-1} at a scan speed of 0.5 cm/s. The second derivative of the FTIR spectra was calculated using the OMNIC software (Thermo scientific, Karlsruhe, Germany).

Results & Discussion

Solubility of theophylline in supercritical carbon dioxide

The solubility of theophylline (TP) was measured in dependency of the amount of methanol and the extraction time (Table 3). Without methanol, the solubility of TP was 0.011 ± 0.0002 g/kg CO_2 at 30 MPa and 50 °C after 3 h of extraction time. Literature data of TP solubility in $scCO_2$ without methanol as cosolvent at a temperature of 40 °C and 22 MPa is reported as 0.04 g/kg (56)[3]. With 4 wt. % methanol, the solubility of TP could be increased by almost one order of magnitude (0.096 g/kg CO_2; Table 3) after an extraction time of 3 h, which is in good agreement with the literature (56). By increasing the extraction time to 18 h, the solubility of TP could be more than doubled (Table 3). With these measures, the dissolved amount of TP could be increased by a factor of almost 25 in comparison to the shorter extraction time and the absence of cosolvent. At these conditions, it was possible to produce a RESS TP with sufficient yield for further characterization.

[3] The discrepancy between the results here and those in the literature are probably due to the different methods of measurement. The static gravimetric approach that was used here is the method that is most susceptible to errors, because the solute is in contact with the SCF for a long time until equilibrium is reached. During long holding times, slight changes in pressure and temperature will change the dissolved mass. Gravimetric sampling is furthermore only recommended for solutes that exhibit solubility greater than 10^{-3} mol fraction, which is not the case for TP (the TP solubility is in the range of 10^{-6} mol fraction). With the equipment at hand, no other method of measurement could be conducted, so that the presented results here cannot be entirely comparable with more accurate results given in the literature. Nevertheless, a good agreement with literature results was obtained when looking at the proportionality of the solubility increase with and without methanol, although the solubility results obtained here are in general lower than the values found in the literature.

Table 3 Solubility s_{CO2} (g/kg CO_2) in dependency of the amount of cosolvent and the extraction time

Extraction time (h)	Amount of cosolvent (wt. %)			
	0	0.5	2	4
3	0.011 ± 0.0002	0.015 ± 0.003	0.049 ± 0.023	0.094 ± 0.003
18	n.a.	n.a.	0.114 ± 0.005	0.267 ± 0.017

n.a. not analyzed

Process yield of RESS experiments with and without cosolvent

Without methanol as cosolvent, the product yield of RESS TP was so low that a gravimetric determination was not possible. With an addition of 4 wt. % of methanol, the yield could be distinctly increased up to 25 %. At the first temperature interval (RESS TP 1; T2 < 0 °C), the obtained RESS product consisted of a liquid methanol phase, which entirely dissolved the precipitated particles. At the following intervals (RESS TP 2; T2 < 30 °C and RESS TP 3; T2 > 50 °C), macroscopically dry powder products were obtained.

Particle size and morphology of RESS theophylline

SEM images of unprocessed TP showed anisometric large particles (Figure 11a). In comparison, the particle size of RESS TP was distinctly reduced. In the case of RESS TP 2, the powders showed clear signs of recrystallization as a probable consequence of a liquid-gas phase separation during the expansion process and consequent partial dissolution of the precipitated material due to liquid methanol. Long adhering needle-shaped particles could be observed among a much finer fraction of particles (Figure 11b). In contrast, RESS TP 3 consisted of homogeneous fine particles while no large micron-sized bundles as in RESS TP 2 were found (Figure 11c). At a higher magnification, it could be observed that the particle shape was rather anisometric, with long and thin, strongly agglomerated fibers (Figure 11d).

Measurement of the particle size via laser diffractometry revealed that unprocessed TP had a D_v90 of 208.7 ± 3.3 µm and a comparatively large span of 3.35 ± 0.01 (Table 4). The particle size reduction of RESS TP produced at the second temperature interval was about one order of magnitude compared to the unprocessed material, but the span was still rather large (24.7 ± 8.1 µm and 3.3 ± 0.6; Table 4). These results reflect the heterogeneous particle collective that was already observed in SEM images. The particle size of RESS TP 3 was distinctly smaller than both unprocessed TP and RESS TP 2 and was therefore measured by dynamic light scattering (Figure 12c). The particle size reduction of RESS TP 3 was about 2 orders of magnitude compared to the unprocessed material, while the span was also distinctly reduced (1.1 ± 0.3; Table 4). Because of the high aspect ratio of the particles, the results of the particle size measurement under-estimate the real particle size as shown by SEM images. Therefore, measurement of the BET surface area appears to be a better method to evaluate the effect of RESS micronization. Unprocessed TP had an average specific surface area of only 0.412 m^2g^{-1}, whereas for RESS TP 2, it was increased to 3.43 m^2g^{-1} and to 5.78 m^2g^{-1} for RESS TP 3, which corresponds to a 14-fold increase.

Table 4 Summary of particle characteristics and thermal properties of unprocessed and RESS theophylline

Product	Particle size (µm)			Span	A (m^2/g)	T_{on} (°C)	ΔH_f (J/g)
	D10	D50	D90				
Unprocessed TP	10.6 ± 0.2	59.2 ± 0.9	208.7 ± 3.3	3.4 ± 0.01	0.41 ± 0.02	271.4 ± 0.03	158.0 ± 0.03
RESS TP 2	1.9 ± 0.5	6.9 ± 1.7	24.7 ± 8.1	3.3 ± 0.6	3.43 ± 0.50	270.5 ± 1.0	152.8 ± 8.0
RESS TP 3	0.085 ± 0.0004	0.143 ± 0.02	0.248 ± 0.07	1.1 ± 0.3	5.78 ± 0.07	270.0 ± 1.0	151.0 ± 0.1

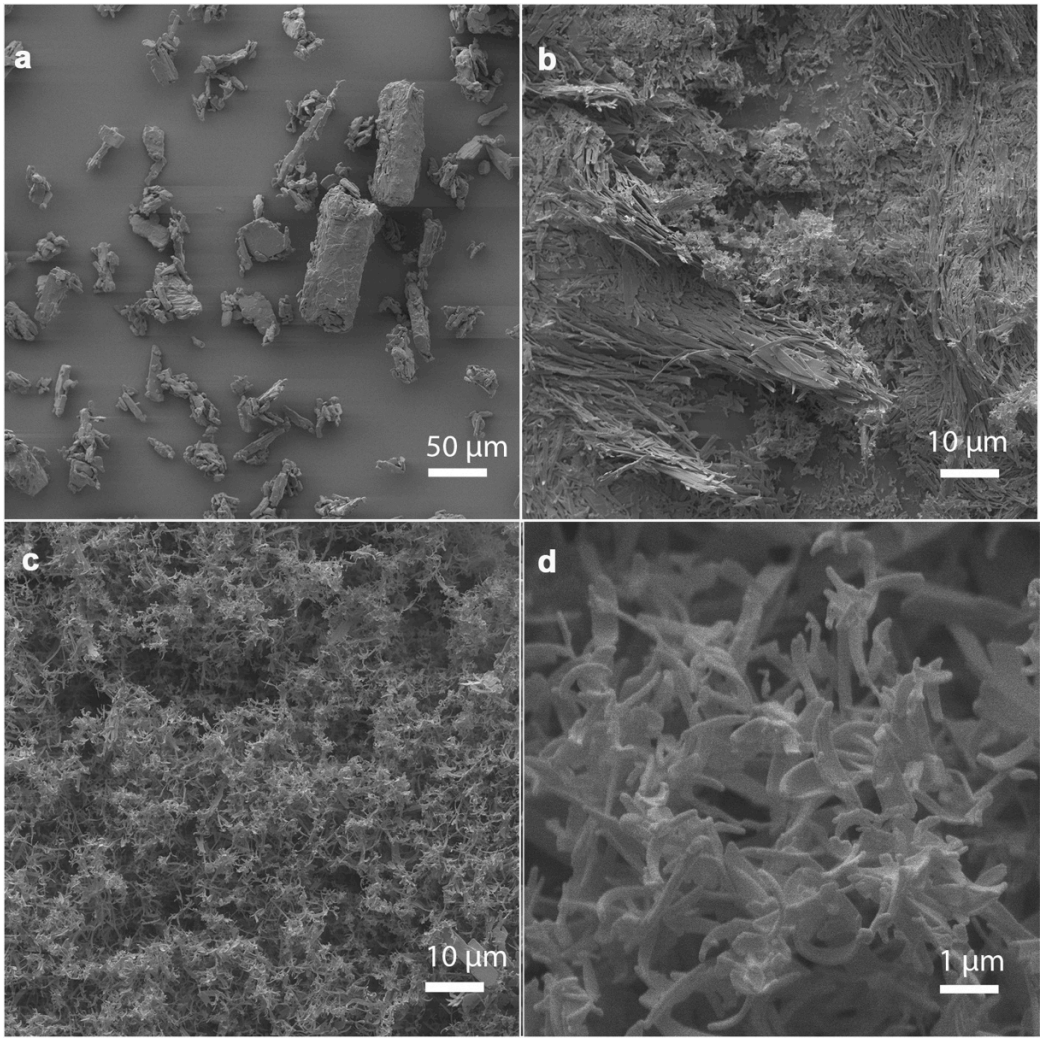

Figure 11 SEM images of a) unprocessed theophylline; b) RESS TP 2; c) & d) RESS TP3

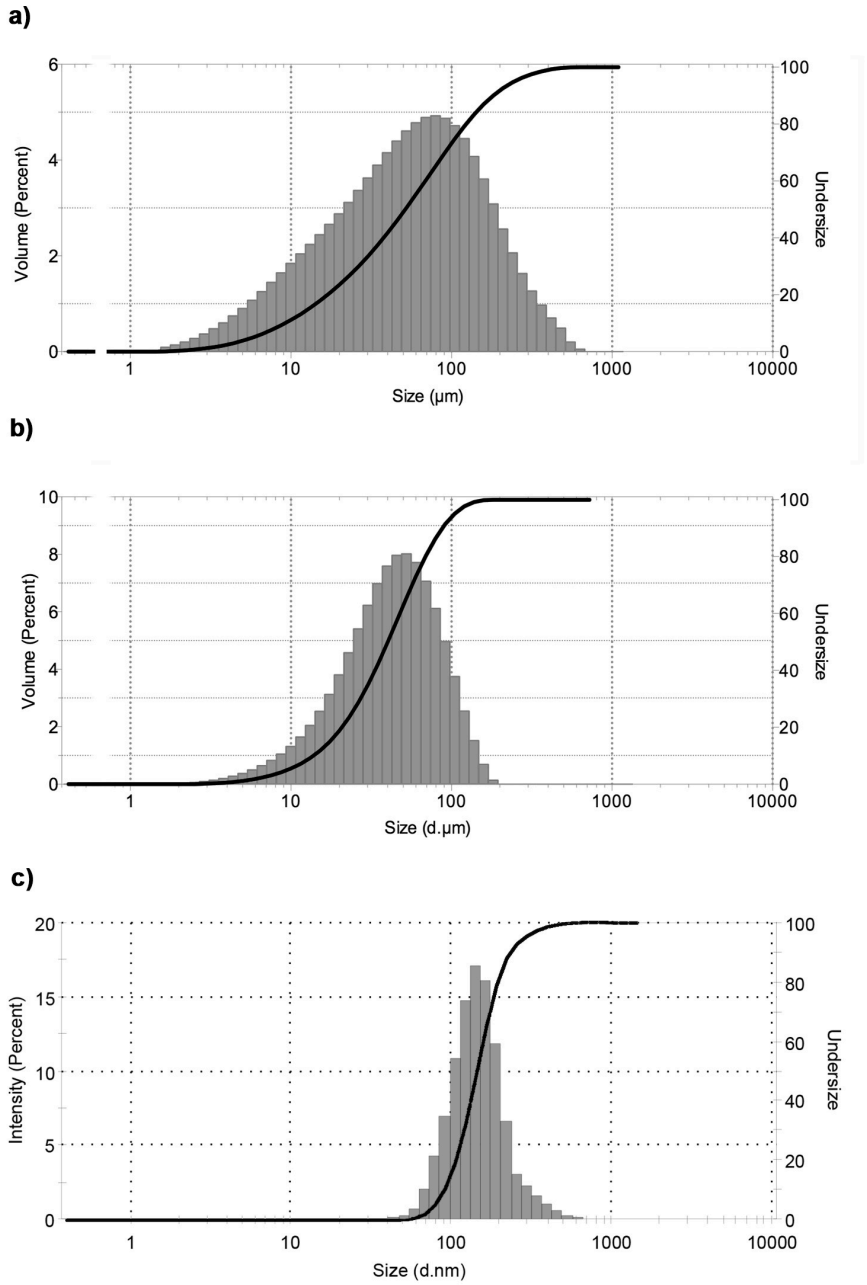

Figure 12 Particle size distribution of a) unprocessed theophylline (µm); b) RESS theophylline produced at temperature interval 2 (µm); c) RESS theophylline produced at temperature interval 3 (nm).

Solid state analysis of RESS theophylline

The melting temperature of unprocessed TP was 271.4 ± 0.03 °C. A slight depression of the melting temperature of RESS TP 2 and 3 was observed, but it was not significant (270.50 ± 0.98 °C and 270.0 ± 0.98 °C, respectively). In contrast, the heat of fusion of RESS TP 2 and RESS TP 3 was distinctly reduced in comparison to the unprocessed material (152.83 ± 7.95 J/g and 151.03 ± 0.12 J/g vs. 157.96 ± 0.03 J/g,. For RESS TP 2, the standard deviation was very high though, meaning that the batch-to-batch variability was much higher than in RESS TP 3. The reduction of the heat of fusion could be caused by a reduced crystallinity or by the reduced particle size in comparison to the bulk material. For a better understanding, PXRD measurements were performed for the bulk material and RESS TP 2. The PY of RESS TP 3 was not sufficient for PXRD analysis due to the fact that the mass flow through the nozzle needed to be reduced distinctly in order to remain inside the defined temperature range, which also lowered the throughput of the process (see Table 2). Diffractograms of RESS TP 2 had identical peaks in comparison to the unprocessed material, but with a strongly decreased intensity (Figure 13).

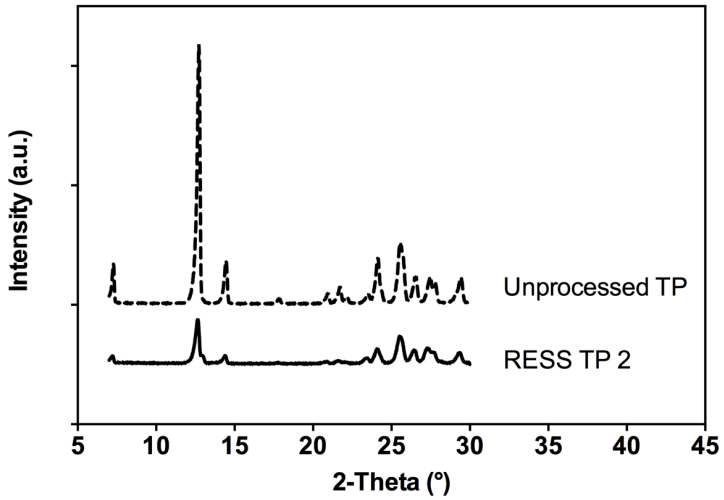

Figure 13 Powder X-Ray Diffractograms of unprocessed TP and RESS TP 2

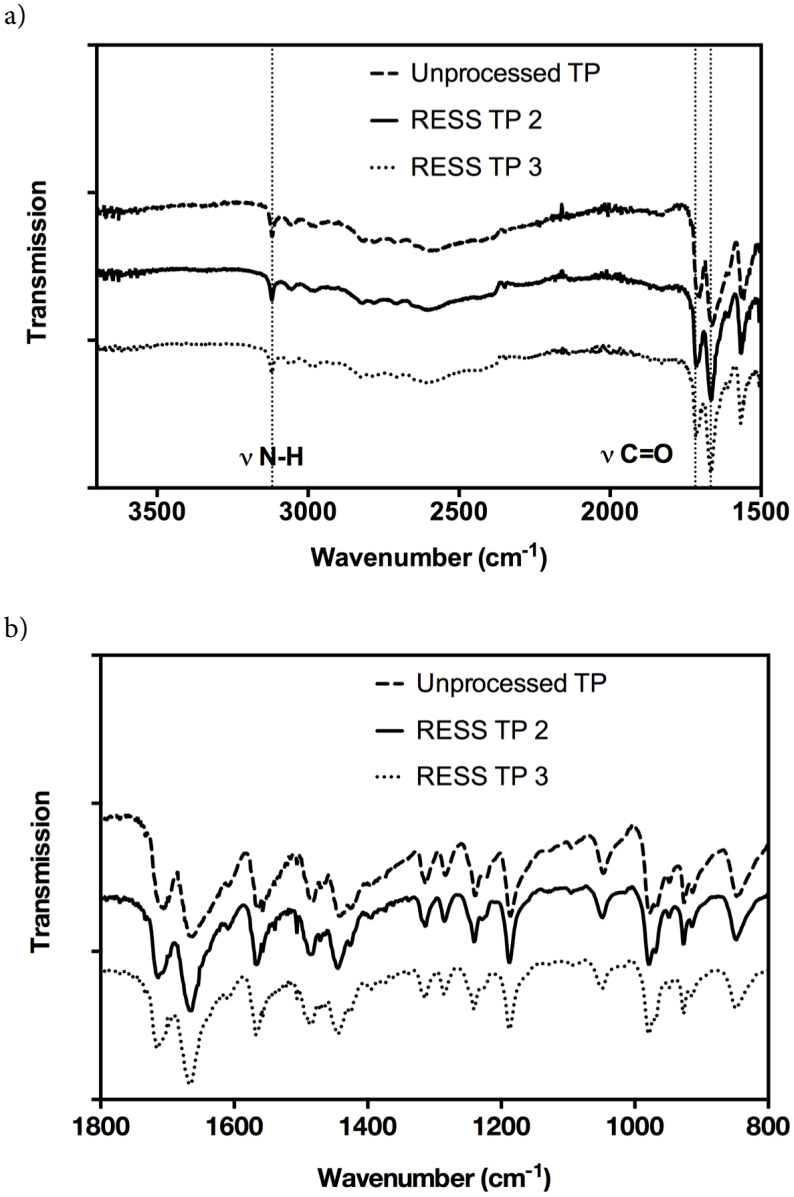

Figure 14 FTIR spectra of unprocessed theophylline and RESS theophylline; a) main stretching vibrations of functional groups (band assignments based on (73)); b) fingerprint region

No direct trace of amorphous material could be found. Many researchers report a reduction in the PXRD peak intensities of RESS precipitated material in comparison to the unprocessed bulk powder, but that could again be related to the decreased particle size of RESS products and is therefore inconclusive for judging a possible reduction of crystallinity (36, 39, 42, 45, 70, 74, 75). The question of whether the material contained an amorphous portion could therefore not be answered conclusively with the presented data.

No difference between unprocessed TP and RESS TP could be observed in FTIR spectra, neither in the vibrations of the functional groups (N-H stretching vibration at 3119 cm^{-1}, C=O stretching vibration at 1718 cm^{-1} and 1667 cm^{-1} (73)) nor in the fingerprint region (Figure 14 a and b).In contrast to a previous study, no hydration of RESS TP could be observed (47). Hydrate formation is most probable to occur after the actual RESS experiment, in cases when the precipitated material is still at a low temperature due to Joule-Thompson cooling and removed from the expansion chamber too early, so that air moisture condensation leads to hydrate formation. More importantly, no solvate formation of RESS TP with remnant methanol could be observed. Judging by DSC, PXRD and FTIR results, it is most likely that RESS TP produced in this study was in the same solid state form as the unprocessed material, regardless of the temperature inside the expansion chamber.

Conclusions

Micronization of poorly soluble API's via RESS is the most important and so far also the most studied application of the technique, but many API's do not have sufficient solubility in $scCO_2$. As this is a prerequisite for a compound to be processed with RESS, in this chapter, the development of a liquid cosolvent-assisted RESS process was described to overcome the problem of poor solubility in $scCO_2$. With the addition of as little as 4 % wt. % methanol as organic cosolvent to the supercritical phase, the solubility of theophylline (TP) in $scCO_2$ and thus the process yield could be increased

from close to 0 % without cosolvent to 25 % with the addition of cosolvent. Micronization of TP with the described process was successful, since a 14-fold increase of the specific surface area could be achieved, while the particle size of RESS TP was distinctly reduced compared to the unprocessed material. It could be demonstrated that a careful control of the expansion conditions is vital to obtain a homogeneous particle size distribution when using a liquid cosolvent in the RESS process. If the liquid-vapor line of the binary mixture CO_2 + methanol was crossed during the expansion, methanol was precipitated in liquid state.

At a very low temperature (0 - 5 °C), the precipitated liquid organic phase dissolved the particles entirely. With increasing temperature, this could be avoided so that a dry powder product was obtained. At an intermediate temperature interval (15 - 30 °C), the formation of a liquid phase during the expansion process still had a distinct influence on particle morphology and the size distribution. Even though solvate formation was not observed, methanol in liquid state caused agglomeration, recrystallization and distinct particle growth of the product during its residence time in the expansion chamber. At a higher temperature (>30 °C), the formation of liquid methanol and thus agglomeration and recrystallization of the product could apparently be restricted, so that RESS TP produced at this temperature interval had a much smaller particle size, a higher specific surface area and a more homogeneous particle size distribution than RESS TP produced at the intermediate temperature interval.

The work presented in this chapter demonstrates that low solubility of many compounds in $scCO_2$ does not necessarily need to be a major restriction for RESS, since small adaptions of the process can render a much wider range of materials applicable for RESS processing.

CHAPTER 3 | FORMATION OF NANOSUSPENSIONS WITH RESS

Introduction

Drug nanocrystals and nanosuspensions are widely considered as an easy approach to overcome low solubility and bioavailability of poorly soluble drugs (76-80). Nanosuspensions are dispersions of drug particles with a size less than 1000 nm in an aqueous medium (78). Due to the large surface energy that promotes agglomeration, nucleation and/or particle growth, they are thermodynamically unstable. In the absence of appropriate stabilizers, flocculation and Ostwald ripening may thus impair their dissolution rate and in vivo performance. Stabilizers for nanosuspensions can basically be classified as steric or electrostatic (81). Non-ionic polymers confer steric repulsion, while ionic surfactants confer electrostatic repulsion to the particles. A combination approach is often chosen, because the mechanisms have a synergistic stabilizing effect and because steric stabilization alone is inherently more sensitive to temperature fluctuations, which can be a problem when the nanosuspension is subjected to temperature cycling e.g. during drying (77).

The advantages of nanosuspensions for drug delivery are the large surface area leading to a much faster dissolution rate and the increased saturation solubility of these formulations[4] (77, 81). With nanosuspensions, it is possible to increase the drug loading, reproducibility of oral absorption and dose-bioavailability proportionality while decreasing toxicity and adverse effects (82). The formulation of nanosuspensions is especially suitable for compounds with a high log P, i.e. substances that are poorly

[4] According to the Ostwald-Freundlich equation, the solubility is only affected, if very small particle sizes are reached:

$$\frac{s(R)}{s_0} = exp\frac{2\gamma V_{atom}}{R\, k_B T}$$

Where $s(R)$ is the solubility of the material with a particle radius R, s_0 is the solubility of the bulk material, γ is the interfacial tension, V_{atom} is the atomic volume, k_B is the Boltzmann constant and T the temperature. With all other factors kept constant, the solubility $s(R)$ increases with decreasing particle size. For $s(R)$ to differ substantially from the bulk solubility (i.e. $\frac{s(R)}{s_0} >> 1$); the exponential term needs to attain values higher than 1, which is only the case for particles in the nanometer range.

soluble in water but soluble in oil (77). Olanzapine (OLZ) is a typical example of a BCS class II drug with poor solubility in water and high lipophilicity (Figure 15).

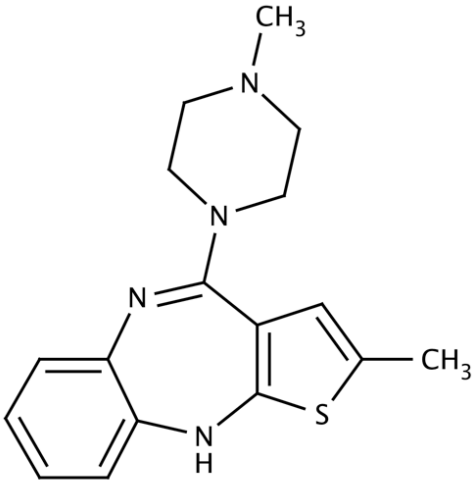

Figure 15 Chemical structure of olanzapine

As an antipsychotic drug, it binds to central dopamine D_2 and serotonin $5HT_{2c}$ receptors (83-85). In addition to its low aqueous solubility, OLZ shows pH dependent solubility because it is a weak base (pK_a = 7.4; Table 5). To date, there are no reports in the literature about the formulation of nanosuspensions with OLZ. Only one study reports the formation of composite OLZ PLGA nanoparticles as a possible dosage form for parenteral administration of the drug (86). The reason for this is most probably the diversity of the compound's solid state forms. It has been reported that OLZ crystallizes in at least 25 different solid forms including polymorphs, hydrates and solvates[5] (83, 87).

The formulation of OLZ as an aqueous nanosuspension is particularly challenging, because the most stable anhydrous OLZ form I converts within hours to the less soluble Dihydrate B in aqueous suspension (87).

[5] In the present work, the nomenclature of OLZ forms is according to the one of Reutzel-Edens et al. (105).

The choice of stabilizer is therefore crucial to suppress recrystallization of the precipitated material to prevent particle growth and polymorphic conversion.

Table 5 Summary of olanzapine properties

Molecular Mass (g/mol)	312.44
Melting point (°C)	195
pKs	(I) 7.4; (II) 14.17
Solubility in water; mg/ml	0.03
Solubility in $scCO_2$	no literature available
Log P	2

Nevertheless, there are a number of reasons why nanosuspensions can be a reasonable strategy for the formulation of OLZ dosage forms. First of all, nanosuspensions reduce food effects on the bioavailability of the drug when administered orally (77). In addition, the increased solubility of drugs formulated as nanosuspensions can reduce the administered dose. Even though OLZ is regarded as well tolerable, the high variability of oral bioavailability can lead to either sub-therapeutic plasma levels or increased adverse affects (81, 88). Parenteral administration of OLZ is indicated in acute agitation of patients with schizophrenia or bipolar mania. The marketed formulation is a fast-acting intra-muscular injection of a solution with a low pH to achieve sufficient solubility of the OLZ base (88, 89). In comparison, nanosuspensions of OLZ could be administered as intravenous fast-acting injection[6] without the need of solubilizing agents or a non-physiological pH,

[6] It is important that for intravenous administration the particles are smaller than 5 µm to avoid capillary blockage.

which often causes irritation and pain, especially with intra-muscular or subcutaneous injections.

Nanosuspensions can be either prepared by nanoprecipitation methods (bottom-up process) or by comminution of larger particles (top-down process). Top-down processes include high-pressure homogenization or media milling. But the high shear forces used in these techniques can generate crystal defects and amorphous domains, which are then subjected to recrystallization throughout storage (82). Other problems are often a high polydispersity of the product, so that subsequent removal of microparticles is required, or the abrasion of milling equipment (76). Nanoprecipitation generally involves the use of organic solvents. This may have adverse effects on the final preparation because of the formation of unstable polymorphs, hydrates or solvates of the drug. In addition, complete removal of the solvents remains a challenge, so that physical and/or chemical instability and increased toxicity are possible consequences (82).

Another critical issue in conventional precipitation techniques is that the speed of precipitation needs to be maximized while the freshly created surface needs to be covered by surfactants quickly, so that growing of the crystals can be limited (80). In contrast, the high supersaturation that can be attained in RESS causes extraordinarily fast nucleation rates (see page 7). A comparable speed of precipitation cannot be attained in conventional nanoprecipitation methods. Considering that nanosuspensions are often regarded as the last resort when it comes to formulating insoluble drugs and that the conventional production techniques are to a certain extent unfavorable, the RESS process can offer a beneficial alternative production method. So in the case of water insoluble drugs, a supercritical solution of the respective solute can be directly sprayed into an aqueous solution containing a stabilizing agent. This technique has also been named RESOLV (Rapid Expansion of Supercritical Solutions into Liquid Solvent) or RESSAS (Rapid Expansion from Supercritical to Aqueous Solution) and has been tested on a lab scale for the

production of nanosuspensions with different pharmaceutical compounds and stabilizing agents (Table 6). When expanding the SCF into a liquid at the receiving end instead of air, particle condensation and coagulation in the expansion jet can apparently be quenched, because the products are often nanosized in contrast to those produced with the classic RESS process (90). Particle sizes in the range of 0.1 - 1 µm (90); but also less than 100 nm are generally reported (42, 48).

A difficulty in expanding a large amount of gas into a restricted volume of stabilizing medium is however that the expansion cooling causes a drastic temperature drop, so that the aqueous medium can freeze within a short time period. The force of the expanding gas can catapult the medium out of the collecting cylinder and foaming of the medium may destabilize the process. The process conditions thus need to be monitored very carefully in order to avoid these issues. Most of the available studies are focused on the influence of the production parameters, i.e. pre-expansion conditions and stabilizing agents, on the generated particle size and particle size distribution (Table 6). But solid state characterization of the drug in suspension, development of a valid drying method, analysis of the release characteristics and especially the stability of the nanosuspension are important issues that are often not included in RESS research.

Table 6 Literature examples of RESSAS/RESOLV applications for pharmaceuticals

Substrates	SCF	Stabilizing agent	Particle size	Reference
Salicylic acid	$scCO_2$	Polysorbate 80	180 nm	Türk (2008) (40)
Naproxen	$scCO_2$	Polysorbate 80 PVP	8 µm 0.56-0.8 µm	Türk (2010) (41)
PLA, Retinyl palmitate	$scCO_2$	Poloxamer; SLS	40 - 110 nm	Sane (2009) (91)
Fenofibrate	$scCO_2$	Polysorbate 80, SLS, Poloxamer, HPMC	0.5 - 5 µm	Dalvi (2013) (44)
Ibuprofen	$scCO_2$	SLS, PVP, PVA, PEG, BSA	25 - 276 nm	Pathak (2006) (42)

The objective of this chapter is to evaluate if RESS nanosuspensions and their freeze-dried products are suitable as pharmaceutical dosage forms. To this end, a RESS process for producing nanosuspensions of OLZ was developed. Nanoparticles of OLZ were also produced with the classic RESS process to assess the influence of precipitation from supercritical solution on the stability and solid state of the drug. The nanosuspensions of OLZ were freeze-dried to improve handling and storage stability. The particle size was measured directly after production and after freeze-drying to evaluate the effectiveness of the respective stabilizer. A solid state analysis via FTIR was included to assess the influence of the stabilizers on the polymorphism of the drug. Finally, the release characteristics of OLZ from freeze-dried nanosuspensions and the conventionally micronized drug product were compared, while the influence of the stabilizers on the drug dissolution rate was also taken into account.

Materials and Methods

Materials

Micronized olanzapine was obtained from Pharmogana, Rosenheim, Germany and carbon dioxide was purchased from Air liquide, Düsseldorf, Germany. Hydroxypropylmethylcellulose (Pharmacoat 615) was obtained from Syntapharm, Mühlheim a.d. Ruhr, Germany; PEG 40000 from Serva, Amstetten, Austria; polysorbate (Tween 80) from Croda, Nettetal, Germany and sodiumlaurylsulfate (SLS; Texapon K12G) from Cognis, Düsseldorf, Germany.

Methods

Solubility of olanzapine in supercritical carbon dioxide

There are very few reports about supercritical fluid processing of OLZ in the literature. A US patent reports the production of OLZ form II with RESS, which is the only published solvent-based SCF technique to process OLZ (92). However, there is no solubility data included. The saturation solubility of Olanzapine (OLZ) in $scCO_2$ was measured at 50 °C and 20 MPa or 30 MPa. At 20 MPa, the solubility was $y = 8.67 \times 10^{6}$ mol fraction, which is comparatively low. At the chosen process conditions and with the used equipment, this equaled a dissolved mass of 241.5 ± 4 mg. At 30 MPa, the solubility could be increased up to $y = 2.15 \times 10^{-5}$ mol fraction. Pilot studies that were conducted to optimize the process conditions for the production of nanosuspensions revealed that a pressure of 20 MPa was more suitable than 30 MPa, which is why a pressure of 20 MPa was chosen for all of the following experiments despite the lower solubility of the drug[7].

[7]At 20 MPa, freezing and/or foaming of the receiving medium during the expansion process were easier to control; and at a lower concentration of the drug in $scCO_2$, smaller particle sizes could be achieved.

Production of olanzapine nanoparticles with the RESS process

The general description of the RESS equipment can be found in **Chapter 2**, page 24. 1.5 g of the solid drug were placed inside the extraction chamber, which was consequently flooded with CO_2, heated to 50 °C and pressurized to 30 MPa. After an equilibration time of 24 h, the solution was expanded during 60 min at a medium mass flow of 1.2 ± 0.4 kg/h CO_2 (average of 3 RESS experiments), using the equipment presented in Figure 10 for particle collection. The heating mantle of the expansion chamber was set to 70 °C. The actual temperature inside the expansion chamber was monitored using the thermocouple T1 close to the nozzle exit (Figure 10). With the temperature drop, an average of 19.3 ± 9.5 °C (average of 3 RESS experiments) was maintained. Prior to particle collection, the expansion chamber was allowed to reach room temperature in order to prevent potential condensation of air moisture on the products.

Production of olanzapine nanosuspensions with the RESS process

The general description of the RESS equipment can be found in **Chapter 2**, page 24. 5.0 g of OLZ were placed inside the extraction chamber, which was consequently heated to 50 °C and pressurized to 20 MPa. After 24 h of equilibration time, the solution was expanded into the expansion chamber during 60 min. The heating mantle of the expansion chamber was set to 55 °C. The temperature inside the expansion chamber was monitored via a thermocouple placed in the water bath surrounding the collection cylinder (Figure 16). The volume of stabilizer medium was 100 ml. The stabilizers were dissolved in phosphate buffer pH 7.4 in order to prevent a pH drift due to dissolved CO_2 and consequent dissolution of OLZ in the medium. In cases when sodium lauryl sulfate (SLS) was added as co-stabilizer, 3.3 ml of a stock solution of 10 wt. % SLS were added to 30 ml of the freshly produced nanosuspension.

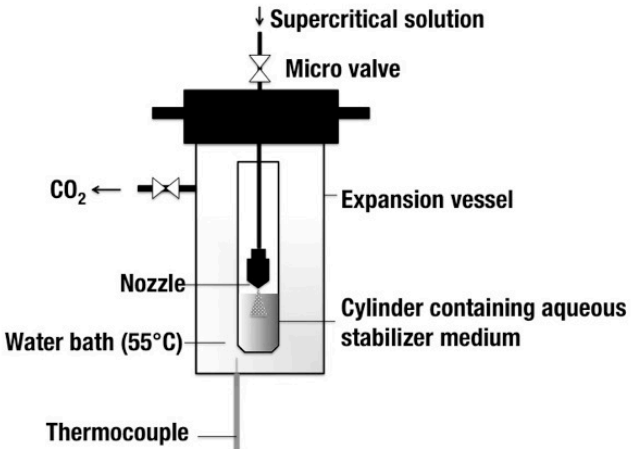

Figure 16 Device in the expansion chamber used for particle collection in the production of nanosuspensions

Determination of the olanzapine content in RESS nanosuspensions

1 ml of the freshly produced nanosuspensions was diluted 1:100 in 0.1N HCl to dissolve the drug. The solutions were analyzed spectrophotometrically at 260 nm for the OLZ concentration c_{NS}. It was ensured that at this dilution and the given wavelength, the stabilizing agents did not interfere with the OLZ absorption.

Calculation of the RESS process yield

For RESS nanoparticles, refer to the calculation presented in **Chapter 2** (page 28). For RESS nanosuspensions, m_E was calculated as the product of the OLZ concentration in nanosuspensions c_{NS} and the final volume of the nanosuspensions V_{NS}:

$$m_E = c_{NS} \cdot V_{NS} \qquad \textit{Eq. 19}$$

The propagated error Δu for PY and m_E was calculated as:

$$\Delta u = |u| \sqrt{\left(\frac{\Delta a}{a}\right)^2 + \left(\frac{\Delta b}{b}\right)^2} \qquad \textit{Eq. 20}$$

Lyophilization of RESS nanosuspensions

3 ml of the nanosuspensions were transferred to 10 ml glass vials and pre-frozen at -18 °C for 24 h prior to freeze-drying. The nanosuspensions were lyophilized at -20 °C for 12 h, followed by a secondary drying phase of 12 h at 20 °C using a Lyovac GT2 freeze-dryer (Finn-Aqua/GEA Pharma Systems, Hildesheim, Germany).

Measurement of the viscosity of stabilizer media used in the production of RESS nanosuspensions

The stabilizers were dissolved in demineralized water at the respective concentration and equilibrated at 37 °C for 30 min. The kinematic viscosity η was measured with a capillary viscometer according to Ubbelohde. The capillary constants were 0.00314 $mm^2 s^{-2}$ and 0.02978 $mm^2 s^{-2}$. Each sample was measured in triplicate.

Particle size measurement via Dynamic Light Scattering (DLS)

The particle size and particle size distribution (PSD) of OLZ nanosuspensions were measured using a Zetasizer Nano ZS (Malvern, Herrenberg, Germany). 1 ml of the freshly produced or reconstituted RESS nanosuspensions was used. All samples were diluted 1:4 and equilibrated during 120 s at a cell temperature of 20 °C. Each sample was measured 3 times and the average values of 3 individual RESS batches are reported.

Laser Diffractometry in aqueous dispersion

This method was used for unprocessed OLZ and for RESS suspensions, where particle growth to the micron range was observed after freeze-drying and reconstitution. A Mastersizer 2000 (Malvern, Herrenberg, Germany) equipped with a Hydro 2000S sample dispersion unit was used. An amount of 10 mg of the unprocessed powder was suspended in demineralized water containing 0.1 % Polysorbate 80 to ensure a good dispersion of the hydrophobic OLZ particles.

The freeze-dried cakes of the RESS suspensions were re-dispersed with 3 ml of demineralized water. Prior to the measurements, ultrasound was applied to desagglomerate the particles during 60 s. 3 measurements were performed per sample and the average values of 3 individual RESS batches are reported. The span was calculated according to Eq. 18.

Measurement of the zeta potential of RESS nanosuspensions

A Zetasizer Nano ZS (Malvern, Herrenberg, Germany) was used. The samples were diluted 1:4 and equilibrated during 120 s at a cell temperature of 20 °C. Each sample was measured 5 times and the average values of 3 individual RESS batches are reported.

Scanning Electron Microscopy (SEM)

The equipment and procedure was described in **Chapter 2** (page 29).

Differential Scanning Calorimetry

The equipment was previously described in **Chapter 2** (page 30). The temperature range was 25 °C - 220 °C at a heating rate of 10 K.

Fourier Transform Infrared Spectroscopy (FTIR)

Measurements were performed using a Nicolet 380 FT-IR spectrometer in absorbance mode (Thermo scientific, Karlsruhe, Germany). A total of 30 scans was performed over a range of 4000-400 cm^{-1} at a scan speed of 0.5 cm/s. The second derivative of the FTIR spectra was calculated using the OMNIC software (Thermo scientific, Karlsruhe, Germany). Flocculated RESS suspensions were filtrated and the solid remnant was dried at room temperature for FTIR analysis.

Determination of the saturation solubility in water

An excess of OLZ powder (approximately 10 mg) was placed into 2 ml Eppendorf cups and 1 ml of the respective stabilizing medium was added. The cups were sealed and placed into a water bath at 37 °C shaking with 60 spm. After 48 h, the Eppendorf cups

were centrifugated at 13,400 rpm for 20 min and diluted in 0.1 N HCl. The concentrations of OLZ were determined with a UV microplate reader at 260 nm (Synergy HT, Biotek, Bad Friedrichshall, Germany).

In vitro dissolution rate

Dissolution studies were conducted with a Pharmatest PT-DT 7 (Hainburg, Germany). A paddle apparatus (USP apparatus 2) at 37.0 °C was used. The freeze-dried cakes of OLZ nanosuspensions were reconstituted with 3 ml of the dissolution medium and immediately added to the dissolution vessels containing 500 ml of phosphate buffer pH 6.8. The rotation speed of the paddles was set to 50 rpm. Samples were drawn at preset time intervals and filtered through a 5 µm sintered filter. The removed sample volume was immediately replaced by fresh medium. The concentration of the samples was analyzed with a UV microplate reader at 260 nm (Synergy HT, Biotek, Bad Friedrichshall, Germany).

Results & Discussion

Production of RESS olanzapine nanoparticles

Because of the described solid state diversity of OLZ, the influence of RESS precipitation on the solid state characteristics of the drug was assessed. The product in these experiments was a very fine powder; and a large fraction of it was thus removed with the outgas. Judging by SEM images, the particles had a round shape and appeared partly merged with a mean diameter of roughly 200 nm (Figure 17). This could be confirmed with particle size measurements via DLS, which yielded a mean particle size of 190 nm and a narrow span of 1.08 (Table 7). In contrast, the unprocessed OLZ powder had a D50 of 39.3 µm, meaning that a 200-fold reduction of the particle size could be achieved with RESS.

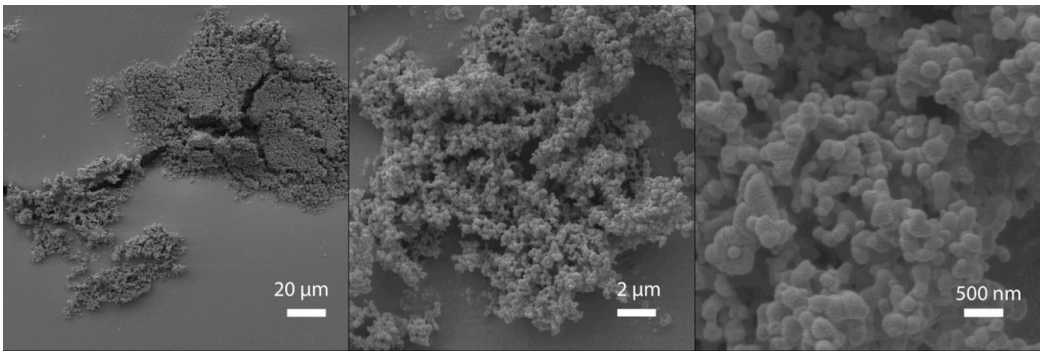

Figure 17 SEM images of RESS olanzapine nanoparticles

Table 7 Particle size and thermal properties of RESS olanzapine (nm) and conventionally micronized olanzapine (µm). Average of 3 individual RESS batches

Particle size	RESS OLZ (nm)[a]	OLZ (µm)[b]
D10	120 ± 2	13.0 ± 1.0
D50	191 ± 10	39.3 ± 1.0
D90	327 ± 40	86.3 ± 1.3
Span	1.08 ± 0.15	1.87 ± 0.04
Thermal Property	**RESS OLZ**	**OLZ**
T_{on} (°C)	190.7 ± 1.1	194.3 ± 0.9
Heat of fusion (J g^{-1})	120.0 ± 2.7	102.2 ± 6.3

a particle size measured via Dynamic Light Scattering
b particle size measured via Laser Diffraction

The melting temperature of RESS OLZ was distinctly reduced from 194.3 °C of the unprocessed material to 190.7 °C (Table 7). In addition, the heat of fusion was decreased from 120.0 J/g to 102.2 J/g, which might indicate a reduced crystallinity of the RESS product. To confirm this, the second derivative of the FTIR spectra of RESS OLZ were compared with crystalline anhydrous OLZ and amorphous OLZ in the range of 900 cm^{-1} to 1100 cm^{-1} (Figure 18). RESS OLZ spectra combined characteristic bands of both the crystalline anhydrous form I and the amorphous form. The band of amorphous OLZ at 998 cm^{-1} for example appeared in RESS OLZ spectra, as well as the sharp peak of the anhydrous form at 927 cm^{-1}. This confirmed that the material was indeed partially precipitated in the amorphous form. Due to the speed of precipitation in RESS, the formation of an amorphous phase appears to be likely and has indeed been shown before[8] (93).

Amorphous conversion is however not a particular issue for RESS, as it has been shown that the degree of crystallinity can vary widely depending on the specific method of production (79). OLZ was apparently not subjected to polymorphic conversion due to RESS processing, because according to FTIR and DSC analysis, the product was precipitated as OLZ form I (87). Polymorphic conversion during the RESS process has been shown before and is supposedly related to the processing conditions such as extraction and expansion pressure and temperature (45, 53, 74). In any case, the crystallization of form I is the preferred result, because it is the most

[8] According to Ostwald's rule of stages, one would expect the less stable form to crystallize first from a solution, because its Gibbs free energy is closest to that of the parent phase (75). This intermediate phase does not have to be a metastable polymorph, but can also be the amorphous form. The following recrystallization to the more stable phase is not necessarily solution-mediated, which would not be possible in the case of RESS, but can also occur via an internal rearrangement of the molecules (solid state transformation) (91). Because SEM, DSC and FTIR results suggested that the RESS OLZ nanoparticles were not entirely crystalline, it is possible that the material was precipitated in the amorphous state and then subjected to such a solid state transformation.

stable crystal form. Form II for example discolors in the presence of air, which makes it less suitable for commercial use (94).

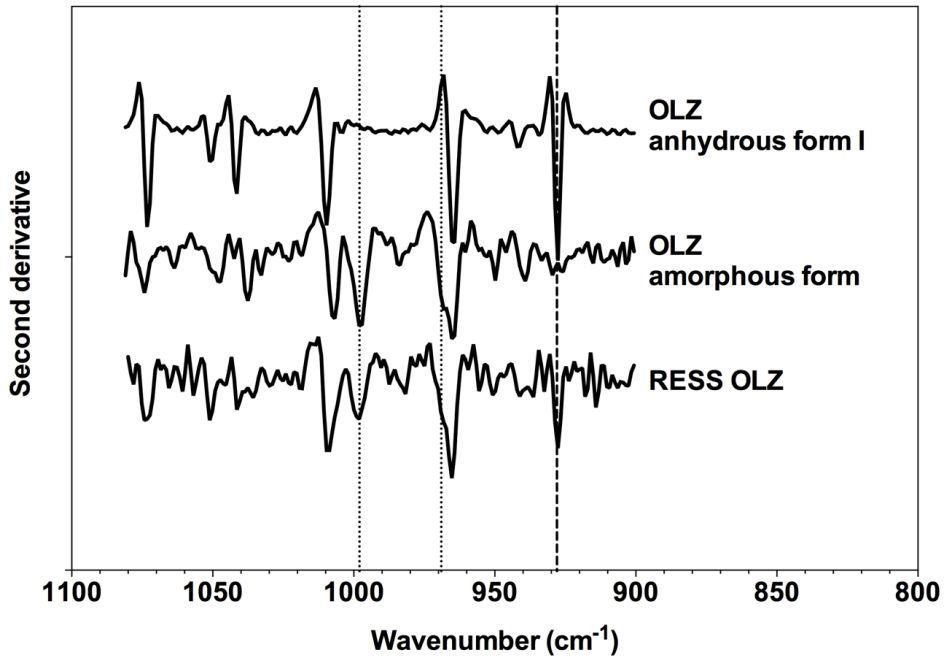

Figure 18 Second derivative of FTIR spectra of anhydrous, amorphous and RESS olanzapine. Dashed line indicates characteristic peak of the anhydrous crystalline form I; dotted lines indicate characteristic peaks of the amorphous form

Optimization of process conditions for RESS nanosuspensions

In RESS, a large amount of gaseous CO_2 is formed during the expansion, which is particularly critical when the solute has a low solubility, so that the ratio of gas to product becomes very large. The expanding gas can lead to distinct foam formation and discharge of the receiving liquid, when it streams out of the collecting cylinder. In addition, the drastic Joule-Thompson cooling can freeze the aqueous medium, especially when the volume is already reduced. Pilot studies were thus conducted to

optimize the mass flow through the nozzle, the post-expansion temperature and the volume of the stabilizing media. The optimized conditions are presented in Table 7. Furthermore, the stabilizers were found to have a critical effect not only on the stability of the formulation but also on the expansion process. It was therefore also necessary to screen for suitable stabilizers. The 2 most important identified stabilizer features were viscosity and foaming tendency. The higher the viscosity, the less medium was discharged from the collection chamber. A high viscosity could be easily achieved with a variety of polymers in increasing concentrations.

But many polymers also distinctly increased the foaming tendency, so that e.g. many cellulose ethers were not feasible. Surfactants providing electro-static stabilization caused extreme foaming and fast depletion of the receiving liquid, so that they were also excluded. Beside the viscosity and foaming, the third important factor was the solubility of the drug in the stabilizing medium, which is crucial regardless of the production method. An increased solubility can induce agglomeration and/or Ostwald ripening (82).

Table 8 Summary of process conditions for the production of OLZ nanosuspensions. (Average of 3 RESS experiments per stabilizer)

Stabilizer	Mass flow of CO_2 (kg/h)	Temperature in expansion	Volume of stabilizing medium
Polysorbate 80 0.1 %	1.55 ± 0.54	40.5 ± 2.3	100
PEG 2 %	3.01 ± 0.34	39.2 ± 2.2	100
HPMC 2 %	2.59 ± 0.77	41.9 ± 2.2	100

The stabilizer should thus have little or no effect on the solubility of the formulated drug. The stabilizers that were chosen based on these selection criteria are presented in Table 9. Polysorbate 80 is a low-molecular weight non-ionic surfactant that has been

used widely in the formulation of nanosuspensions and, apart from stabilizing the system, helps as a wetting and dispersing agent with very hydrophobic drugs (95). PEG and HPMC are polymers that confer steric repulsion (82). None of these stabilizers increased the saturation solubility of OLZ in comparison to phosphate buffer pH 7.4 (Table 9). In contrast to PEG, Polysorbate and HPMC caused foaming when CO_2 during the expansion.

Table 9 Viscosity (η) of stabilizing media and saturation solubility (s) of olanzapine

Stabilizer	wt. % stabilizer	s (mg/ml)	η (cSt)	Foaming tendency
Buffer pH 7.4	-	0.16 ± 0.06	0.81 ± 0.001	-
Polysorbate 80	0.1	0.11 ± 0.003	0.72 ± 0.001	+
PEG	2	0.16 ± 0.01	1.63 ± 0.001	-
HPMC	2	0.16 ± 0.01	7.27 ± 0.005	+

Production of RESS olanzapine nanosuspensions

Nanosuspensions could be successfully produced with the 3 stabilizers HPMC, PEG and Polysorbate 80. But because of the foaming caused by HPMC and Polysorbate 80, the volume of the receiving liquid was decreased by more than 50 % by the end of the expansion process (Table 10). With PEG on the contrary, almost no foaming was observed, and it was possible to quantitatively recover the drug that was initially dissolved in $scCO_2$, corresponding to a process yield of almost 100 % (Table 10). With an average concentration of about 3 mg/ml, the drug load was comparably low, given that with top-down techniques such as high-pressure homogenization or wet media milling, drug loads of at least one order of magnitude more can be achieved (96, 97).

But low drug loads are indeed a common problem for all bottom-up techniques, and not at all particular to the RESS process (82).

Table 10 Quantitative analysis of RESS olanzapine nanosuspensions

Stabilizer	Volume of final suspension (V_{NS}; ml)[a]	c OLZ in final suspension (c_{NS}; mg/ml)[a]	Recovered mass of OLZ (m_E; mg)[b]	Process yield (PY; %)[b]
Polysorbate 80	30 ± 11	3.3 ± 1.4	99 ± 55.5	41.0 ± 23.0
PEG	70 ± 5	3.4 ± 0.4	238 ± 32.8	98.6 ± 13.6
HPMC	45 ± 10	2.4 ± 1.3	108 ± 63.2	44.7 ± 26.2

a: average ± standard deviation of 3 individual experiments; b: average ± absolute propagated uncertainty

Stability of RESS olanzapine nanosuspensions

The smallest particle size after production was achieved with Polysorbate 80 as stabilizing agent. The D_i50 value was 158.7 ± 12.7 nm with a narrow PSD (span = 1.15 ± 0.12; Figure 19a). The largest particles were obtained with HPMC with a D_i50 of 341.3 ± 42 nm and a broader PSD with a span of 1.5 ± 0.4 (Figure 19a). The particle size of PEG stabilized nanosuspensions was between that of Polysorbate 80 and HPMC with a D_i50 of 213.8 ± 23.7 nm and a narrow span of 0.99 ± 0.08 (Figure 19a). After production, PEG and Polysorbate 80 nanosuspensions remained macroscopically stable for a couple of hours, until the transparent suspensions suddenly started to turn cloudy and agglomeration became visible quite rapidly. After freeze-drying and reconstitution of the PEG and Polysorbate 80 nanosuspensions, the particle sizes were measured again and indeed distinctly increased (D_v50 of 8.5 ± 0.9 µm for PEG and 15.1 ± 2.6 µm for Polysorbate 80; Figure 19b). For both stabilizers, the PSD was also distinctly increased after freeze-drying. The particle size of OLZ in HPMC nanosuspensions was initially slightly larger than with the other stabilizers, but no visible particle growth was observed macroscopically during 24 h.

When measured again after freeze-drying, only a slight particle growth was detected (365.8 ± 72.3 nm after freeze-drying vs. 341.3 ± 42 nm before freeze-drying; Figure 19b). This could be attributed to the higher viscosity of HPMC suspensions compared to PEG and Polysorbate 80, which reduced the diffusivity of the drug molecules in suspension (Table 9).

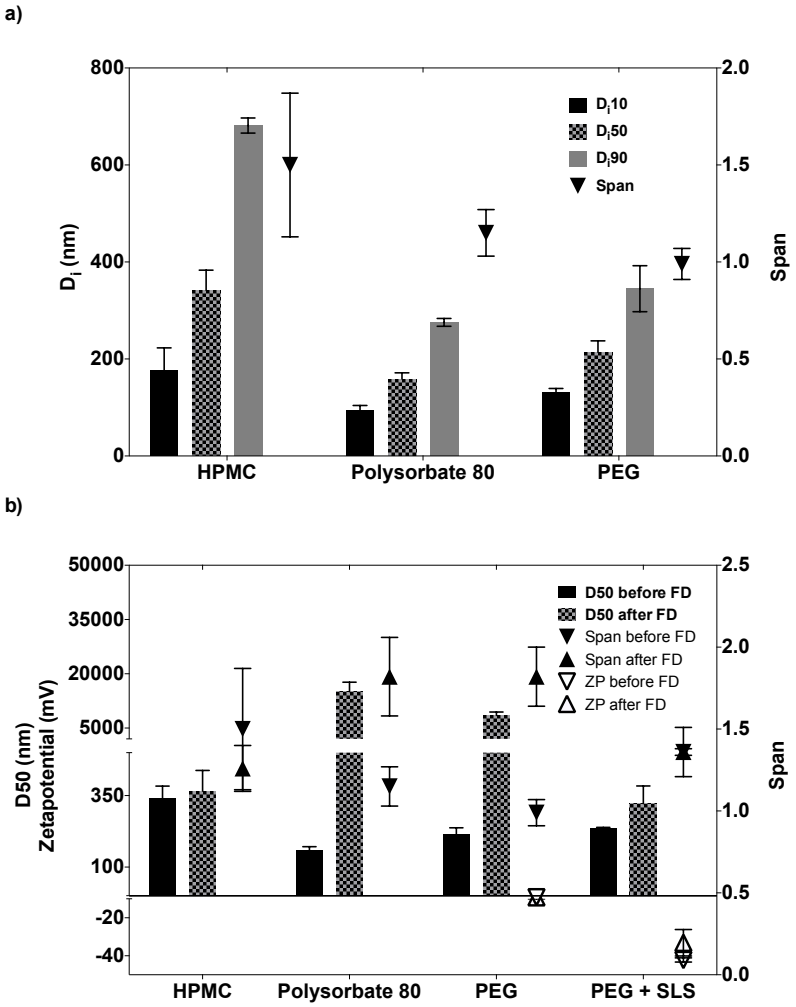

Figure 19 Particle size, span and zetapotential (ZP) a) before and b) after freeze-drying (FD) and reconstitution of the RESS nanosuspensions. Error bars represent standard deviation of 3 separately produced RESS batches

In bottom-up techniques, a fast adsorption process and slow desorption of the stabilizer molecules onto the freshly created drug surface are crucial to ensure fast and complete surface coverage of the precipitated nanoparticles and therefore a well stabilized system (77). If the drug particle surface is not covered fast enough, or if the interaction is of a weak nature, then agglomeration and particle growth are naturally observed after production. It has been argued that Polysorbate 80 as a small molecule size sometimes does not provide a very effective stabilization and co-stabilizers should be used in such cases (98).

In the case of PEG, the insufficient stabilization could be attributed to the molecular weight of the polymer, because its adsorption rate onto the drug surface decreases with increasing molecular weight of the steric stabilizer (96). Because the PEG derivative used here had a molecular weight of $M_w \sim 40{,}000$, this could explain the insufficient stabilization. A derivative with a lower molecular weight might be a better choice regarding the stabilization, but would also mean a lower viscosity, which, as explained above, is a disadvantage during the production process. This shows that the choice of excipients can be somewhat limited and that it is vital to find a compromise between process operability and formulation stability when using RESS as a tool for the production of nanosuspensions.

Effect of retro-active co-stabilization with SLS

Because steric stabilization was not entirely effective, it was attempted to co-stabilize the OLZ nanosuspensions with sodium lauryl sulfate (SLS). SLS is an electrostatic stabilizer; it could thus not be added during the precipitation process due to the increased foaming tendency of the receiving liquid (see page 56). But since agglomeration of the particles was only observed a couple of hours after the actual production process, it was hypothesized that there is a time window for retrograde stabilization of the nanosuspensions.

Especially anionic surfactants like SLS are known to increase the saturation solubility of a large number of compounds, which can cause Ostwald ripening (99). Indeed, the saturation solubility of OLZ was increased to 0.8 ± 0.01 mg/ml in combination with PEG, and to 1.62 ± 0.2 mg/ml in combination with HPMC when 1 % m/V of SLS was used (Table 11). Because of the low average drug load, the attempt was only feasible for PEG stabilized nanosuspensions. With the addition of SLS to PEG stabilized nanosuspensions, the particle growth could be effectively suppressed, because only a slight increase of the particle size was measured after freeze-drying and reconstitution (Figure 19b). The addition of 1 % SLS resulted in a zeta potential of -33 mV, which reflects that the suspensions were indeed physically stable (80).

Table 11 Saturation solubility s of OLZ in different stabilizing media with 1 % m/V of SLS

Medium	Saturation solubility s of OLZ with 1 % SLS (mg/ml)
Phosphate buffer pH 7.4	1.82 ± 0.05
Polysorbate 80 0.1 %	n.a.
PEG 2 %	0.8 ± 0.01
HPMC 2 %	1.62 ± 0.2

n.a. not analyzed

It was suggested that production of nanosuspensions via RESS can be divided into two related processes, the first being the actual precipitation step and the second the stabilization of the initially formed particles (42). Although one would expect that if the co-stabilizer is not present at the actual precipitation process to immediately cover the freshly created surface, then the final particle size is not that of the initially precipitated particles (77). But with the addition of SLS immediately after production, the particle size of OLZ in PEG nanosuspensions was only slightly bigger than

nanoparticles produced with the classic RESS process (see page 53). It could thus be demonstrated that there is a time span after the actual production process in RESS that can be used for retroactive stabilization.

Solid state characterization of olanzapine in nanosuspensions after freeze-drying

As explained in the introduction, OLZ tends to form a hydrate in aqueous suspension within a couple of hours (87). With second derivative FTIR, it is possible to enhance the resolution of overlapping and complex bands in original FTIR spectra. A range of the spectrum (950 - 1050 cm^{-1}) was chosen, where the stabilizers did not interfere with the OLZ spectra (Figure 20). Hydration to the dihydrate B became apparent from two peak shifts of the anhydrous form at 965 cm^{-1} and 1009.6 cm^{-1} to 1003.8 cm^{-1} and 971 cm^{-1}, respectively (Figure 20). OLZ in the flocculated suspensions with PEG and Polysorbate 80 was completely transformed to the dihydrate B (Figure 20). After freeze-drying, the hydrated form was maintained by OLZ in PEG suspensions, while OLZ in Polysorbate 80 suspensions was dehydrated during the drying process so that the solid remnant again contained the anhydrous form I. Judging by the appearance of double bands in OLZ spectra of freeze-dried HPMC nanosuspensions, the drug was probably partially hydrated (Figure 20).

Only OLZ in freeze-dried nanosuspensions stabilized with PEG and SLS showed no trace of hydrate formation. This also became apparent macroscopically, because flocculated and hydrated OLZ turned white, while nanosuspensions stabilized with PEG and SLS appeared yellow and transparent after freeze-drying and reconstitution just like the freshly produced samples (Figure 21).

Particle growth and hydrate formation coincided in the insufficiently stabilized nanosuspensions. This is because the anhydrous form I is more soluble than the dihydrate B and thus, solvent-mediated recrystallization occurs (87). The

supersaturation will be higher with respect to the dihydrate B than to the anhydrate, because it is less soluble so that its nucleation rate will be higher (87, 100).

In previous studies, it was observed that the hydrate formation of carbamazepine could be suppressed by the addition of several polymeric excipients to suspensions of the drug (101, 102). Apparently, the polymeric agents stabilized smaller nuclei of the hydrate and prevented them from growing to the critical size, from where nucleation and particle growth start (see page 7). The interaction was ascribed to the H-bonding capacity of the polymeric agents with the drug and also the increase of viscosity caused by the excipients, which reduced the diffusivity of the drug molecules. Similarly in this study, HPMC strongly increased the viscosity of the medium, thus constraining the diffusivity of the drug molecules. The polymer has both hydrogen acceptor and donor groups in the ring structure, which could provide a strong interaction with the drug surface. PEG on the other hand caused only a slight increase of the viscosity and has only hydrogen bond donor groups at the end of the polymeric chains, while the hydrogen acceptor in the hydroxyl group is very weak. It therefore seems plausible that the protective effect of HPMC is more pronounced than that of PEG. Polysorbate 80, on the other hand, as a non-polymeric small molecule prevented neither particle growth nor hydrate formation.

In vitro dissolution rate

OLZ from RESS suspensions dissolved distinctly faster compared to the micronized powder reference, regardless of the drastic particle growth in Polysorbate 80 and PEG suspensions (Figure 22a). Since the stabilizing agents all possessed more or less pronounced surface activity, their influence on the dissolution rate of the reference material was also investigated (Figure 22b-d). Therefore, suspensions of the micronized drug powder in the respective stabilizing media were also tested. A distinct acceleration of the dissolution rate was observed for all stabilizing agents, which shows

that their effect cannot be underestimated. The effect of the size reduction was, however, still apparent in all RESS suspensions (Figure 22c).

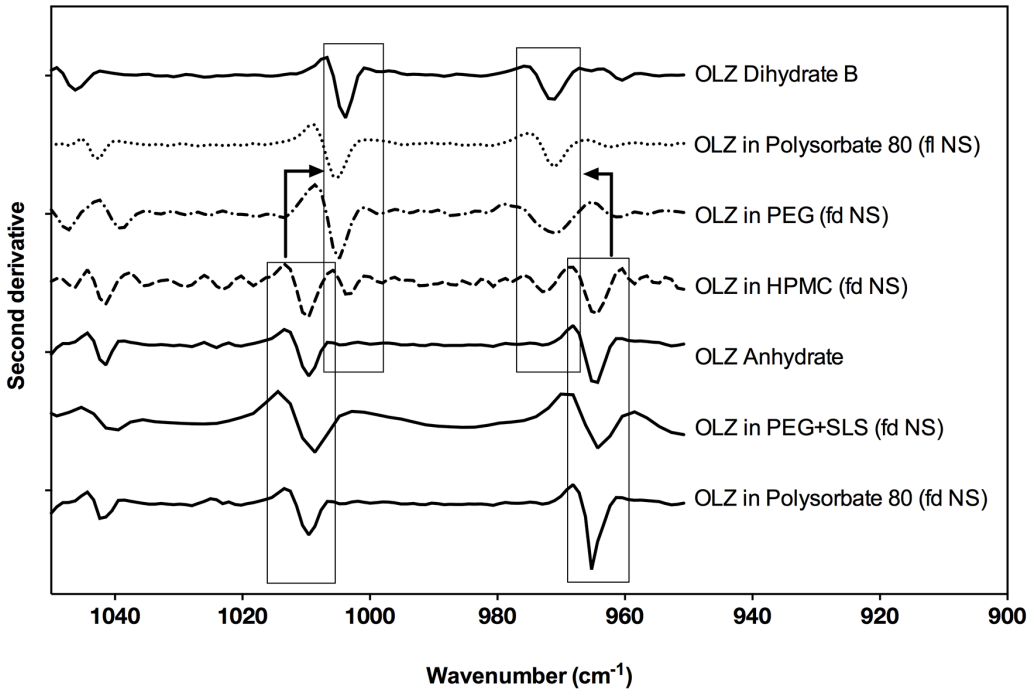

Figure 20 Second derivative FTIR spectroscopy of olanzapine (OLZ) in flocculated nanosuspensions (fl NS) or freeze-dried nanosuspensions (fd NS) with different stabilizing agents

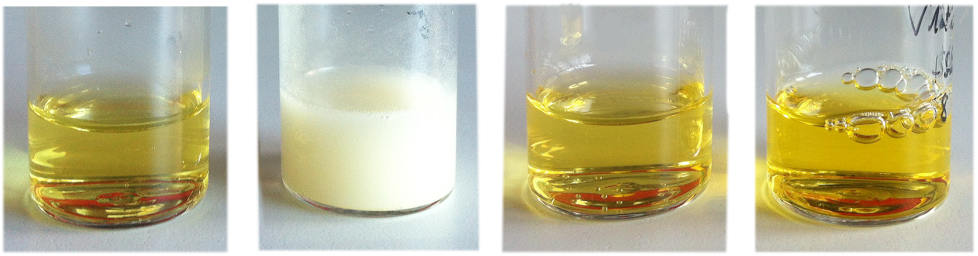

Figure 21 Comparison of nanosuspensions (NS) before and after freeze-drying (FD) with and without the addition of SLS

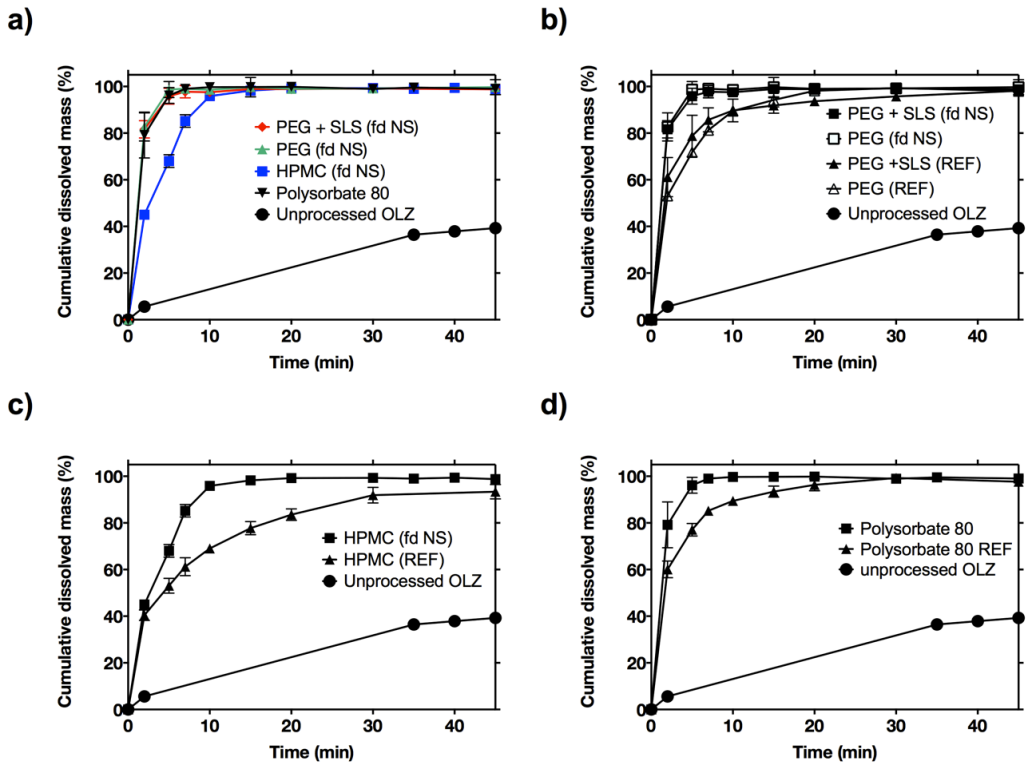

Figure 22 Dissolution profiles in phosphate buffer pH 6.8, USP apparatus II (Paddle)
a) Release profiles of freeze-dried RESS nanosuspensions (fd NS) and unprocessed olanzapine; b-d) Release profiles of unprocessed olanzapine suspensions with the respective stabilizing agent (REF) in comparison to freeze-dried RESS nanosuspensions (fd NS)

Conclusions

Conventional techniques for the production of nanoparticles and nanosuspensions often involve harsh processing conditions and/or the use of organic solvents, which can cause chemical or physical instability of the product. In this chapter, it could be demonstrated that nanosuspensions can be successfully prepared with the RESS process as an alternative solvent free production technique. The mean particle size of RESS olanzapine nanosuspensions ranged from 160 to 340 nm depending on the stabilizer and all suspensions had a narrow particle size distribution, while the drug could be preserved in the most stable polymorphic state.

It was found that during the expansion period, the post expansion temperature and the CO_2 flux through the nozzle are crucial parameters to ensure successful precipitation of the solute into the stabilizing medium. If carefully controlled, freezing or discharge of the receiving liquid with the expanding gas could be avoided, so that a quantitative recovery of the dissolved material could be achieved. At the same time, the pilot equipment used for collection of nanoparticles in suspension introduced in this work still leaves ample room for optimization. For instance, an optical cell for in-line monitoring of the expansion process can greatly speed up the process of defining suitable expansion conditions. Furthermore, an additional inert gas flow around the nozzle and the liquid surface could help to reduce excessive foaming. It is thus expected that the process efficiency can still be enhanced significantly.

An important finding in this chapter is that the choice of stabilizer has a critical influence on both the stability of the nanosuspensions and the expansion process itself. This is because excessive foaming of the receiving medium caused by some steric and all of the tested electrostatic stabilizers could cause depletion of the medium and disruption of the process. Polymeric stabilizers are therefore the better choice from a processing standpoint. But steric repulsion is often not a sufficient stabilizing mechanism for nanosuspensions. On the one hand, it is thus vital to find a compromise between process operability and formulation stability when using RESS as

a tool for the production of nanosuspensions. But on the other hand, it could be shown that retroactive electrostatic stabilization will still lead to preservation of the nanosized particles. Theoretically, it is thus possible to divide the process of precipitation and stabilization to disconnect the adverse effect of electrostatic stabilizers on the precipitation process. But whether this is a viable approach for other compounds remains to be tested.

OLZ from reconstituted RESS nanosuspensions showed a distinct increase of the dissolution rate in comparison to both the micronized drug powder and suspensions of the micronized drug powder in the respective stabilizing media. But the drug load of the RESS nanosuspensions was comparatively low. There are however a number of suggestions to be made how this could be improved in future work. Firstly, a supercritical solution could be expanded over various cycles into the same receiving medium to increase the final drug concentration (44). Furthermore, the volume of the stabilizer could be decreased in order to achieve higher final drug loads. In this study, the approach was not feasible because it increased the risk of ice formation around the nozzle due to Joule-Thompson cooling. This could however be effectively prevented with an additional nozzle heating. Finally, the solubility of OLZ in $scCO_2$ was shown to be much higher with increased fluid density, so that a higher concentration of the drug in $scCO_2$ can be achieved, which will also increase the final drug load of the nanosuspensions.

Considering the beneficial features of the RESS process like the mild process conditions and the absence of organic solvents, but especially the narrow particle size distributions and the small particle sizes, it is concluded that the RESS process may present a superior alternative to other bottom-up techniques for the production of pharmaceutical nanosuspensions; especially if the suggested developments of the equipment and collection device were to be realized.

CHAPTER 4 | FORMATION OF COCRYSTALS WITH RESS

Introduction

Crystal engineering in the pharmaceutical sector traditionally encompasses hydrate and solvate formation, salt formation and polymorphic forms of crystalline API's. Cocrystallization in this field has emerged in the past 10 years as an alternative way of improving the physicochemical properties of pharmaceuticals; especially, if the respective drug is non-ionisable and thus salt formation is not possible (103-113). For a number of cocrystal systems, an increased dissolution rate could be observed, which makes cocrystallization an interesting additional tool for drugs with dissolution-limited bioavailability (111, 114-117). The need for regulatory clarification of what is and what is not a cocrystal has been met recently by an issued draft guideline by the FDA, which reflects the growing importance of pharmaceutical cocrystals in industrial applications (104).

In cocrystals, an API and a structurally related additive are distributed homogeneously in a definite stoichiometric ratio and engage on a supramolecular level via non-ionic interactions (103, 104). If a cocrystal is composed of an acid and a base, the only difference between salt and cocrystal is the location of a proton (103, 113, 118). To establish whether a compound should then be classified as cocrystal or salt, the FDA proposes to consider the following: If the API and the coformer have a ΔpKa of (pKa (base) - pKa (acid)) $\geqq$ 1, a substantial proton transfer will lead to ionization and salt formation. On the other hand, if ΔpKa is lower than 1, no substantial proton transfer will occur, so that API and coformer are present in unionized state and form a cocrystal rather than a salt (104).

Cocrystals are most commonly prepared by slow evaporation of organic solvent, or slow cooling from a solution of the cocrystal formers in organic solvent. But these production methods often do not lead to a pure cocrystal product, because there is always the risk of crystallizing the single components as a physical mixture (115, 119). To avoid this, experimental conditions need to be determined empirically, which often involves a lot of laboratory work, or knowledge of the ternary phase

diagrams of the cocrystal formers and the respective solvent is required (119). In addition, remaining residues of the solvents may contaminate the product. A production method that avoids this and invariably leads to the formation of cocrystals would therefore be desirable.

In this context, supercritical fluid assisted coprecipitation might provide crystallization conditions that suppress the segregation of the single components. Vemavarapu *et al.* first assessed RESS as a technique for crystal doping and coprecipitation of a large number of pharmaceuticals, and found that depending on the solubility and affinity of the components towards the supercritical solvent, cocrystal formation could be observed among other phenomena such as hydrate formation or polymorphic transition (47). The authors however found that supercritical solvent assisted cocrystallization was limited due to the fact that selective extraction of the components leads to inhomogeneous mixtures and thus incorrect stoichiometry of the supercritical solution. Selective extraction can occur, if one of the components presents a much higher solubility in $scCO_2$ than the other, which was reported for theophylline and caffeine (47). Caffeine was found to exceed the solubility of theophylline by one order of magnitude, which will lead to a supercritical solution with according stoichiometry if the solids are presented in a 1:1 ratio (56).

In a different study, cocrystallization of indomethacin and saccharin was attempted via a supercritical solvent technique, which proved unsuccessful, since the solubility in $scCO_2$ of both the pure components was too low (120). It is therefore most essential to consider the solubility limits of the cocrystal formers in $scCO_2$ at the respective extraction conditions, since otherwise, the composition of the supercritical solution may not allow the formation of a pure cocrystal product. But this issue has so far not been addressed sufficiently in an experimental manner (47, 120).

Cocrystal precipitation via RESS compared to cocrystal precipitation from organic solvents

Cocrystal precipitation from supercritical fluids differs from precipitation from organic solvents mainly in the speed with which the products are formed and the fact that in the RESS process, no equilibria between the crystallized solid product and the cocrystal formers in supercritical solution exist. In the RESS process, the precipitation of the solutes is irreversible, because after the expansion, the fluid returns to the gaseous state in which it has negligible solvent power (13). In contrast to this, for ternary systems of cocrystal formers in an organic solvent the equilibria between solid phase and the cocrystal formers in solution must be considered, since during slow evaporation of the solvent, the system may pass through several phase regions in the ternary phase diagram. This may result in precipitation of the cocrystal as well as of the pure coformer and the pure API (119). This again is dependent on the solubility limits of the cocrystal and the respective cocrystal formers.

As stated above, the solubility limits of the cocrystal formers in $scCO_2$ are also important when considering RESS as an alternative way of cocrystal formation, because of the issue of selective extraction. But a large difference in solubility of the components in the supercritical solvent could also prohibit successful cocrystal precipitation because their precipitation is induced at different coordinates regarding the expansion path. As explained initially, the supersaturation S plays a fundamental role in the RESS process, because it is the driving force for nucleation and particle growth (22). A substance with higher solubility in the respective fluid undergoing the same expansion path as a substance with lower solubility will experience a different supersaturation rate. For the two solutes, particle nucleation will thus be theoretically initiated at different spatial or time coordinates regarding the expansion path (30). Nevertheless, a simultaneous precipitation of both components is plausible, if the affinity of the coformer is sufficiently high towards the host molecule in relation to the

solvent. A phase transition of the components would then coincide and dictate the nucleation and growth rate of the cocrystal (47).

Model cocrystal of ibuprofen and nicotinamide

The model API under investigation in this chapter is ibuprofen (IBU). IBU is a non-steroidal anti-inflammatory drug used as analgesic in the short-term management of painful conditions and long term inflammatory conditions such as osteoarthritis (121). Especially in the first case, a fast absorption from the digestive tract is essential to ensure prompt and efficient pain relief. IBU however classifies as a BCS class II drug due to its low dissolution rate and aqueous solubility (Table 12). A 1:1 cocrystal structure of IBU and nicotinamide (NA) obtained by solvent evaporation and grinding has been previously described (115, 121, 122). This cocrystal could also be successfully prepared via hot melt extrusion (123, 124). The cocrystal assembly consists of a central NA amide dimer and linkages to carboxylic acid functions of IBU via the pyridine ring of NA (Figure 23) (122).

IBU has been shown to have a higher intrinsic dissolution rate from the cocrystal than the pure drug (115, 123). NA is the amine of nicotinic acid. It is a commonly used coformer in cocrystal architecture, since it has the structural prerequisites and is a non-toxic, FDA-approved additive (115, 121, 122, 125-127). In addition, NA has a well-studied hydrotropic effect and increases the apparent drug solubility via solution complexation (128, 129).

The IBU NA cocrystal is suitable as a model system for RESS processing, because both components show good solubility in $scCO_2$, but they differ by at least one order of magnitude (14, 130) (Table 12). With the difference in solubility, selective extraction as well as separately induced nucleation of the components are issues that might prevent successful cocrystal formation via RESS.

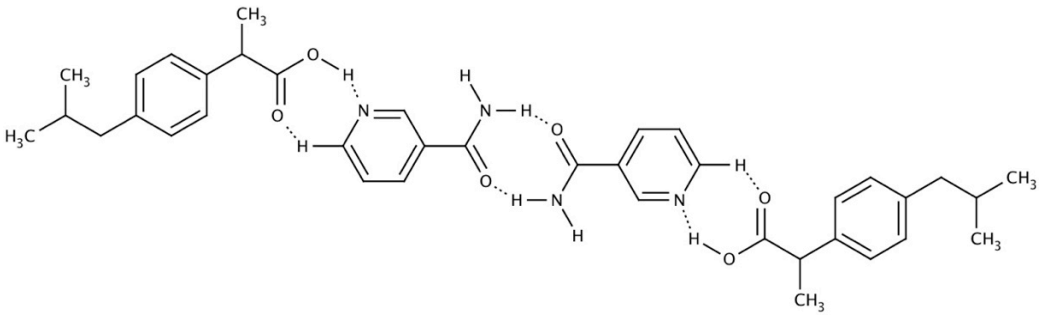

Figure 23 Cocrystal assembly of ibuprofen and nicotinamide (122)

The objective of this chapter is to investigate whether the RESS process is a beneficial alternative production method for cocrystals. In theory, RESS offers a one-step procedure for simultaneous cocrystal formation and micronization of the product. It is hypothesized that the additional micronization will lead to a better dissolution rate than cocrystals produced by the established solvent evaporation technique. But if RESS is to be used successfully for cocrystal formation, then both selective extraction and separately induced nucleation need to be prevented.

To test this, supercritical solutions of IBU and NA in different stoichiometric ratios were precipitated with the RESS technique to assess whether and how the stoichiometry of the supercritical solution could be controlled. Furthermore, the influence of the stoichiometry in supercritical solution on the formation of cocrystals was analyzed. The particle size, specific surface area and morphology were measured and compared to the unprocessed API powder. In addition, the pure API was micronized with RESS to assess the influence of the process on its particle characteristics and crystallinity. Finally, the dissolution rate was measured and the mean dissolution time was calculated as an indicator of improved dissolution performance.

Table 12 Summary of ibuprofen and nicotinamide properties

Property	Ibuprofen	Nicotinamide
Molecular Mass (g/mol)	206.29	122.12
Melting point (°C)	76	128-131
pKs	4.4	(I) 0.5; (II) 3.4
Solubility in water; mg/ml	0.021	Freely soluble
Solubility in $scCO_2$; mol fraction; 40°C	6.49×10^{-3} (22 MPa)(14)	7.5×10^{-4} (20 MPa) (130)

Materials and Methods

Materials

Micronized R,S ibuprofen (IBU) with a median particle size (D_v50) of 50 µm was obtained from BASF, Ludwigshafen, Germany. Nicotinamide (NA) was purchased from Caelo, Bonn, Germany and carbon dioxide from Air liquide, Düsseldorf, Germany. Ethanol and Acetonitrile were purchased from Avantor, Deventor, The Netherlands.

Methods

Solubility of ibuprofen and nicotinamide in supercritical carbon dioxide

For a general description of the procedure and the calculation calculation, refer to **Chapter 2**; page 28. IBU was freely soluble at the extraction conditions of 50 °C and 30 MPa. Within a period of 3 h, 2 g of the compound were dissolved completely. NA on the contrary was not freely soluble at the given conditions and consequently dissolved much slower, so that the extraction time needed to be increased to 24 h. With a further increase of the extraction time, no significant enhancement of the

dissolved material could be achieved. The solubility of NA was thus y = 5.62 x 10^{-5} mol fraction[9] .

Micronization of ibuprofen and cocrystals with the RESS process

For a general description of the RESS equipment and calculation of the RESS process yield, refer to **Chapter 2**, page 28. An accurately weighed amount of the solid material (see Table 13) was placed inside the extraction chamber, which was consequently flooded with CO_2, heated to 50 °C and pressurized to 30 MPa. For the micronization of IBU, the equilibration time was 3 h. In all other experiments, the equilibration time was 24 h.

Supercritical solutions of IBU and NA were prepared in 3 different stoichiometric compositions (Table 13). Since NA was less soluble than IBU, it was attempted to control selective extraction of IBU in the following manner: the amount of NA placed inside the extraction chamber and thus the dissolved fraction of the drug was kept constant in all experiments, while the amount of IBU was varied accordingly (Table 13). After the respective equilibration time, the solution was expanded into the expansion chamber during 60 min, using the equipment presented in Figure 10 for particle collection.

[9] The solubility measured here was much lower than the one found for NA in the literature (1.86 x 10^{-3} mol fraction (128)). This issue has already been discussed in **Chapter 2**.

Table 13 Summary of process conditions for the micronization of olanzapine, ibuprofen and coprecipitates (CP) of IBU and NA

API	Extraction time (h)	Amount in extraction	T in expansion chamber (°C)	Mass flow of CO_2 (kg/h)
IBU	3	2.0	21.3 ± 0.9	2.98 ± 2.12
RCC 0.5 : 1[a]	24	0.5 + 1.0[b]	18.3 ± 9.3	0.87 ± 0.57
RCC 1 : 1[a]	24	1.0 + 1.0[b]	13.0 ± 1.3	0.89 ± 0.29
RCC 2 : 1[a]	24	2.0 + 1.0[b]	14.7 ± 1.8	0.86 ± 0.59

a intended molar ratio (IBU:NA) in supercritical solution and the products
b m (IBU) + m (NA); IBU was freely soluble at the given extraction conditions (i.e. 100 % of the mass was dissolved), while only roughly 60 % of the mass were dissolved in the case of NA (i.e. ~0.6 g)

To improve the particle yield, a suction pump was attached at the outlet and the expansion path was optimized for a shorter connection between the extraction chamber and the expansion chamber. Further details can be found in the Appendix. The heating mantle of the expansion chamber was set to 70 °C. The actual temperature inside the expansion chamber was monitored using thermocouple T1 close to the nozzle exit (Figure 10). Prior to particle collection, the expansion chamber was allowed to reach room temperature in order to prevent potential condensation of air moisture on the products.

Preparation of cocrystals by slow solvent evaporation

Cocrystals of IBU and NA in a molar ratio of 1:1 were prepared by slow solvent evaporation as a reference production method for cocrystals. Equimolar solutions of IBU and NA were prepared in ethanol (purity 96 %) and then joined in equal volumes into petri dishes. The solvent was left to evaporate slowly at ambient conditions during 24 hours. The petri dishes were then placed into an oven at 30 °C for 6 hours to

remove the remaining solvent. Subsequently, the samples were triturated gently with a pestle and mortar and passed through a 250 µm sieve.

Laser Diffractometry in dry dispersion

A Mastersizer 2000 (Malvern, Herrenberg, Germany) equipped with a dry dispersion unit (Scirocco 2000) was used. The disperser pressure was set to 0.07 MPa. The span was calculated according to Eq. 18.

Measurement of the specific surface area with the Brunauer-Emmet-Teller (BET) method

The specific surface area was measured with nitrogen gas adsorption at -196 °C. The material was accurately weighed and analyzed with a SA 3100 Beckman Coulter system (Beckman Coulter, Krefeld, Germany). The outgas temperature was set to 25 °C at an outgas time of 180 min. The average results reported are those of 3 individual RESS batches.

Scanning Electron Microscopy (SEM)

The equipment and sample preparation was the same as described in **Chapter 2**, page 29. In the case of RESS IBU and cocrystals, loose material recovered from the expansion chamber was used as samples. The material was fixed onto double-sided adhesive tape and otherwise prepared in the same fashion.

Differential Scanning Calorimetry (DSC)

The equipment used was described in **Chapter 2**, page 30. A heating rate of 25 °C to 150 °C and a heating rate of 10 K/min was used for the measurement of melting points and specific heat of fusion of IBU, NA and cocrystals. The cocrystal yield α was calculated as

$$\alpha = \frac{\Delta H_f}{\Delta H_f^{100\%}} \qquad \textit{Eq. 21}$$

With $\Delta H_f^{100\%}$ as specific heat of fusion of the cocrystals prepared by solvent evaporation.

Powder X-Ray Diffraction (PXRD)

The equipment and procedure was described in **Chapter 2** (page 30).

Fourier Transform Infrared Spectroscopy (FTIR)

The equipment and procedure was described in **Chapter 2** (page 30).

Confocal Raman Microscopy (CRM) and Imaging

Raman spectra and color-coded images were obtained using an alpha 500R Raman microscope (WiTec, Ulm, Germany) equipped with a 532 nm excitation laser, UHTS 300 spectrometer and a DV401-BV CCD camera. An area of 50 µm x 50 µm or 30 µm x 30 µm was mapped using a 40x objective (numerical aperture 1.25). Color-coded images were calculated after cosmic ray removal and baseline correction using the software WiTec Project Plus 2.10 (WiTec, Ulm, Germany).

Measurement of dynamic contact angles with the modified Wilhelmy plate method

The dynamic contact angles were determined using a tensiometer (K12, Krüss GmbH, Hamburg, Germany) with the modified Wilhelmy plate method (131). Adhesive tape was cut accurately to a length of 50 mm and a height of 20 mm, attached to a Wilhelmy plate and coated with the respective powders on both sides. Superfluous material was removed by gentle air pressure. The plate was suspended from an electronic microbalance and moved with a speed of 3 mm/min in and out of a test vessel containing demineralized water at 22.0 °C to a maximum immersion depth of 5 mm. The contact angle θ_c was calculated according to

$$cos\ \theta_c = \frac{F_{tot} - F_b}{l \cdot \sigma} \qquad \textit{Eq. 22}$$

Where F_{tot} is the measured vertical force (N), F_b is the buoyancy force (N), l is the wetted length (m), and σ is the surface tension of the test liquid (Jm^{-2}). F_b was calculated with the laboratory desktop software 3.1. The wetted length was measured with a micrometer caliper for each measurement. The average values reported are those of 3 individual RESS batches.

Determination of the equilibrium solubility in water

The solubility of IBU as a pure drug, from physical mixtures and from RESS cocrystals was determined using a 48 h shake flask method in sealed 2.0 ml Eppendorf cups (132). 1.0 ml of demineralized water was added to the solids. To measure complexation between IBU and NA, known amounts of NA of increasing concentration were added to an excess of IBU (132). The cups were placed in a thermostated water bath at 25.0 °C and shaken at 60 spm for 48 h. Subsequently, the cups were centrifugated at 13,400 rpm for 20 minutes, the supernatant withdrawn and analyzed with HPLC (see below). The solid remnants of IBU NA physical mixtures and cocrystals were dried and analyzed with DSC to check for possible phase transitions.

In vitro dissolution rate

The in vitro dissolution rate was measured using a Stricker flow-through cell apparatus (Sartorius AG, Göttingen, Germany). Samples were placed into the rotating dissolution chamber together with 80 g of glass beads in 100 ml phosphate buffer pH 6.4 (Ph. Eur.) at 37.0 °C. Samples of 3.5 ml were withdrawn at preset time intervals, filtered through a 0.2 µm cellulose nitrate filter and collected in test tubes. The removed sample volume was immediately replaced with fresh medium. For a detailed description of the calculation of the cumulative released mass with this apparatus, see (12). For a description of the validation procedure, see the Appendix.

The mean dissolution time (MDT) was calculated as

$$MDT = \frac{\sum_{j=1}^{n} t_j^d \Delta M_j}{\sum_{j=1}^{n} \Delta M_j} \qquad \textit{Eq. 23}$$

Statistical evaluation of dissolution data

The MDT values were compared using one-way analysis of variance (ANOVA) with a significance level of 95 % ($p < 0.05$) and the Scheffé test using SPSS statistics V22 (Armonk, US).

High Pressure Liquid Chromatography (HPLC)

Concentrations of IBU and NA in aqueous solutions were measured with an HPLC system (LC 20AT, Shimadzu, Duisburg, Germany) equipped with a UV-detector (SPD-6A, Shimadzu, Duisburg, Germany) and a Nucleosil 100-5 C18 column (Macherey-Nagel, Düren, Germany). The detection wavelength was set to 230 nm. The mobile phase consisted of 60:40 (V/V) acetonitrile and 20 mM phosphoric acid pH 3.0 at a flow rate of 1.0 ml/min. The injection volume was adjusted to 20 µl.

Results & Discussion

Process yield and quantitative composition of RESS coprecipitates

RESS IBU and RESS coprecipitates could be produced with product yields of up to 30 wt. % and 20 wt. %, respectively, in relation to the dissolved material. This corresponds to a comparatively high production rate of 0.4 to 0.6 g/h. RESS coprecipitates of IBU and NA were produced in 3 stoichiometric ratios, namely 0.5:1, 1:1 and 2:1 (IBU:NA; Table 14). Quantitative analysis of the coprecipitates with HPLC revealed slight deviations of the actual molar composition of the products from the supercritical solution and from the intended composition, most distinctly in

coprecipitates with a molar ratio of 0.5:1[10] (IBU:NA). During the long extraction times, leakage of CO_2 via fittings could cause a loss of pressure, which reduced the solubility of NA. The solubility of IBU was not susceptible to these changes because of its relatively higher saturation solubility in $scCO_2$ (Table 14).

A shorter extraction time would make the problem of pressure fluctuation easier to handle. But then the speed of mass transport also needs to be increased efficiently, so that phase equilibria can be reached during shorter extraction times. This could for example be achieved with mechanic stirrers that intimately mix the solid and the supercritical phase inside the extraction chamber (130). Apart from the fluctuations of the NA concentration due to the equipment, selective extraction of IBU could be controlled successfully, so that an overall correct stoichiometric composition of the components in supercritical solution could be achieved.

[10] For RCC 0.5:1, the molar fraction of IBU in supercritical solution was higher than in the products. This can be explicable by assuming that a portion of the API was lost because it crystallized separately. Judging by SEM images, pure IBU forms smaller particles than the cocrystal (Figure 29). It is thus possible that a small fraction of pure IBU was removed from the expansion chamber through the gas outlet, resulting in the observed shift of the molar composition of the products. Another possibility is that this part of the material was precipitated before the nozzle. In any case, the calculation of the concentration in supercritical solution is based on gravimetric measurement of the solid remnants, and is therefore not very accurate.

Table 14 Molar fraction of IBU in supercritical solution and in RESS products

Sample	Molar fraction of IBU in sc solution[b]	Molar fraction of IBU in product[c]
RCC 1:1[a]	1.01 ± 0.09	0.94 ± 0.09
RCC 0.5:1[a]	0.78 ± 0.09	0.56 ± 0.001
RCC 2:1[a]	2.12 ± 0.4	2.05 ± 0.64

a: Intended molar ratio (IBU:NA) in supercritical solution and products
b: Measured by gravimetric evaluation of the remaining solid material in the extraction chamber
c: Measured by HPLC

Cocrystal identification in RESS coprecipitates

To establish whether RESS coprecipitates consisted of a physical mixture of the cocrystal formers or if cocrystals were formed, different techniques of solid state characterization were used. As a reference, cocrystals produced by slow solvent evaporation (SCC 1:1) were used.

Differential Scanning Calorimetry (DSC)

DSC is a valid tool to establish whether cocrystal formation was successful, because the cocrystal of IBU and NA has a distinct melting point that is located between those of the single components (115, 121). RESS processing had no influence on the melting point of IBU, but a slight reduction of the heat of fusion was observed for RESS IBU in comparison to unprocessed IBU (Table 15). Reference cocrystals (SCC 1:1) exhibited a single sharp endotherm with an onset temperature of 90.6 ± 0.5 °C corresponding to the melting point of the cocrystal, which was in good agreement with the data reported in the literature (115, 121). A small trace of an impurity was repeatedly detected at ~64 °C, which probably corresponds to a eutectic of IBU and NA (Figure 24). Thermograms of RESS coprecipitates with a molar ratio of 1:1 (RCC 1:1) also exhibited a single melting peak with an onset temperature of 90.2 ± 0.4 °C, while the

melting points of the pure components were absent (Figure 24). Because RESS processing had no distinct influence on the heat of fusion of RESS IBU, it was assumed that the same holds true for RESS cocrystals. The heat of fusion was thus used as a quantitative readout for the cocrystal yield α of RESS cocrystals. For RCC 1:1, α was 0.96 ± 0.07 (Table 15), which indicates that the starting material was almost completely transformed to cocrystals upon RESS precipitation. RESS coprecipitates with a molar ratio of 0.5:1 IBU:NA (RCC 0.5:1) also exhibited the cocrystal melting point, but at a slightly decreased temperature (89.8 ± 0.2 °C). Additionally, a second broad endotherm at roughly 105 °C was recorded. The latter probably corresponds to NA melting in the presence of the cocrystal, because a similar endothermic event was detected in a physical mixture of cocrystals and NA (Figure 24).

The cocrystal yield α was 0.69 ± 0.02, which indicates that the API was almost completely transformed to cocrystals[11], while the superfluous amount of coformer crystallized separately. RESS coprecipitates with a molar ratio of 2:1 (RCC 2:1) showed two endothermic events. The first onset temperature was below those of the single components, which again probably corresponds to a eutectic of IBU and NA (65.3 °C vs. 75.0 °C for IBU and 128.6 °C for NA). The second endotherm had an onset temperature below that of the cocrystal (82 °C). Because these samples exhibited no clear evidence of cocrystal formation, they were excluded from further analysis.

[11] With a molar ratio of 0.5:1 (IBU:NA), the maximum cocrystal yield is limited by the amount of API: $m\,(\text{cocrystal}) = 0.5\ \text{mol} \times M_r(\text{cocrystal})$ with $M_r(\text{cocrystal}) = 328\ \text{g/mol}$. If the surplus of NA crystallizes separately, then the total product mass is given by:
$m_{tot} = m_{cocrystal} + m_{nicotinamide} = 0.5\ \text{mol} \times 328\ \text{g/mol} + 0.5\ \text{mol} \times 122\ \text{g/mol}$
This means that at a stoichiometric ratio of 0.5:1, the maximum cocrystal yield with regard to the product mass can be calculated as $\alpha = \frac{m_{cocrystal}}{m_{tot}} = 0.73$

Table 15 Thermal key features of starting material and RESS products

Sample	Molar ratio IBU:NA	T_{on} (°C)	ΔH_f (J g^{-1})	cocrystal yield α
SCC 1:1	1:1	90.6 ± 0.5	133.2 ± 2.6	1
RCC 1:1	1:1	90.2 ± 0.4	127.8 ± 10.4	0.96 ± 0.08
RCC 0.5:1	0.5:1	89.8 ± 0.2	91.4 ± 3.3	0.69 ± 0.02
RCC 2:1	2:1	65.2 ± 0.6	-	-
IBU		75.0 ± 0.3	124.1 ± 2.2	
RESS IBU		74.5 ± 0.7	120.3 ± 0.5	
NA		127.8 ± 0.1	192.2 ± 0.6	

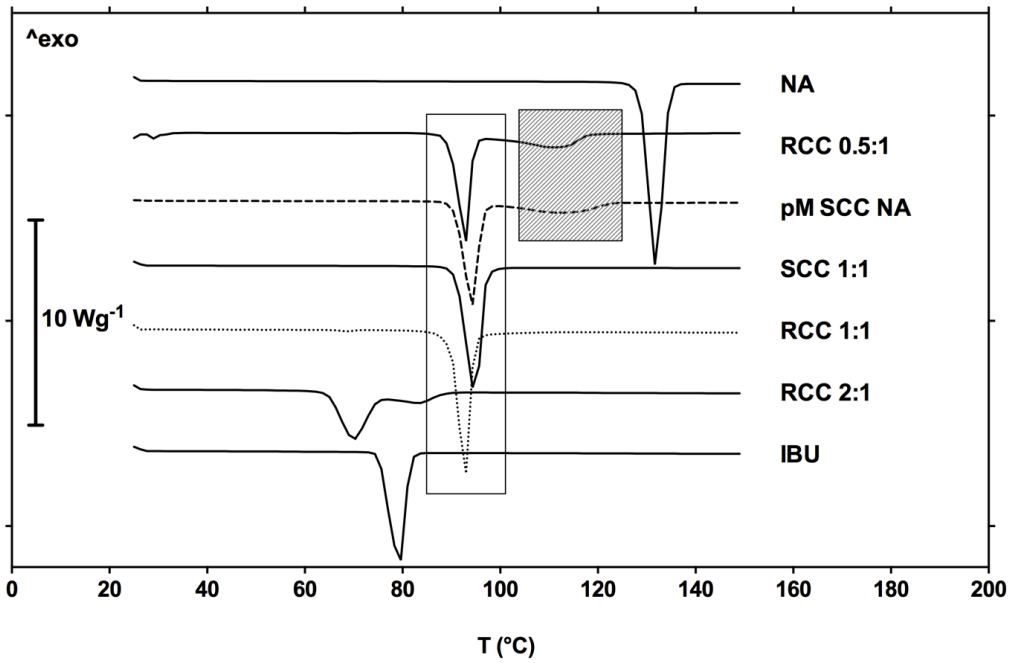

Figure 24 DSC Thermograms of ibuprofen (IBU), nicotinamide (NA), RESS coprecipitates (RCC), reference cocrystals (SCC 1:1) and a physical mixture of cocrystal and NA (pM SCC NA). Clear square marks the cocrystal melting peak; hatched square marks the endothermic event detected for melting of the cocrystal in the presence of NA

Powder X-Ray Diffractometry (PXRD)

The cocrystal of IBU and NA has an individual diffractogram that differs from those of the single components, which can be used to identify cocrystals and mixtures of cocrystals with the single components. Diffractograms of RCC 1:1 showed characteristic peaks at 9.41° and 12.55° 2θ, which were in good agreement with the reference cocrystals produced in this study (SCC 1:1) and the literature (122, 124) (Figure 25). The characteristic peaks of IBU (19.46° and 20.05 2θ) and NA (14.75° and 27.25° 2θ) were absent in the diffraction patterns of RCC 1:1 (Figure 25). RCC 0.5:1 exhibited the above-mentioned cocrystal peaks in addition to the NA peaks, but no pure IBU was detected. These findings are in good agreement with the DSC

measurements and support that IBU was fully transformed to cocrystals upon RESS precipitation, while, if a surplus of the coformer NA was present in the supercritical solution, it was precipitated separately. RCC 0.5:1 is therefore likely to be a physical mixture consisting of cocrystal and NA. The intensity of PXRD diffractograms of RESS products was distinctly reduced in comparison to reference cocrystals and the crystalline starting material. This could be caused by a reduction in crystallinity, but since there is no significant reduction of the melting peak, in this case it seems probable that the reduced intensity of the PXRD signals of RESS products is caused by the reduced particle size.

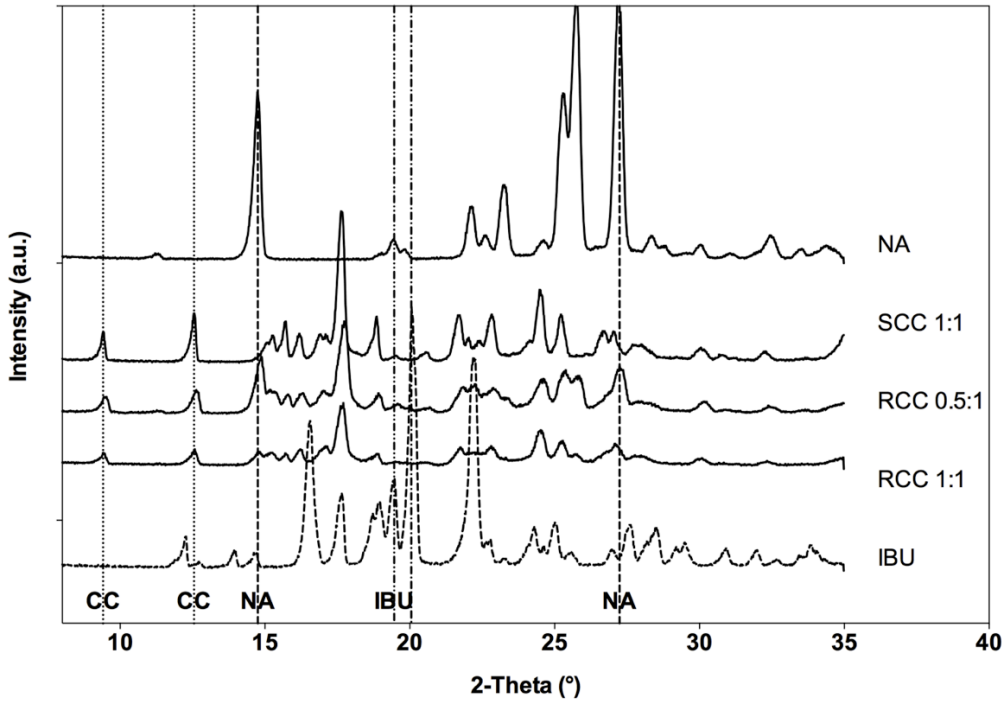

Figure 25 PXRD diffractograms of ibuprofen (IBU), nicotinamide (NA), RESS coprecipitates (RCC) and reference cocrystals (SCC). Characteristic peaks of cocrystals (CC), NA and IBU are marked with dashed and dotted lines

Fourier Transform Infrared Spectroscopy (FTIR)

In contrast to PXRD, RCC 1:1 and RCC 0.5:1 could not be clearly distinguished with FTIR, because the fingerprint region was nearly identical for these samples (Figure 26). Two broad peaks could be observed at 2459 and 1948 cm^{-1}, which were attributed to hydrogen bonding between the carboxylic acid and the amine group of IBU and NA in the cocrystal assembly (dashed lines in Figure 26) (115). The δ NH_2 vibration at 1620 cm^{-1} was however more distinctive in RCC 0.5:1, which may indicate the presence of coformer not engaged in supramolecular hydrogen bonding.

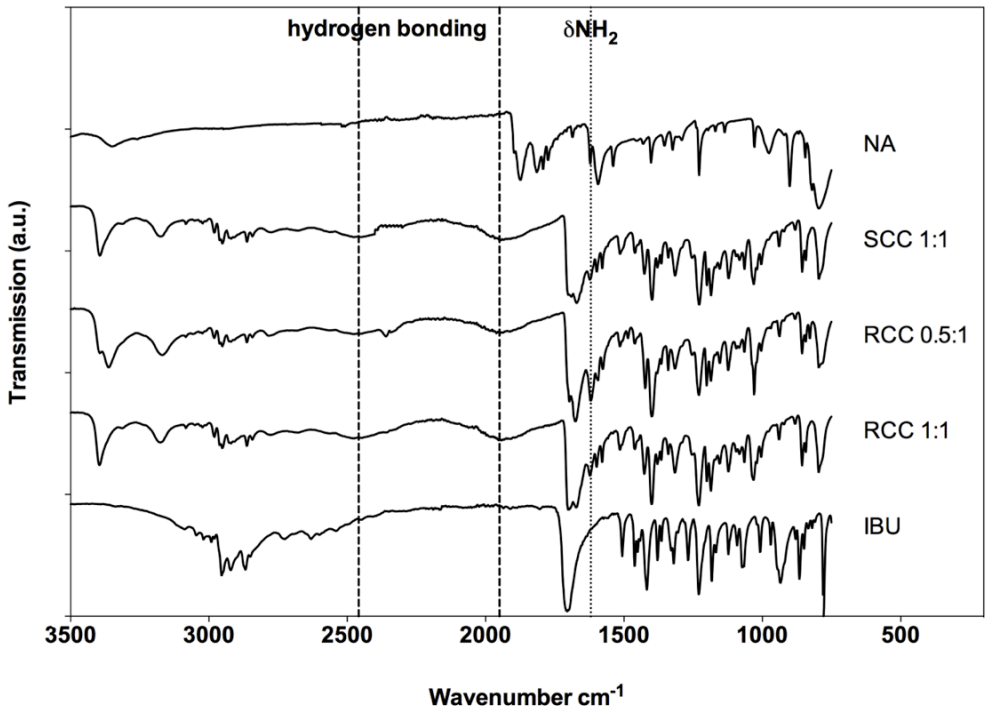

Figure 26 FTIR spectra of ibuprofen (IBU), nicotinamide (NA), RESS coprecipitates (RCC) and reference cocrystals (SCC); dashed lines mark hydrogen bonding and dotted line marks δ NH_2 vibration

Confocal Raman Microscopy (CRM)

CRM is a highly interesting technique for solid state analysis, because with color-coded Raman imaging, the chemical information of the samples can be spatially resolved. This helps to identify crystals of the pure substances, cocrystals and/or mixed crystals. The prerequisite for this is that the spectra of the components differ in at least one of their characteristic peak positions. IBU and NA each exhibited such characteristic peaks and could be well distinguished (Figure 27). The characteristic peaks of IBU and NA in the Raman spectra at 1048 cm^{-1} (NA) and 1013.5 cm^{-1} (IBU) correspond to an aromatic ring deformation mode (Table 16; band assignments were based on previous studies (133-135)). The characteristic C-H stretching vibrations of IBU were located in the region of 2869 cm^{-1} to 2955 cm^{-1}, and =C-H stretching vibrations were identified for both molecules at 3050 cm^{-1} (IBU) and at 3063 and 3101 cm^{-1} (NA). NA also exhibited a weak N-H stretching mode at 3370 cm^{-1} and a NH_2 deformation mode at 1620 cm^{-1}. For both molecules, the O-H stretching vibration was a weak band located in the region of 3155 cm^{-1} (NA) and 3218 cm^{-1} (IBU).

The Raman spectra of cocrystals exhibited characteristic bands of both components (Table 16) and were equivalent for the RESS cocrystals (RCC 1:1) and reference cocrystals (SCC 1:1; Figure 27). The peak corresponding to the C=C deformation vibration was shifted from 1048 cm^{-1} in NA spectra to 1035 cm^{-1} in cocrystal spectra. This peak was used for imaging (highlighted in Figure 27a). Several peaks generated by structures involved in forming hydrogen bonds in the cocrystal were absent in cocrystal spectra, including the δ NH_2 scissoring vibration and the ν N-H stretching vibration of NA (Figure 27b &c). In addition, the bonds assigned to the C=O stretching vibration at 1680 cm^{-1} (NA) and at 1658 cm^{-1} (IBU) were shifted to 1686 cm^{-1} in the cocrystal spectrum (Figure 27b).

Table 16 Main vibrational modes in the Raman spectra of IBU, NA and cocrystals (cm^{-1})

Description	NA	Cocrystal	IBU
δ C=C	1048	1035	1013.5
ν C-N	1397	1403	-
ν C=C	1600	1612	1613
δ NH_2	1620	-	-
ν C=O	1680	1686	1658
ν C-H	-	2866; 2907; 2939	2869; 2920; 2955
ν =C-H	3063; 3101	3050; 3079	3050
ν OH	3155	3161	3218
ν N-H	3370	-	-

ν: stretching; δ: deformation

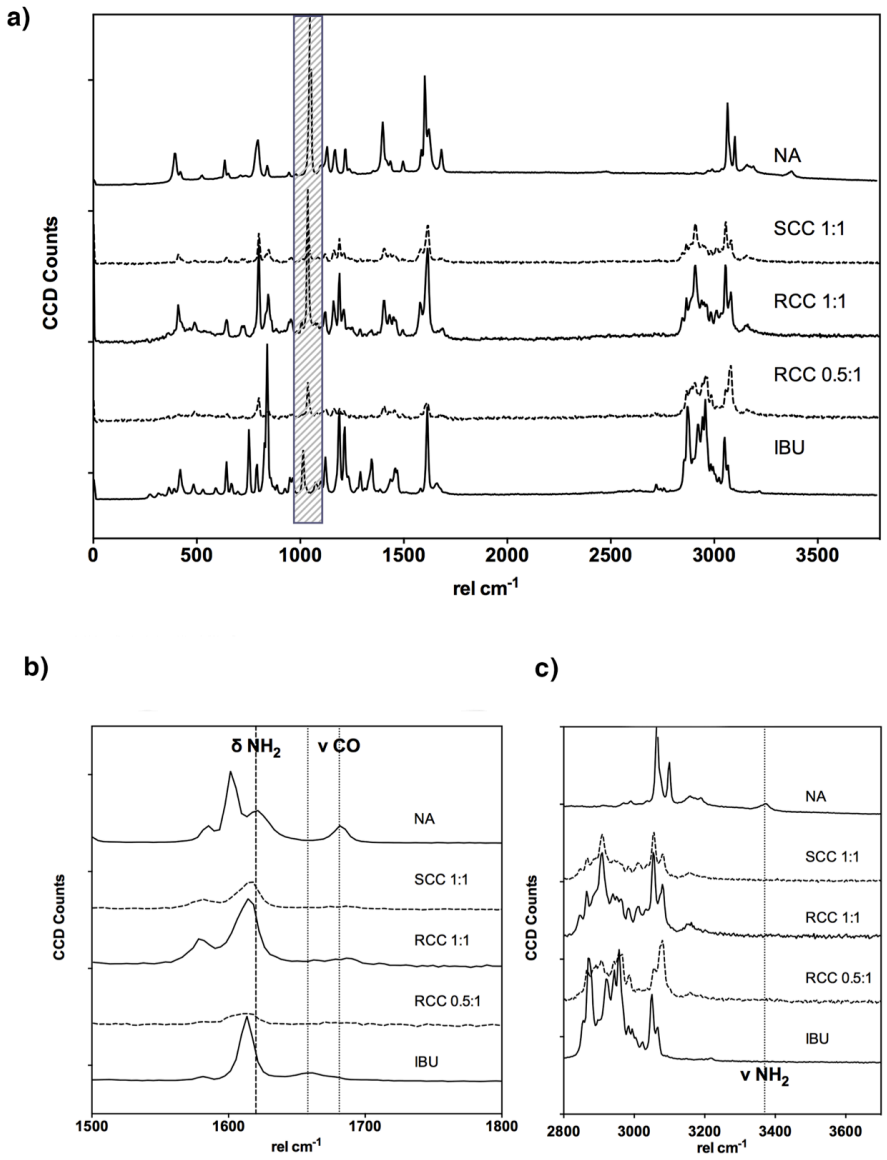

Figure 27 a) Raman vibrational spectra of cocrystal samples and single components; peak positions used for imaging are highlighted; b) enlargement of δ NH_2 vibration of nicotinamide (NA) at 1620 cm^{-1} (absent in cocrystal spectra) and ν C=O vibration region (ibuprofen (IBU): 1658 cm^{-1}; NA: 1680 cm^{-1}; cocrystal (very weak): 1686 cm^{-1}); c) enlargement of ν NH_2 vibration of NA at 3370 cm^{-1} (absent in cocrystal)

In Raman image scans, a sample area is scanned and a spectrum is recorded for every pixel of the image. From these data, the distribution of the material in the sample can be calculated according to the spectral information. The resulting color-coded images of the samples contain the spatially resolved chemical information of the sample. With this technique, it is thus possible to obtain more accurate information about the distribution of the pure components and cocrystals throughout the RESS products. In image scans of physical mixtures, the single components and cocrystals could be well distinguished from each other (Figure 28). Raman imaging could thus be used as a tool to detect phase impurities in cocrystal samples, which is shown in Figure 28c and d; where image scans of RCC 0.5:1 are depicted. In these samples, cocrystals were detected in addition to separate NA crystals while no single IBU crystals could be found.

DSC, PXRD, FTIR and CRM all confirmed that a pure cocrystal phase was precipitated from supercritical solution, if the cocrystal formers were present in the correct stoichiometric ratio. But also with a surplus of coformer, the API was fully transformed to cocrystals. This shows that indeed the individual nucleation rates are not the determining factors dictating the precipitation, but that the affinity of the coformers towards each other causes a simultaneous precipitation and subsequent particle growth.

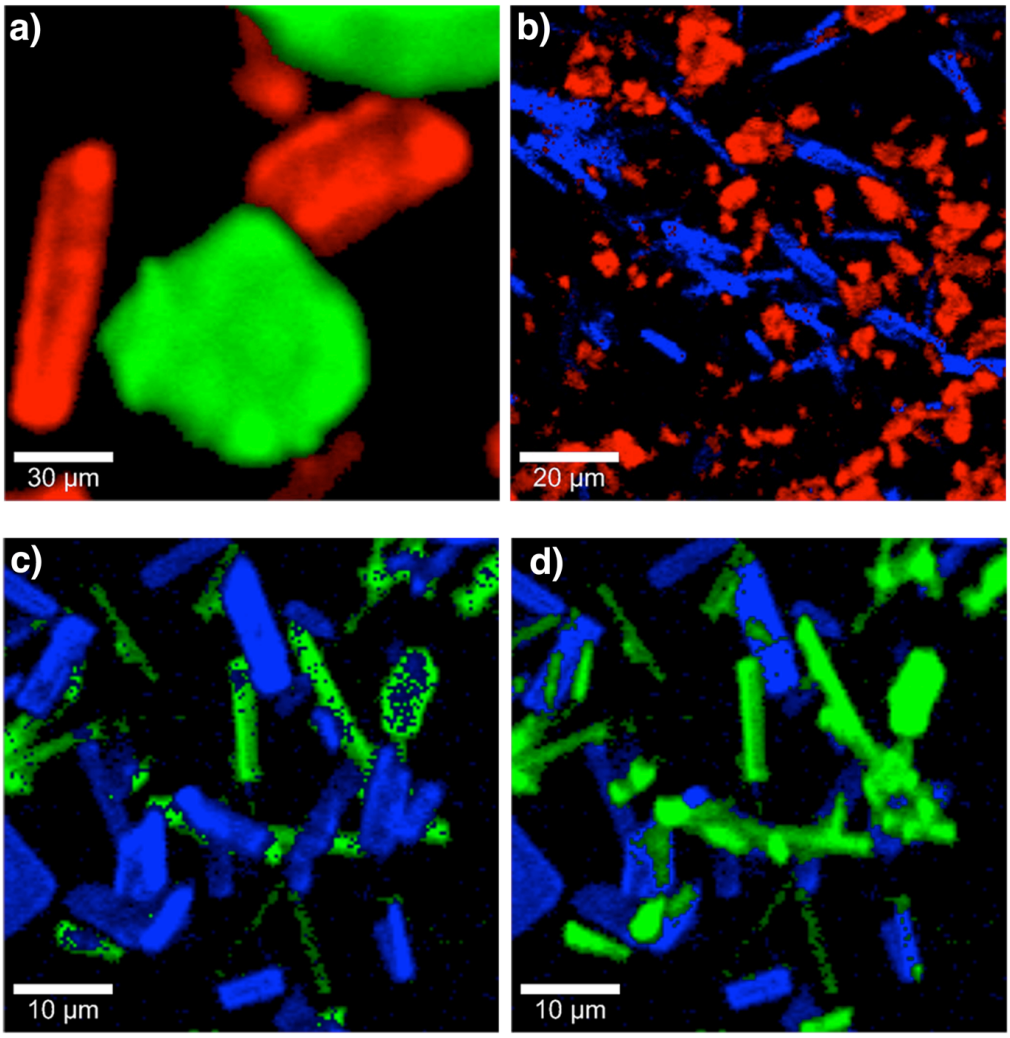

Figure 28 Raman image scans; color code: red: ibuprofen; blue: cocrystal; green: nicotinamide (a) Physical mixture of unprocessed ibuprofen and nicotinamide; (b) Physical mixture of RESS ibuprofen and RCC 1:1; (c) RCC 0.5:1; top color layer: cocrystal; d) RCC 0.5:1; top color layer: nicotinamide

Particle size and morphology of the starting material and RESS products

SEM images revealed that the particle size of RESS IBU was distinctly reduced in comparison to the starting material (Figure 29a-d). The particles were strongly agglomerated and anisometrical. They also seemed partly molten and fused at the edges (Figure 29c). This may have been caused by the mantle temperature in the expansion chamber, which compensates the cooling in the immediate expansion zone but might provoke partial melting of the downstream deposited material. RESS cocrystals did not show this, which is most probably related to their higher thermal stability (90.2 °C). RESS cocrystals exhibited a noticeably different morphology compared to the starting material, since they precipitated as fibers with a high aspect ratio (Figure 29g). Furthermore, the particle size distribution of RESS cocrystals was comparatively large due to fiber-shaped particles that distinctly exceeded 10 µm. The same morphology was also observed in coprecipitates with a different molar ratio (data not shown). In contrast, IBU crystals were rather compact, while NA particles were porous and consisted of agglomerated and partly fused single crystals (Figure 29a; e; f).

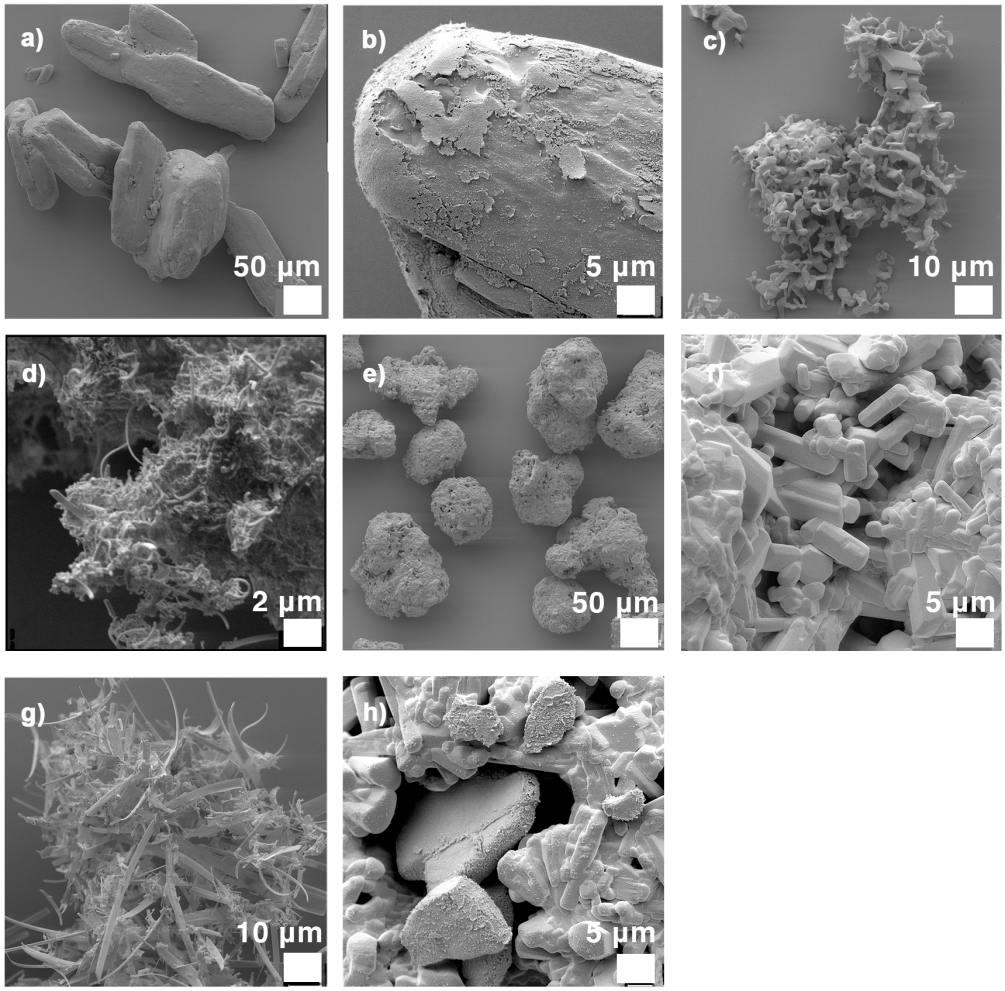

Figure 29 SEM images of a) & b) ibuprofen; c) & d) RESS IBU; e) & f) nicotinamide; g) RCC 1:1; h) equimolar physical mixture of ibuprofen and nicotinamide

The median particle size (D_v50) of RESS IBU and RESS cocrystals measured by laser diffraction was 9.0 ± 1.6 µm and 16.7 ± 0.7 µm, respectively (Table 17). These values are however equivalent diameters, because the high agglomeration tendency of the RESS material may have prevented a proper dispersion of the primary particles and the anisometric nature of the particles is not ideal for laser diffraction measurements,

since the algorithms for calculation of size from diffraction patters are based on a spherical particle shape. A better quantitative parameter for the size reduction is therefore the specific surface area as measured by BET. The specific surface area of RESS IBU was increased 4-fold in comparison to unprocessed IBU, while RESS cocrystals exhibited an almost 10-fold increase (Table 17). Because of the slow crystallization process, cocrystals produced by slow solvent evaporation (SCC 1:1) tended to form crystals with a large size distribution (Table 17).

Table 17 Summary of median particle size (D_v50) , span, specific surface area (A) and contact angle θ_C

Sample	D_v50 (µm)	Span	A ($m^2 g^{-1}$)	θ_C (°)
IBU	49.6 ± 0.4	1.87	0.31 ± 0.01	80.5 ± 1.7
NA	123.8 ± 2.5	1.25	1.14 ± 0.01	66.9 ± 5.3
RESS IBU	9.0 ± 1.6	4.51	1.38 ± 0.08	91.0 ± 2.0
SCC 1:1	39.9 ± 0.7	6.53	0.41 ± 0.02	84.4 ± 0.9
RCC 1:1	16.7 ± 0.7	2.86	2.89 ± 0.22	87.8 ± 1.1

Wetting properties and apparent solubility of RESS products

In previous studies, many hydrophobic compounds have been successfully micronized via RESS, but quite often, the increase in dissolution rate was not as high as expected from the increase in specific surface area, or no increase could be observed at all (136). This was attributed to re-agglomeration and poor wettability of the RESS material. For this reason, the contact angle of water was measured with the modified Wilhelmy plate. RESS products apparently also had a slightly increased hydrophobicity, as indicated by an increased contact angle (Table 17). For RESS IBU, it was distinctly

increased to 91.0° ± 2.0° compared to unprocessed IBU (80.5° ± 1.7; Table 17). RESS cocrystals exhibited a similar value (87.8° ± 1.1°). Surprisingly, the same tendency was observed for cocrystals produced by slow solvent evaporation, but the effect was less pronounced (84.4° ± 0.9°). However, it is important to note that cocrystals did not exhibit a better wettability than pure IBU, regardless of the production method and despite the presence of the much more hydrophilic coformer NA in the host matrix. The increased contact angle may be the cause for the reduced equilibrium solubility of RESS IBU (0.277 ± 0.001 mM vs. 0.298 ± 0.049 mM for unprocessed IBU; Table 18).

A linear increase of the apparent solubility of IBU was observed with increasing NA concentrations in physical mixtures of IBU and NA. This was expected because NA is known to act as a hydrotrope for a variety of substances (115, 128, 129). The apparent solubility of IBU from RESS cocrystals was increased in the same order as observed for physical mixtures and corresponded to the concentration of NA present in the respective solutions (Table 18). DSC analysis of the undissolved solid remnants proved that they consisted of undissolved IBU with a minor trace of eutectic impurity (Figure 30). NA was thus completely dissolved from cocrystals, which indicates dissociation of the cocrystal upon dissolving (115).

Table 18 Equilibrium solubility (mM) of IBU from physical mixtures (pM) and RESS cocrystals in dependence of the NA concentration

Sample	NA concentration (mM)							
	0	SD*	20	SD*	30	SD*	40	SD*
RESS IBU	0.277	0.001	-		-		-	
Physical Mixture	0.298	0.049	0.9122	0.091	0.992	0.097	1.116	0.097
RESS cocrystals	-	-	0.863	0.145	0.993	0.043	1.065	0.062

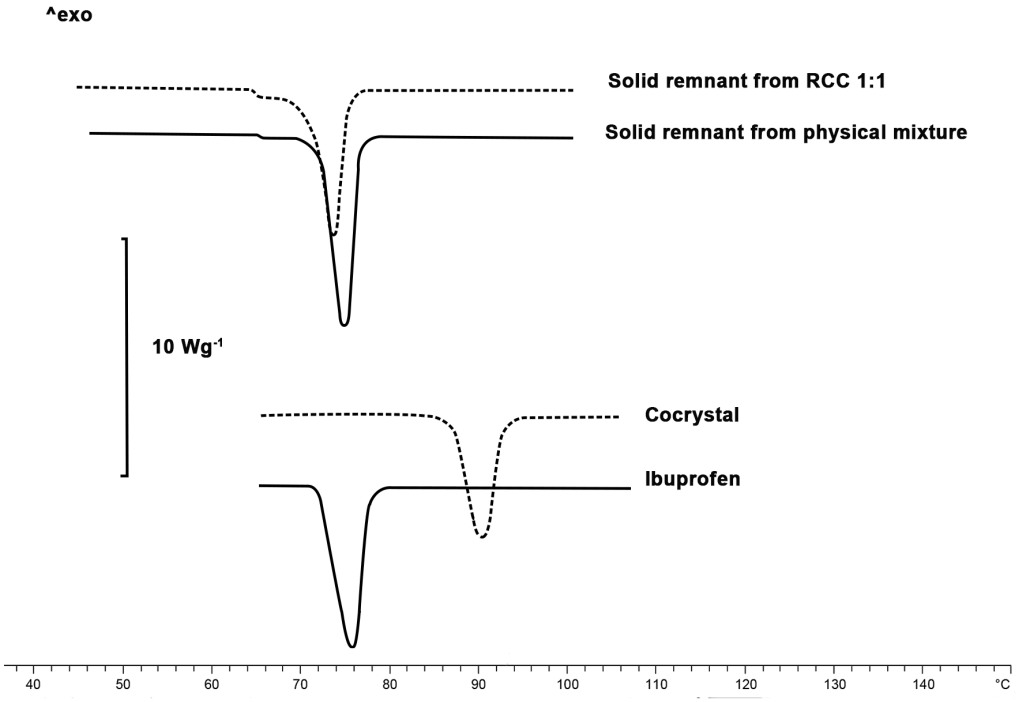

Figure 30 DSC analysis of solid undissolved remnants from equilibrium solubility studies

In vitro dissolution rate

To assess whether RESS micronization had an additional impact on the dissolution rate of IBU from cocrystals, powder dissolution studies with the Stricker flow-through cell apparatus were performed. The dissolution rate of cocrystals was distinctly increased for both production methods, which is in agreement with previous studies (115). The observed increase was however greater for RESS cocrystals (Figure 31b). Calculation of the mean dissolution time (MDT) and statistical analysis revealed that the MDT of IBU from RESS cocrystals was significantly decreased ($p < 0.05$) to almost the order of the faster dissolving co-former NA (Table 19). RESS micronization therefore had an additional positive effect on the dissolution rate of IBU from cocrystals. The dissolution rate of RESS IBU on the contrary was decreased despite the

larger specific surface area (Table 17). This is probably attributed to the poor wettability of the material as shown by the contact angle measurements. This was already observed in a previous study for RESS IBU, where a much slower dissolution rate was obtained for the RESS product in comparison to the unprocessed material (137). It is therefore likely that RESS processing increases the surface hydrophobicity of the material to a certain extent. This could of course have diminished the observed effect on the dissolution rate of IBU from RESS cocrystals.

Table 19 Mean Dissolution Time (MDT; min) of ibuprofen (IBU) and nicotinamide (NA) from different formulations

	Unprocessed	SCC 1:1	RCC 1:1	pM*
IBU	$10.9 \pm 1.0^{a;b}$	10.0 ± 1.1^{b}	6.2 ± 0.6^{c}	13.3 ± 1.4^{a}
NA	4.8 ± 0.3^{a}	7.7 ± 0.6^{b}	4.6 ± 0.8^{a}	8.1 ± 1.2^{b}

*pM = physical mixture; Values with different letters a-c in a row are significantly different at $p < 0.05$ (Scheffé Test)

The MDT of NA from cocrystals produced by solvent evaporation was increased in comparison to free NA (Table 19). This reflects the entrapment of NA in the host matrix of less soluble IBU molecules. Due to the overall larger surface area available for dissolution in RESS cocrystals, the MDT of NA from cocrystals was in the same range as NA alone. Surprisingly, the MDT of NA from equimolar physical mixtures was significantly increased ($p < 0.05$) compared to NA alone. This might be explained by an adsorption of IBU on the surface of NA particles, which could be observed by SEM images of dry physical mixtures of the 2 components (Figure 29b; f; h). In any case, this shows that the mere presence of the hydrotrope NA does not increase the dissolution rate of IBU, but that cocrystallization is indeed a prerequisite (123).

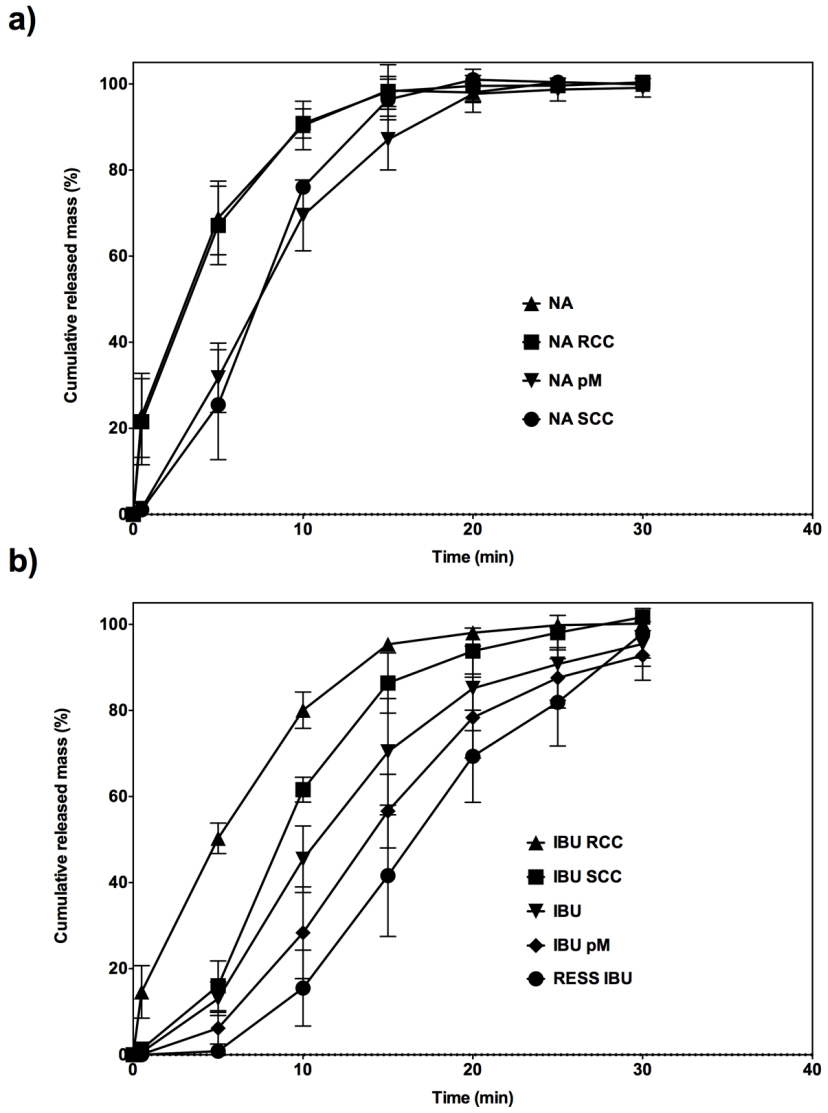

Figure 31 Comparison of in vitro dissolution profiles from different formulations of a) nicotinamide; b) ibuprofen. pM = physical mixture; RCC = RESS cocrystals; SCC = Cocrystals produced by slow solvent evaporation.

Conclusions

Cocrystal formation can provide a successful strategy to improve the apparent solubility and dissolution rate of poorly soluble API's. Cocrystals are however often prepared via solvent evaporation techniques, which bear the disadvantage of crystallizing a mixed solid phase, while the products may be contaminated with remnant solvents. In this chapter, it could be demonstrated that RESS is a promising alternative production method for the formation and micronization of pharmaceutical cocrystals.

Selective extraction of the coformer with higher solubility in $scCO_2$ could be controlled, so that the stoichiometric composition of the supercritical solution could effectively be tailored. This was important, because it was observed that precipitation of the cocrystal mainly depended on the molar composition of the cocrystal formers in supercritical solution. With a surplus of coformer dissolved in $scCO_2$, the API was almost completely precipitated as cocrystals, while the excess coformer precipitated separately. With a surplus of API on the other hand, a mixed solid phase was precipitated, in which the cocrystal could not be clearly identified. The precipitation of a supercritical solution with the molar ratio of 1:1 led to the formation of a remarkably pure cocrystal phase. This can often not be achieved with conventional cocrystal production techniques, because during the evaporation of the organic solvent, the system passes through several phases of the ternary phase diagram. In RESS, on the contrary, the equilibria between dissolved and undissolved phase need not be considered, because the precipitation step is irreversible.

Due to the optimized expansion path and the additional suction pump attached at the outlet of the expansion chamber, a comparatively high process yield of 20 - 30 % in relation to the dissolved material could be achieved.

RESS cocrystals had a distinctly increased specific surface area, which effectively led to a better dissolution performance in comparison to cocrystals produced by slow solvent evaporation. The particle morphology on the other hand was

not ideal, because an anisometric particle shape may negatively affect flowability and trigger demixing tendencies in powder mixtures. It has however been shown that the RESS process conditions can have a distinct impact on both particle size and morphology (46, 74). It is therefore expected that an optimization of the pre-expansion temperature, pressure and the post-expansion conditions offers ample room for improvement in the matter of particle size and morphology. With RESS being a solvent free one-step procedure for cocrystal formation and micronization, further drying and size reduction steps can be dispensed. The most important advantage of RESS can however be seen in the high product purity of cocrystals, which clearly distinguishes RESS from organic solvent-based production techniques. RESS can thus present a valuable additional tool for crystal engineering of poorly soluble API's.

CHAPTER 5 | SUMMARY, CONCLUDING REMARKS AND PERSPECTIVES

Summary

An increasing number of newly developed pharmaceutical compounds are classified as poorly soluble according to the Biopharmaceutics Classification System (BCS). At the same time, many of the established processing techniques in pharmaceutical technology for enhancement of drug dissolution and solubility suffer from drawbacks arising from harsh process conditions such as high temperature, mechanical stress and the use of organic solvents. The Rapid Expansion of Supercritical Solutions (RESS) is an alternative processing technique for particle design and crystal engineering. In contrast to many established pharmaceutical processing techniques, RESS uses little or no organic solvents that can contaminate the products and raise their toxic potential or cause physical and chemical instabilities. The absence of organic solvents furthermore makes RESS a green technology, which is a growing demand of today's environment that is increasingly focused on sustainability. Finally, RESS avoids harsh processing conditions such as heat and mechanical forces that can negatively affect the crystallinity and polymorphic state of sensitive material.

The aim of this thesis was therefore to investigate the potential of RESS as an alternative technique for crystal engineering and particle design to improve aqueous solubility and dissolution of poorly soluble drugs. To this end, three applications of RESS were developed for dissolution rate and solubility enhancement in the fields of micronization, nanotechnology and crystal engineering.

In **Chapter 2**, a process for liquid cosolvent-assisted RESS micronization was developed in order to overcome the issue of poor drug solubility in supercritical carbon dioxide. It could be shown that with the addition of 4 wt. % of methanol to the supercritical phase, the solubility of theophylline could be increased by almost a factor of 25, while the process yield of RESS theophylline could be increased from around 0 % to 25 %.

Theophylline could be successfully micronized with RESS as shown by a 14-fold increase of the specific surface area. With increasing expansion temperatures, the

precipitation of methanol in liquid state could be suppressed so that recrystallization and agglomeration of the product could be minimized, while no solvent contamination or distinct reduction of the crystallinity could be detected in the product. This development of the classic RESS process could thus render a large variety of compounds applicable for RESS micronization and overcome what is generally considered a major restriction of the technique.

In **Chapter 3**, a process for the production of RESS nanoparticles and nanosuspensions of olanzapine, a poorly soluble BCS class II compound, was developed. With RESS, nanoparticles and nanosuspensions of olanzapine with a medium particle size of 160-340 nm and a narrow size distribution could be produced, while no polymorphic conversion of the drug was caused by RESS. Depending on the stabilizer, almost 100 % of the dissolved API could be recovered in nanosuspensions. The process parameters such as expansion temperature and CO_2 flux through the nozzle were found to be critical for the successful production of RESS nanosuspensions, because freezing or discharge of the receiving liquid with the expanding gas could disrupt the process.

Polymeric stabilizers were found to be the better choice from a processing standpoint in comparison to ionic surfactants, because they caused less foaming and an increased viscosity of the stabilizing medium, which was beneficial during the expansion process. But the steric repulsion conveyed by polymers is often not a sufficient stabilizing mechanism for nanosuspensions. On the one hand, it is thus vital to find a compromise between process operability and formulation stability when using RESS as a tool for the production of nanosuspensions. But on the other hand, it could be shown that retroactive electrostatic stabilization will still lead to preservation of the nanosized particles in the suspension.

Finally, reconstituted RESS nanosuspensions showed a distinct increase of the olanzapine release rate in comparison to the reference material. Considering the absence of organic solvents, the mild process conditions and the high process yield

that can be achieved, production of nanosuspensions via RESS may represent a superior alternative to established bottom-up techniques for the production of nanosuspensions.

In **Chapter 4**, RESS was investigated as a tool for crystal engineering; namely the simultaneous formation and micronization of ibuprofen-nicotinamide cocrystals. Different molar ratios of the cocrystal formers were precipitated from supercritical solution and it was found that with an excess of coformer, the API was nearly completely precipitated as cocrystals while the excess coformer crystallized separately. With a surplus of API on the other hand, a mixed solid phase was precipitated, in which the cocrystal could not be clearly identified. A cocrystalline phase with remarkable purity was obtained when precipitating the cocrystal formers from a supercritical solution with the molar ratio of 1:1.

RESS cocrystals had a distinctly increased specific surface area, which effectively led to a better dissolution rate in comparison to cocrystals produced by a conventional solvent evaporation technique. The high product purity and the fact that cocrystals can be formed and micronized in a one-step procedure make RESS a promising alternative for conventional organic solvent-based production techniques.

Concluding remarks and perspectives

Rapid Expansion of Supercritical Solutions (RESS) is a promising and versatile technology for crystal engineering and particle design of poorly soluble drug molecules. Although RESS processing bears a number of immanent advantages over established pharmaceutical processing techniques, many applications of RESS are still on an experimental level and no commercial use for drug products is presently made of it. One of the critical issues related to RESS is the low process yield due to insufficient particle separation from the gaseous stream after expansion and the low solubility of many compounds in $scCO_2$. As a consequence, RESS process yields of less than 5 % are commonly reported in the literature. In contrast to this, it could be shown

in **Chapter 3** that the right choice of stabilizer and careful control of the expansion conditions in the production of nanosuspensions increase the process yield up to almost 100 %. In **Chapter 2**, due to the use of very low amounts of liquid cosolvent, the process yield of RESS micronization could be significantly improved from 0 % to around 25 % without negatively impacting the crystallinity or precipitating solvates of the model compound with the employed solvent. In **Chapter 4**, a process yield of 20 - 30 % could be achieved in the precipitation of the model API and its cocrystal by mechanical improvements of the expansion path and the collection device. Even though these figures are still not ideal, this work shows that effective measures can be taken towards improved process yields. Considering the easy recycling of the expanded gas, an additional possible approach is the design of a continuous RESS process, so that low solubility and thus a lower throughput can be circumvented by a closed loop technology or even an array of nozzles.

Critical reports related to RESS often claim poor control over the particle size, morphology and size distribution. Indeed, the cocrystals produced in **Chapter 4** had an anisometric needle-shaped morphology and a broad particle size distribution, so that further optimization of the process conditions is clearly necessary at this point. On the contrary, the nanoparticles and nanosuspensions of olanzapine produced with RESS in **Chapter 3** had a highly homogeneous particle size and a very narrow size distribution. In **Chapter 2**, it could be shown that by simple modification of the post expansion temperature, the particle size, size distribution and specific surface area could be significantly improved. So there clearly is a dependence of particle size and morphology on both the material type and the RESS process conditions, and further research should address as to how the process conditions can effectively tailor particle morphology.

The RESS process probably bears the highest resemblance to spray drying when considering efficient particle collection and the concern regarding the product particle characteristics. Although spray drying is a well established technique and has

long been a common tool in the food and pharmaceutical industry, its history of more than 150 years of intense research concerning the optimization of atomization, flowability of the products and process efficiency is still ongoing. The immense research effort made in the field of spray drying and the significantly improved output that was consequently achieved may help to place the comparatively short history of RESS and the improvements shown in this thesis in a wider perspective. Specifically the issue of low process yields will require further scientific attention from a process-engineering perspective. But from a pharmaceutical standpoint, it can be concluded that with the successful applications shown in the field of micronization, nanotechnology and crystal engineering, RESS offers a highly interesting and valuable technology platform with an up-to-date unexploited potential for particle design of poorly soluble drug molecules. At the same time, an increasing number of newly developed pharmaceutical compounds are classified as poorly soluble and the stability issues that arise from the use of organic solvents and rough process conditions in traditional pharmaceutical processing techniques call for alternative technologies. In the light of this development, RESS represents a more than fitting candidate. If future technological advances can further improve the efficiency and control of the process parameters, then research on scale-up is possibly the next step on the way of the RESS technique into the market.

REFERENCES

1. Vandecruys R, Peeters J, Verreck G, Brewster ME. Use of a screening method to determine excipients which optimize the extent and stability of supersaturated drug solutions and application of this system to solid formulation design. Int J Pharm. 2007;342(1-2):168-75.

2. Amidon GL, Lennernas H, Shah VP, Crison JR. A theoretical basis for a biopharmaceutic drug classification: the correlation of in vitro drug product dissolution and in vivo bioavailability. Pharm Res. 1995;12(3):413-20.

3. WHO model lists of essential medicines. 13th Ed., 2003 [cited 2014]; Available from: http://www.who.int/medicines/publications/essentialmedicines/en/.

4. FDA new molecular entities approval. 2011-2013 [cited 2014]; Available from: http://www.fda.gov/Drugs/DevelopmentApprovalProcess/DrugInnovation/ucm381263.html.

5. Hannay J, Hogarth J. On the solubility of solids in gases. Proceedings of the Royal Society of London (1854-1905). 1879;30:178-88.

6. Eckert CA, Van Alsten JG, Stoicos T. Supercritical fluid processing. Environ Sci Technol. 1986;20(4):319-25.

7. Wahl MA. Supercritical Fluid Technology. In: Parikh DM (Editor). Handbook of Pharmaceutical Granulation Technology. New York, London: Informa Healthcare; 2009. p. 126-37.

8. Ginty PJ, Whitaker MJ, Shakesheff KM, Howdle SM. Drug delivery goes supercritical. Mater Today. 2005;8(8, Supplement):42-8.

9. Gupta RB, Shim J-J. Solubility in Supercritical Carbon Dioxide. Boca Raton: CRC Press; 2007.

10. Vemavarapu C, Mollan MJ, Lodaya M, Needham TE. Design and process aspects of laboratory scale SCF particle formation systems. Int J Pharm. 2005;292(1-2):1-16.

11. Hussein K, Türk M, Wahl MA. Drug loading into β-cyclodextrin granules using a supercritical fluid process for improved drug dissolution. Eur J Pharm Sci. 2008;33(3):306-12.

12. Metzger P. Systematische Untersuchung der kontrollierten Partikelabscheidung aus überkritischem Kohlendioxid und Entwicklung geeigneter Trägersysteme. Tübingen: Eberhard Karls Universität Tübingen; 2011.

13. Matson DW, Fulton JL, Petersen RC, Smith RD. Rapid expansion of supercritical fluid solutions: solute formation of powders, thin films, and fibers. Ind Eng Chem Res. 1987;26(11):2298-306.

14. Charoenchaitrakool M, Dehghani F, Foster NR, Chan HK. Micronization by Rapid Expansion of Supercritical Solutions to Enhance the Dissolution Rates of Poorly Water-Soluble Pharmaceuticals. Ind Eng Chem Res. 2000;39(12):4794-802.

15. Weidner E, Knez, Ž., Novak, Z, inventor Process for preparing particles or powders. patent WO 95/21688. 1995.

16. Gallagher PM, Coffey MP, Krukonis VJ, Klasutis N. Gas Antisolvent Recrystallization: New Process To Recrystallize Compounds Insoluble in Supercritical Fluids. Supercritical Fluid Science and Technology: American Chemical Society; 1989. p. 334-54.

17. Rossmann M, Braeuer A, Dowy S, Gallinger TG, Leipertz A, Schluecker E. Solute solubility as criterion for the appearance of amorphous particle precipitation or crystallization in the supercritical antisolvent (SAS) process. J Supercrit Fluids. 2012;66(0):350-8.

18. Pereira VJ, Matos RL, Cardoso SG, Soares RO, Santana GL, Costa GMN, Vieira de Melo SAB. A new approach to select solvents and operating conditions for supercritical antisolvent precipitation processes by using solubility parameter and group contribution methods. J Supercrit Fluids. 2013;81(0):128-46.

19. Bodmeier R, Wang H Fau - Dixon DJ, Dixon Dj Fau - Mawson S, Mawson S Fau - Johnston KP, Johnston KP. Polymeric microspheres prepared by spraying into compressed carbon dioxide. Pharm Res. 1995;12(8):1211-7.

20. Kang Y, Yin G, Ouyang P, Huang Z, Yao Y, Liao X, Chen A, Pu X. Preparation of PLLA/PLGA microparticles using solution enhanced dispersion by supercritical fluids (SEDS). J Colloid Interface Sci. 2008;322(1):87-94.

21. Chattopadhyay P, Gupta RB. Production of griseofulvin nanoparticles using supercritical CO2 antisolvent with enhanced mass transfer. Int J Pharm. 2001;228(1-2):19-31.

22. Debenedetti PG, Tom JW, Kwauk X, Yeo SD. Rapid expansion of supercritical solutions (RESS): fundamentals and applications. Fluid Phase Equilib. 1993;82(0):311-21.

23. Weber M, Thies MC. A simplified and generalized model for the rapid expansion of supercritical solutions. J Supercrit Fluids. 2007;40(3):402-19.

24. Volmer M, Weber A. Keimbildung in übersättigten Gebilden. Z Phys Chem. 1926;119:277-301.

25. Becker R, Döring W. Kinetische Behandlung der Keimbildung in übersättigten Dämpfen. Ann Phys. 1935;24:719-52.

26. Gebauer D, Kellermeier M, Gale JD, Bergstrom L, Colfen H. Pre-nucleation clusters as solute precursors in crystallisation. Chem

Soc Rev. [10.1039/C3CS60451A]. 2014;43(7):2348-71.

27. Zeldovich JB. On the theory of new phase formation: cavitation. Acta Physicochem USSR. 1943;18:1-22.

28. Debenedetti PG. Homogeneous nucleation in supercritical fluids. AlChE J. 1990;36(9):1289-98.

29. Tom JW, Debenedetti PG. Particle formation with supercritical fluids--a review. J Aerosol Sci. 1991;22(5):555-84.

30. Türk M. Formation of small organic particles by RESS: experimental and theoretical investigations. J Supercrit Fluids. 1999;15(1):79-89.

31. Türk M, Hils P, Helfgen B, Schaber K, Martin HJ, Wahl MA. Micronization of pharmaceutical substances by the Rapid Expansion of Supercritical Solutions (RESS): a promising method to improve bioavailability of poorly soluble pharmaceutical agents. J Supercrit Fluids. 2002;22(1):75-84.

32. Helfgen B, Türk M, Schaber K. Hydrodynamic and aerosol modelling of the rapid expansion of supercritical solutions (RESS-process). J Supercrit Fluids. 2003;26(3):225-42.

33. Jung J, Perrut M. Particle design using supercritical fluids: Literature and patent survey. J Supercrit Fluids. 2001;20(3):179-219.

34. Pasquali I, Bettini R. Are pharmaceutics really going supercritical? Int J Pharm. 2008;364(2):176-87.

35. Hirunsit P, Huang Z, Srinophakun T, Charoenchaitrakool M, Kawi S. Particle formation of ibuprofen-supercritical CO2 system from rapid expansion of supercritical solutions (RESS): A mathematical model. Powder Technol. 2005;154(2-3):83-94.

36. Hezave AZ, Esmaeilzadeh F. Micronization of drug particles via RESS process. J Supercrit Fluids. 2010;52(1):84-98.

37. Sane A, Thies MC. Effect of material properties and processing conditions on RESS of poly(l-lactide). J Supercrit Fluids. 2007;40(1):134-43.

38. Hezave AZ, Esmaeilzadeh F. The effects of RESS parameters on the diclofenac particle size. Adv Powder Technol. 2011;22(5):587-95.

39. Baseri H, Lotfollahi MN. Formation of gemfibrozil with narrow particle size distribution via rapid expansion of supercritical solution process (RESS). Powder Technol. 2013;235(0):677-84.

40. Türk M, Lietzow R. Formation and stabilization of submicron particles via rapid expansion processes. J Supercrit Fluids. 2008;45(3):346-55.

41. Türk M, Bolten D. Formation of submicron poorly water-soluble drugs by rapid expansion of supercritical solution (RESS): Results for Naproxen. J Supercrit Fluids. 2010;55(2):778-85.

42. Pathak P, Meziani MJ, Desai T, Sun Y-P. Formation and stabilization of ibuprofen nanoparticles in supercritical fluid processing. J Supercrit Fluids. 2006;37(3):279-86.

43. Songtipya L, Sane A. Effect of concentration and degree of saturation on co-precipitation of catechin and poly(l-lactide) by the RESOLV process. J Supercrit Fluids. 2013;75(0):72-80.

44. Dalvi SV, Azad MA, Dave R. Precipitation and stabilization of ultrafine particles of Fenofibrate in aqueous suspensions by RESOLV. Powder Technol. 2013;236(0):75-84.

45. Gosselin PM, Thibert R, Preda M, McMullen JN. Polymorphic properties of micronized carbamazepine produced by RESS. Int J Pharm. 2003;252(1-2):225-33.

46. Yim J-H, Kim W-S, Lim JS. Recrystallization of adefovir dipivoxil particles using the rapid expansion of supercritical solutions (RESS) process. J Supercrit Fluids. 2013;82(0):168-76.

47. Vemavarapu C, Mollan MJ, Needham TE. Coprecipitation of pharmaceutical actives and their structurally related additives by the RESS process. Powder Technol. 2009;189(3):444-53.

48. Meziani MJ, Pathak P, Beacham F, Allard LF, Sun Y-P. Nanoparticle formation in rapid expansion of water-in-supercritical carbon dioxide microemulsion into liquid solution. J Supercrit Fluids. 2005;34(1):91-7.

49. Young TJ, Mawson S, Johnston KP, Henriksen IB, Pace GW, Mishra AK. Rapid Expansion from Supercritical to Aqueous Solution to Produce Submicron Suspensions of Water-Insoluble Drugs. Biotechnol Progr. 2000;16(3):402-7.

50. Türk M, Lietzow R. Stabilized nanoparticles of phytosterol by rapid expansion from supercritical solution into aqueous solution. AAPS PharmSciTech. 2004;5(4):36-45.

51. Pathak P, Meziani MJ, Desai T, Foster C, Diaz JA, Sun Y-P. Supercritical Fluid Processing of Drug Nanoparticles in Stable Suspension. J Nanosci Nanotechno. 2007;7(7):2542-5.

52. Senčar-Božič P, Srčič S, Knez Z, Kerč J. Improvement of nifedipine dissolution characteristics using supercritical CO2. Int J Pharm. 1997;148(2):123-30.

53. Bolten D, Türk M. Micronisation of carbamazepine through rapid expansion of supercritical solution (RESS). J Supercrit Fluids. 2012;62(0):32-40.

54. Benedetti L, Bertucco A, Pallado P. Production of micronic particles of biocompatible polymer using supercritical carbon dioxide. Biotechnol Bioeng. 1997;53(2):232-7.

55. Page SH, Sumpter SR, Lee ML. Fluid phase equilibria in supercritical fluid chromatography with CO2-based mixed mobile phases: A review. J Microcolumn Sep. 1992;4(2):91-122.

56. Johannsen M, Brunner G. Measurements of Solubilities of Xanthines in Supercritical Carbon Dioxide + Methanol. J Chem Eng Data. 1995;40(2):431-4.

57. Page SH, Goates SR, Lee ML. Methanol/CO2 phase behavior in supercritical fluid chromatography and extraction. J Supercrit Fluids. 1991;4(2):109-17.

58. Brunner E, Hültenschmidt W, Schlichthärle G. Fluid mixtures at high pressures IV. Isothermal phase equilibria in binary mixtures consisting of (methanol + hydrogen or nitrogen or methane or carbon monoxide or carbon dioxide). J Chem Thermodyn. 1987;19(3):273-91.

59. Hong JH, Kobayashi R. Vapor-liquid equilibrium studies for the carbon dioxide-methanol system. Fluid Phase Equilib. 1988;41(3):269-76.

60. Robinson DB, Peng D-Y, Chung SYK. The development of the Peng - Robinson equation and its application to phase equilibrium in a system containing methanol. Fluid Phase Equilib. 1985;24(1-2):25-41.

61. Chang T, Rousseau RW. Solubilities of carbon dioxide in methanol and methanol-water at high pressures: experimental data and modeling. Fluid Phase Equilib. 1985;23(2-3):243-58.

62. Weber W, Zeck S, Knapp H. Gas solubilities in liquid solvents at high pressures: apparatus and results for binary and ternary systems of N2, CO2 and CH3OH. Fluid Phase Equilib. 1984;18(3):253-78.

63. Dombro Jr RA, McHugh MA, Prentice GA, Westgate CR. Dielectric constant behavior of carbon dioxide-methanol mixtures in the mixture-critical and liquid-phase regions. Fluid Phase Equilib. 1991;61(3):227-41.

64. Johannsen M, Brunner G. Solubilities of the xanthines caffeine, theophylline and theobromine in supercritical carbon dioxide. Fluid Phase Equilib. 1994;95(0):215-26.

65. Rodrigues MA, Padrela L, Geraldes V, Santos J, Matos HA, Azevedo EG. Theophylline polymorphs by atomization of supercritical antisolvent induced suspensions. J Supercrit Fluids. 2011;58(2):303-12.

66. Roy C, Vega-González A, Subra-Paternault P. Theophylline formulation by supercritical antisolvents. Int J Pharm. 2007;343(1-2):79-89.

67. Franceschi E, Kunita MH, Tres MV, Rubira AF, Muniz EC, Corazza ML, Dariva C, Ferreira SRS, Oliveira JV. Phase behavior and process parameters effects on the characteristics of precipitated theophylline using carbon dioxide as antisolvent. J Supercrit Fluids. 2008;44(1):8-20.

68. Roy C, Vrel D, Vega-González A, Jestin P, Laugier S, Subra-Paternault P. Effect of CO2-antisolvent techniques on size distribution and crystal lattice of theophylline. J Supercrit Fluids. 2011;57(3):267-77.

69. Subra P, Laudani C-G, Vega-González A, Reverchon E. Precipitation and phase behavior of theophylline in solvent-supercritical CO2 mixtures. J Supercrit Fluids. 2005;35(2):95-105.

70. Thakur R, Gupta RB. Formation of phenytoin nanoparticles using rapid expansion of supercritical solution with solid cosolvent (RESS-SC) process. Int J Pharm. 2006;308(1-2):190-9.

71. Larson KA, King ML. Evaluation of Supercritical Fluid Extraction in the Pharmaceutical Industry. Biotechnol Progr. 1986;2(2):73-82.

72. Asghari I, Esmaeilzadeh F. Investigation of key influence parameters for synthesis of submicron carboxymethylcellulose particles via rapid expansion of supercritical CO2 solution by Taguchi method. J Supercrit Fluids. 2012;69(0):34-44.

73. Lin H-L, Hsu P-C, Lin S-Y. Theophylline-citric acid co-crystals easily induced by DSC-FTIR microspectroscopy or different storage conditions. Asian Journal of Pharmaceutical Sciences. 2013;8(1):19-27.

74. Lin P-C, Su C-S, Tang M, Chen Y-P. Micronization of ethosuximide using the rapid expansion of supercritical solution (RESS) process. J Supercrit Fluids. 2012;72(0):84-9.

75. Asghari I, Esmaeilzadeh F. Formation of ultrafine deferasirox particles via rapid expansion of supercritical solution (RESS process) using Taguchi approach. Int J Pharm. 2012;433(1-2):149-56.

76. Müller RH, Peters K. Nanosuspensions for the formulation of poorly soluble drugs: I. Preparation by a size-reduction technique. Int J Pharm. 1998;160(2):229-37.

77. Rabinow BE. Nanosuspensions in drug delivery. Nat Rev Drug Discov. 2004;3(9):785-96.

78. Sinha B, Müller RH, Möschwitzer JP. Bottom-up approaches for preparing drug nanocrystals: Formulations and factors affecting particle size. Int J Pharm. 2013;453(1):126-41.

79. Möschschwitzer J, Rainer HM. Drug Nanocrystals - The Universal Formulation Approach for Poorly Soluble Drugs. Nanoparticulate Drug Delivery Systems: Informa Healthcare; 2007. p. 71-88.

80. Müller RH, Jacobs C, Kayser O. Nanosuspensions as particulate drug formulations in therapy: Rationale for development and what we can expect for the future. Adv Drug Deliver Rev. 2001;47(1):3-19.

81. Patravale VB, Date AA, Kulkarni RM. Nanosuspensions: a promising drug delivery strategy. J Pharm Pharmacol. 2004;56(7):827-40.

82. Wang Y, Zheng Y, Zhang L, Wang Q, Zhang D. Stability of nanosuspensions in drug delivery. J Controlled Release. 2013;172(3):1126-41.

83. Polla GI, Vega DR, Lanza H, Tombari DG, Baggio R, Ayala AP, Filho JM, Fernández D, Leyva G, Dartayet G. Thermal behaviour and stability in Olanzapine. Int J Pharm. 2005;301(1-2):33-40.

84. Rao PS, Ray UK, Hiriyanna SG, Rao SV, Sharma HK, Handa VK, Mukkanti K. Identification of oxidative degradation impurities of Olanzapine drug substance as well as drug product. J Pharm Biomed Anal. 2011;56(2):413-8.

85. Ayala AP, Siesler HW, Boese R, Hoffmann GG, Polla GI, Vega DR. Solid state characterization of olanzapine polymorphs using vibrational spectroscopy. Int J Pharm. 2006;326(1-2):69-79.

86. Seju U, Kumar A, Sawant KK. Development and evaluation of olanzapine-loaded PLGA nanoparticles for nose-to-brain delivery: In vitro and in vivo studies. Acta Biomater. 2011;7(12):4169-76.

87. Reutzel-Edens SM, Bush JK, Magee PA, Stephenson GA, Byrn SR. Anhydrates and Hydrates of Olanzapine: Crystallization, Solid-State Characterization, and Structural Relationships. Cryst Growth Des. 2003;3(6):897-907.

88. Di Lorenzo R, Brogli A. Profile of olanzapine long-acting injection for the maintenance treatment of adult patients with schizophrenia. Neuropsychiatr Dis Treat. 2010 (6):573-81.

89. Heres S, Kraemer S Fau - Bergstrom RF, Bergstrom Rf Fau - Detke HC, Detke HC. Pharmacokinetics of olanzapine long-acting injection: the clinical perspective. Int Clin Psychopharmacol. 2014;29(6):299-312.

90. Sun Y-P, Meziani MJ, Pathak P, Qu L. Polymeric Nanoparticles from Rapid Expansion of Supercritical Fluid Solution. Chem Eur J. 2005;11(5):1366-73.

91. Sane A, Limtrakul J. Formation of retinyl palmitate-loaded poly(l-lactide) nanoparticles using rapid expansion of supercritical solutions into liquid solvents (RESOLV). J Supercrit Fluids. 2009;51(2):230-7.

92. Keltjens R, Thijs L, inventors; A process and composition for making olanzapine form (i). US patent US 20070021605. 2007 Jan 25.

93. Perrut M, Jung, J., Leboeuf, F., 2002 Solid state morphology of particles prepared by supercritical fluid processes. In: Bertucco A, (Editor). Proceedings of the Fourth International Symposium on High Pressure Process Technology and Chemical Engineering; Venice.

94. Bunnell CA, Hendriksen BA, Larsen SD, inventors; Eli Lilly And Company, assignee. Slurrying impure material in anhydrous ethyl acetate, then crystallization yields pure stable drug for treatment of anxiety, psychological disorders and gastrointestinal disorders. US patent US5736541 A. 1998 Apr 7.

95. Verma S, Kumar S, Gokhale R, Burgess DJ. Physical stability of nanosuspensions: Investigation of the role of stabilizers on Ostwald ripening. Int J Pharm. 2011;406(1-2):145-52.

96. Ghosh I, Bose S, Vippagunta R, Harmon F. Nanosuspension for improving the bioavailability of a poorly soluble drug and screening of stabilizing agents to inhibit crystal growth. Int J Pharm. 2011;409(1-2):260-8.

97. Hu J, Ng WK, Dong Y, Shen S, Tan RBH. Continuous and scalable process for water-redispersible nanoformulation of poorly aqueous soluble APIs by antisolvent precipitation and spray-drying. Int J Pharm. 2011;404(1-2):198-204.

98. Ain-Ai A, Gupta PK. Effect of arginine hydrochloride and hydroxypropyl cellulose as stabilizers on the physical stability of high drug loading nanosuspensions of a poorly soluble compound. Int J Pharm. 2008;351(1-2):282-8.

99. He W, Lu Y, Qi J, Chen L, Hu F, Wu W. Food proteins as novel nanosuspension stabilizers for poorly water-soluble drugs. Int J Pharm. 2013;441(1-2):269-78.

100. Wikström H, Rantanen J, Gift AD, Taylor LS. Toward an Understanding of the Factors Influencing Anhydrate-to-Hydrate Transformation Kinetics in Aqueous Environments. Cryst Growth Des. 2008;8(8):2684-93.

101. Otsuka M, Ohfusa T, Matsuda Y. Effect of binders on polymorphic transformation kinetics of carbamazepine in aqueous solution. Colloids Surf, B. 2000;17(3):145-52.

102. Tian F, Baldursdottir S, Rantanen J. Effects of Polymer Additives on the Crystallization of Hydrates: A Molecular-Level Modulation. Mol Pharm. 2008;6(1):202-10.

103. Elder DP, Holm R, Diego HLd. Use of pharmaceutical salts and cocrystals to address the issue of poor solubility. Int J Pharm. 2013;453(1):88-100.

104. U.S. Food and Drug Administration, 2013. U.S. Department of Health and Human Services, Food and Drug Administration, Center for Drug Evaluation and Research. Guidance for Industry: Regulatory Classification of Pharmaceutical Cocrystals.

105. Friscic T, Jones W. Cocrystal architecture and properties: design and building of chiral and racemic structures by solid-solid reactions. Faraday Discuss. 2007;136(0):167-78.

106. Friscic T, Jones W. Recent Advances in Understanding the Mechanism of Cocrystal Formation via Grinding. Cryst Growth Des. 2009;9(3):1621-37.

107. Qiao N, Li M, Schlindwein W, Malek N, Davies A, Trappitt G. Pharmaceutical cocrystals: An overview. Int J Pharm. 2011;419(1-2):1-11.

108. Schultheiss N, Newman A. Pharmaceutical Cocrystals and Their Physicochemical Properties. Cryst Growth Des. 2009;9(6):2950-67.

109. Schartman RR. On the thermodynamics of cocrystal formation. Int J Pharm. 2009;365(1-2):77-80.

110. Shan N, Zaworotko MJ. The role of cocrystals in pharmaceutical science. Drug Discov Today. 2008;13(9-10):440-6.

111. Thakuria R, Delori A, Jones W, Lipert MP, Roy L, Rodríguez-Hornedo N. Pharmaceutical cocrystals and poorly soluble drugs. Int J Pharm. 2013;453(1):101-25.

112. Tomaszewska I, Karki S, Shur J, Price R, Fotaki N. Pharmaceutical characterisation and evaluation of cocrystals: Importance of in vitro dissolution conditions and type of coformer. Int J Pharm. 2013;453(2):380-8.

113. Aakeröy CB, Fasulo ME, Desper J. Cocrystal or Salt: Does It Really Matter? Mol Pharm. 2007;4(3):317-22.

114. Shayanfar A, Jouyban A. Physicochemical characterization of a new cocrystal of ketoconazole. Powder Technol. 2014;262(0):242-8.

115. Chow SF, Chen M, Shi L, Chow AHL, Sun CC. Simultaneously Improving the Mechanical Properties, Dissolution Performance, and Hygroscopicity of Ibuprofen and Flurbiprofen by Cocrystallization with Nicotinamide. Pharm Res. 2012;29(7):1854-65.

116. Shayanfar A, Asadpour-Zeynali K, Jouyban A. Solubility and dissolution rate of a carbamazepine-cinnamic acid cocrystal. J Mol Liq. 2013;187(0):171-6.

117. Masuda T, Yoshihashi Y, Yonemochi E, Fujii K, Uekusa H, Terada K. Cocrystallization and amorphization induced by drug-excipient interaction improves the physical properties of acyclovir. Int J Pharm. 2012;422(1-2):160-9.

118. Childs SL, Stahly GP, Park A. The Salt-Cocrystal Continuum: The Influence of Crystal Structure on Ionization State. Mol Pharm. 2007;4(3):323-38.

119. Ainouz A, Authelin J-R, Billot P, Lieberman H. Modeling and prediction of cocrystal phase diagrams. Int J Pharm. 2009;374(1-2):82-9.

120. Padrela L, Rodrigues MA, Velaga SP, Matos HA, de Azevedo EG. Formation of indomethacin-saccharin cocrystals using supercritical fluid technology. Eur J Pharm Sci. 2009;38(1):9-17.

121. Oberoi LM, Alexander KS, Riga AT. Study of interaction between ibuprofen and nicotinamide using differential scanning calorimetry, spectroscopy, and microscopy and formulation of a fast-acting and possibly better ibuprofen suspension for osteoarthritis patients. J Pharm Sci. 2004;94(1):93-101.

122. Berry DJ, Seaton CC, Clegg W, Harrington RW, Coles SJ, Horton PN, Hursthouse MB, Storey R, Jones W, Friscic T, Blagden N. Applying Hot-Stage Microscopy to Co-Crystal Screening: A Study of Nicotinamide with Seven Active Pharmaceutical Ingredients. Cryst Growth Des. 2008;8(5):1697-712.

123. Dhumal RS, Kelly AL, York P, Coates PD, Paradkar A. Cocrystalization and Simultaneous Agglomeration Using Hot Melt Extrusion. Pharm Res. 2010;27(12):2725-33.

124. Kelly AL, Gough T, Dhumal RS, Halsey SA, Paradkar A. Monitoring ibuprofen-nicotinamide cocrystal formation during solvent free continuous cocrystallization (SFCC) using near infrared spectroscopy as a PAT tool. Int J Pharm. 2012;426(1-2):15-20.

125. Chan HCS, Kendrick J, Neumann MA, Leusen FJJ. Towards ab initio screening of co-crystal formation through lattice energy calculations and crystal structure prediction of nicotinamide, isonicotinamide, picolinamide and paracetamol multi-component crystals. Cryst Eng Comm. 2013;15(19):3799-807.

126. Qiao N, Wang K, Schlindwein W, Davies A, Li M. In situ monitoring of carbamazepine-nicotinamide cocrystal intrinsic dissolution behaviour. Eur J Pharm Biopharm. 2013;83(3):415-26.

127. Soares FLF, Carneiro RL. Evaluation of analytical tools and multivariate methods for quantification of co-former crystals in ibuprofen-nicotinamide co-crystals. J Pharm Biomed Anal. 2014;89(0):166-75.

128. Sanghvi R, Evans D, Yalkowsky SH. Stacking complexation by nicotinamide: A useful way of enhancing drug solubility. Int J Pharm. 2007;336(1):35-41.

129. Truelove J, Bawarshi-Nassar R, Chen NR, Hussain A. Solubility enhancement of some developmental anti-cancer nucleoside analogs by complexation with nicotinamide. Int J Pharm. 1984;19(1):17-25.

130. Kotnik P, Škerget M, Knez Ž. Solubility of Nicotinic Acid and Nicotinamide in Carbon Dioxide at T = (313.15 to 373.15) K and p = (5 to 30) MPa: Experimental Data and

Correlation. J Chem Eng Data. 2011;56(2):338-43.

131. Sheridan PL, Buckton G, Storey DE. The extent of errors associated with contact angles II. Factors affecting data obtained using a Wilhelmy plate technique for powders. Int J Pharm. 1994;109(2):155-71.

132. Grossjohann C, Eccles KS, Maguire AR, Lawrence SE, Tajber L, Corrigan OI, Healy AM. Characterisation, solubility and intrinsic dissolution behaviour of benzamide: dibenzyl sulfoxide cocrystal. Int J Pharm. 2012;422(1-2):24-32.

133. Akalin E, Akyuz S. Vibrational analysis of free and hydrogen bonded complexes of nicotinamide and picolinamide. Vib Spectrosc. 2006;42(2):333-40.

134. Rossi B, Verrocchio P, Viliani G, Mancini I, Guella G, Rigo E, Scarduelli G, Mariotto G. Vibrational properties of ibuprofen–cyclodextrin inclusion complexes investigated by Raman scattering and numerical simulation. J Raman Spectrosc. 2009;40(4):453-8.

135. Jubert A, Legarto ML, Massa NE, Tévez LL, Okulik NB. Vibrational and theoretical studies of non-steroidal anti-inflammatory drugs Ibuprofen [2-(4-isobutylphenyl)propionic acid]; Naproxen [6-methoxy-α±-methyl-2-naphthalene acetic acid] and Tolmetin acids [1-methyl-5-(4-methylbenzoyl)-1H-pyrrole-2-acetic acid]. J Mol Struct. 2006;783(1-3):34-51.

136. Perrut M, Jung J, Leboeuf F. Enhancement of dissolution rate of poorly-soluble active ingredients by supercritical fluid processes: Part I: Micronization of neat particles. Int J Pharm. 2005;288(1):3-10.

137. Cristini F, Delalonde, M., Joussot-Dubien, C., Bataille, B., 2003 Elaboration of ibuprofen microcomposites in supercritical CO2. In: Brunner G, Kikic, I., Perrut, M., (Editor). Proceedings of the Sixth International Symposium on Supercritical Fluids.

APPENDIX

Modifications of the expansion path

The expansion path for the production of RESS products as designed by Sitec is depicted in Figure 32a). The configuration allows interruption of the RESS process in case of clogging of the nozzle, but it has the disadvantage of the fluid passing through a long distance between the micro-metering valve and the nozzle inside the expansion chamber. The pressure loss caused phase transitions and thus product loss before the fluid passed the nozzle, which could not be prevented by additional heating. Thereby, clogging of the nozzle and thus interruptions of the RESS process occurred frequently and product yields were unstable. For this reason, alternative configurations were built in house and tested, which are depicted in Figure 32b) and c).

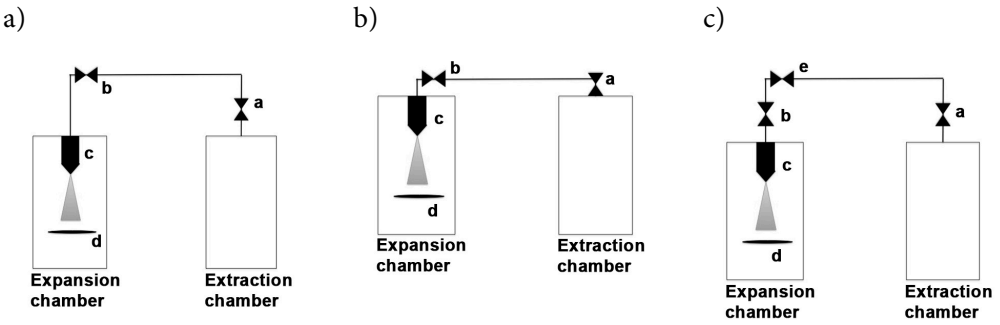

Figure 32 Modifications of the expansion path a) Sitec configuration b) modified configuration with short distance between micro-metering valve and nozzle c) modified setup with short distance between micro-metering valve and nozzle and security valves between extraction and expansion chamber.

a	valve V35
b	micro-metering valve V45 for regulation of the CO_2 flow through the nozzle
c	nozzle
d	Filter for particle collection
e	security valve between extraction and expansion chamber

In configuration b), the distance between micro-metering valve and nozzle was shortened, which distinctly improved both the continuity of the expansion process and the product yields. If clogging of the nozzle did occur however, the process needed to be abandoned since no security valve could be operated between the extraction and the expansion chamber. Therefore, a security valve was added (Figure 32c). Configuration c combines both a short distance between micro-metering valve and the nozzle, and the possibility of process interruption if needed.

Validation of the Stricker dissolution apparatus

The sampling specifications for the Stricker flow-through cell apparatus are met, if the deviation of every individual sample volume is maximum 4 % of the intended sample volume, except for the first sample, since it cannot be avoided that a certain amount of air enters the apparatus while introducing the sample into the chamber. The chamber volume at the end of the experiment is allowed a total deviation of ± 5 %. To test if the equipment is within the specifications, 3 runs were performed, where during 30 min a sample of 3.5 ml was withdrawn and accurately measured every minute. The chamber volume at the end of the runs was determined.

Run	Chamber volume [ml]	Deviation allowed [ml]	Satisfies
1	97.5	5	yes
2	99.0	5	yes
3	101.0	5	yes
Time (min)	**Sample volume 1**	**Sample volume 2**	**Sample volume 3**
0	3.5	3.5	3.5
1	3.5	3.5	3.5
2	3.5	3.5	3.5
3	3.5	3.5	3.5
4	3.5	3.5	3.5
5	3.5	3.5	3.5
6	3.5	3.5	3.5
7	3.5	3.5	3.5
8	3.5	3.5	3.5
9	3.5	3.5	3.5
10	3.5	3.5	3.5
11	3.5	3.5	3.5
12	3.5	3.5	3.5
13	3.5	3.5	3.6
14	3.5	3.5	3.5
15	3.5	3.5	3.4
16	3.5	3.5	3.5
17	3.5	3.55	3.5
18	3.5	3.5	3.5
19	3.5	3.5	3.55
20	3.5	3.5	3.5
21	3.5	3.5	3.5
22	3.5	3.5	3.5
23	3.5	3.5	3.5
24	3.5	3.5	3.5
25	3.5	3.5	3.5
26	3.5	3.5	3.5
27	3.5	3.5	3.5
28	3.5	3.5	3.5
29	3.5	3.5	3.5
30	3.5	3.5	3.5
Mean [ml]	3.5	3.5	3.5
St Dev [ml]	0.00	0.01	0.03
Allowed dev[ml]	0.14	0.14	0.14
Satisfies	yes	yes	yes

UV calibration and quantitative determination of theophylline

Theophylline solutions were quantified in phosphate buffer pH 7.4 at 270 nm. 5 stock solutions were prepared by accurately weighing an amount of TP (50 mg) and placing it into 100 ml volumetric flasks. The material was dissolved in 100 ml of phosphate buffer pH 7.4 and diluted appropriately. Each concentration was measured in triplicate.

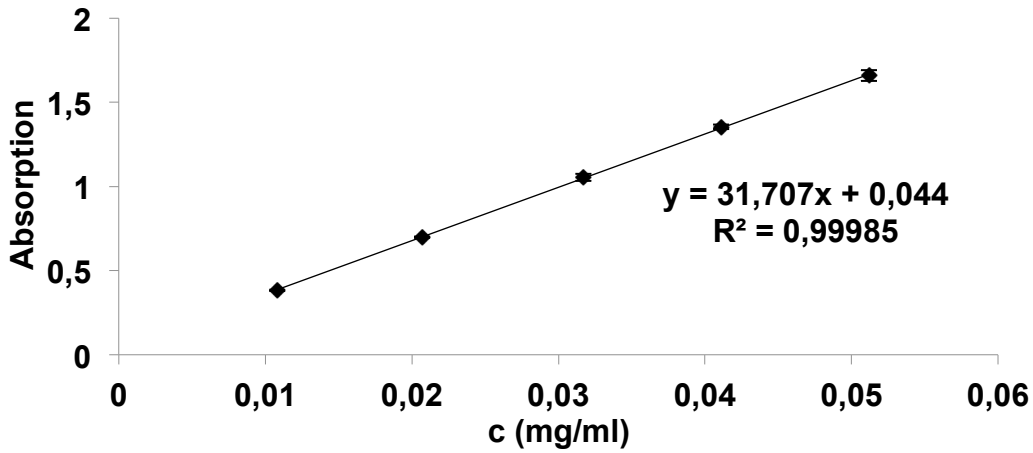

Figure 33 UV calibration curve of theophylline at 270 nm in phosphate buffer pH 7.4. Error bars represent standard deviation of the mean (n = 6)

UV calibration and quantitative determination of olanzapine

Olanzapine was quantified at 260 nm in phosphate buffer pH 6.8 for dissolution testing. 3 stock solutions of 5 mg olanzapine in 250 ml buffer were prepared and each was diluted 5 times. For the quantitative determination of olanzapine in nanosuspensions, a calibration in 0.1 N hydrochloric acid (HCl) was used at a wavelength of 260 nm. 3 stock solutions of 10 mg olanzapine in 100 ml HCl were prepared and diluted 6 times.

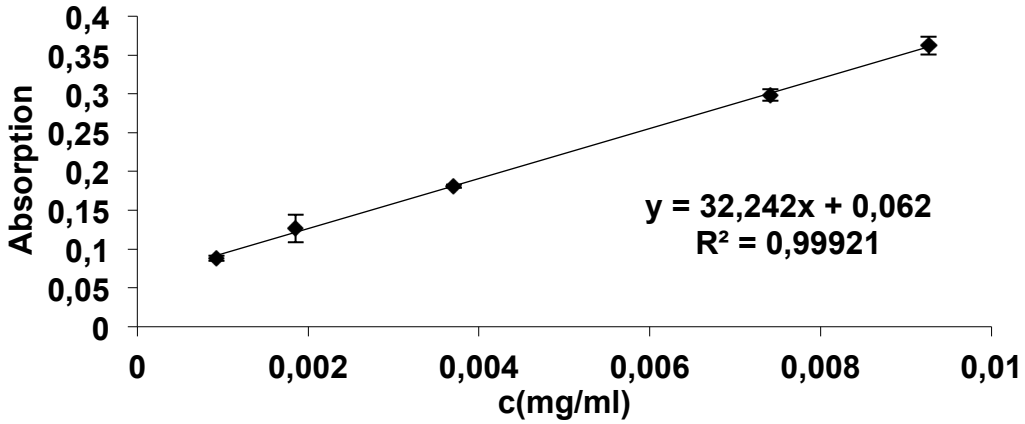

Figure 34 UV calibration of olanzapine at 260 nm in phosphate buffer pH 6.8. Error bars represent standard deviation of the mean (n = 6)

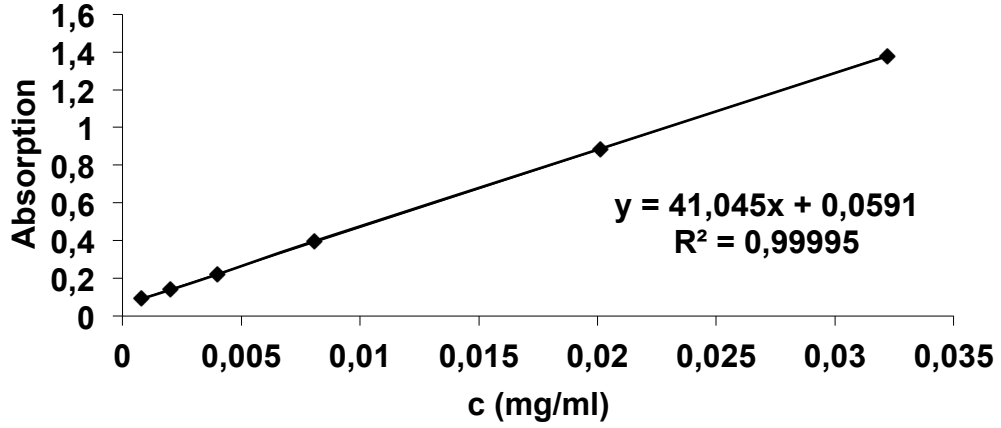

Figure 35 UV calibration curve of olanzapine at 260 nm in 0.1 N HCl. Error bars represent standard deviation of the mean (n = 6)

HPLC calibration and quantitative determination of ibuprofen and nicotinamide

Ibuprofen and nicotinamide were quantified with HPLC at a detection wavelength of 230 nm. 6 stock solutions were prepared of 8 mg API in 100 ml of phosphate buffer pH 6.4 and each stock solution was diluted 7 times.

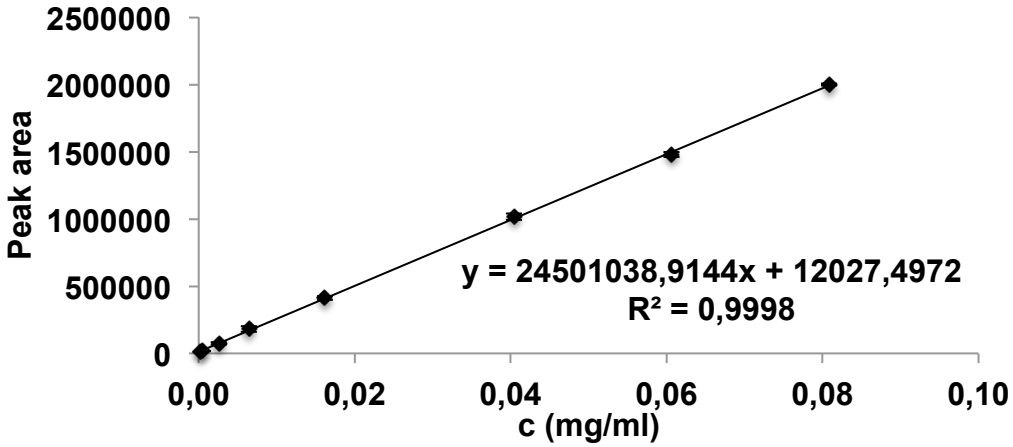

Figure 36 HPLC calibration over the peak area of ibuprofen. Error bars represent standard deviations of the mean (n = 6)

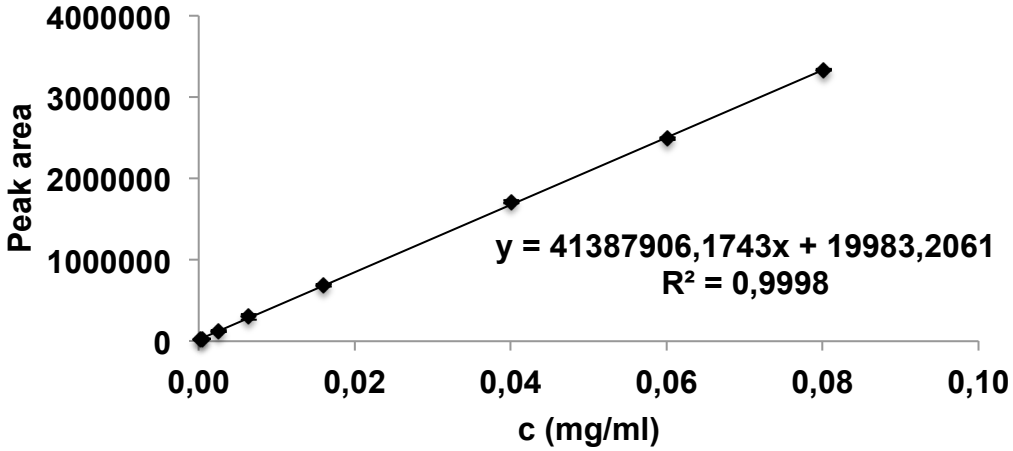

Figure 37 HPLC calibration over the peak area of nicotinamide. Error bars represent standard deviations of the mean (n = 6)